Journal of the Electrochemical Society of India

Indian Institute of Science Campus,
Bengaluru - 560 012, India

Guest Editor

Dr. S.T. Aruna

Vol.No.73 (7&8), Oct-Dec 2024

CODEN - JESIA 73 [7&8] 2024 ISSN:0013-466X

INSTRUCTIONS TO AUTHORS

GENERAL

Address all manuscripts to the Managing Editor, Electrochemical Society of India,(JECSI) Bengaluru-560012 and send it by email to arunaecsi@gmail.com / ecsiiisc@gmail.com. Submission of an article will be taken to imply that it has not been previously published and is not under consideration for publication elsewhere. And further that if accepted, it will not be published elsewhere. Submit an electronic version of the paper in WORD format along with a pdf version in order not to miss any portion due to transmission faults. Identify the address, affiliation, email address of the author (corresponding author in case of multiple authors). Also, identify the category in which the paper qualifies for publication.

Journal of the Electrochemical Society of India (JECSI) is a multidisciplinary journal in the general area of Electrochemical Science and Technology. Research and review papers of general significance that are written clearly and well organized will be given preference. All submitted papers will be reviewed by three experts to determine suitability. Paper found unsuitable in terms of the overall requirements of the Journal and those not accepted by the reviewers will be returned to the authors. Both solicited and unsolicited papers will be reviewed. Authors will be notified of acceptance, rejection or any need for revision before acceptance for publication. Any illustrations or other material reproduced from other publications must be properly credited. It is the author's responsibility to obtain the necessary permission in such cases.

CATEGORIES OF MANUSCRIPTS

GeneralArticles, not exceeding 5000 words in length, should discuss current trends in research in a field that will be of interest to readers outside the field; interdisciplinary topics; Science policy and administration; Impact of Science and Technology on Society, etc. The paper should include a summary not exceeding 200 words, introductory paragraph(s), brief subheads at appropriate places to point to what follows, Illustrations that will help a general reader and references.

Review Articles, not exceeding 5000 words, are expected to survey and discuss recent developments in a relevant field. They should be well focused and organized. General text book style is not acceptable. Research Articles should report and discuss results of work of a fairly major significance. They should include an Abstract, introductory paragraph(s) and brief subheads indicating materials and methods used, major results and discussion of results, relevant illustrations and references.

Research Communications, not exceeding 2000 words, should contain important findings that are novel and are of fairly broad interest. They should not be broken up under subheads. Correspondences include letters, not exceeding 500 words that are of general interest to Scientist, Engineers and Technologists. Only selected letters will be published. Scientific Correspondence contains technical comments, including those on articles or communications published in JECSI. Appropriate letters will be published.

Book Reviews are reviews of books published in the major areas of Electrochemical Science, Technology and Engineering. Unsolicited reviews will also be considered. Reviews that simply 'list' the contents will not be acceptable for publication. Reviews should have 'context' and convey information about the subject of the book. Historical Comments and Notes inform readers about interesting aspects of personalities or institutions of Science or about watershed events in the history/ development of science. Most are expected to relate to India. Illustrations are welcome with due credit if already published elsewhere.

MANUSCRIPT PREPARATION

The manuscript should be in double line spacing in an area corresponding to A-4 size paper with 25 mm margin all around. Page numbers, including that for the first page should be given at the bottom centre of the page. The title should be brief, specific and amenable to indexing. Give a maximum of 5 keywords which are carefully chosen and not phrases of several words. Summary and abstract should not have more than 200 words and should convey the main point of the paper, outline the results and conclusions and explain the significance of the work and results.

Text

Papers should begin with an introduction. The text should be intelligible to readers in different disciplines and technical terms should be defined. Tables and figures should be arranged in numerical order and referred to in that order. All symbols and abbreviations must be defined and used only when absolutely necessary. Superscripts and subscripts and ambiguous characters should be clearly indicated. Units of measure should be metric and preferably SI. Methods should, as far as possible, be described briefly in appropriate table and figure legends.

Figures are to be drawn in sizes that are clearly intelligible. Location and orientation of figures is the entire responsibility of the author(s). The actual location of figures and tables may be clearly indicated in the pdf format that accompanies the main word format submission. The same data should not be given in both tables and figures. Photomicrographs and other photographs that require a scale bar or a micron marker should be defined clearly in the caption. Magnifications are not acceptable in place of micron markers. Primary data should be submitted as far as possible as for example actual photograph of an electrophoretic gel rather than an idealized diagram.

References should be numbered in the order in which they appear first through the text and then through table and figure legends. Following examples indicate the different ways of writing the references:

Reference to a journal publication:

[1] J. Name, J.A.J. Name, R.A. Name, Title of article, J. Sci. Commun. Vol.no (year) page number xx–xy. https://doi.org/10.1016/ j.Sc.2010.00372.

Reference to a book:

[3] W. Name, E.B. Name, Title of the book, Edition, Publisher, Place name, year.

Reference to a chapter in an edited book:

[4] G.R. Name, L.B. Name, Chapter title, in: B.S. Name, R.Z. Name
(Eds.), Title of book, Publisher, Place name, Year, pp. xxx–yyy.

Acknowledgments should be brief and clear.

Funding: This work was supported by Granting Agency Name [grant numbers xxxx, yyyy];

Cover Photographs. Good photographs (colour or black and white) that pertain to a submitted paper will be considered for use on the cover of an issue.

Proofs and Publication: A final pdf version of the paper may be sent to the author before publication if there are any inaccuracies or doubts of any nature. Such a procedure is redundant in case no major editorial changes are made in the paper.

About Guest Editor

Dr. S.T. Aruna

Chief Scientist
CSIR-National Aerospace Laboratories
Bangalore-560017

Dr. S.T. Aruna is currently working as a Chief Scientist at Council of Scientific and Industrial Research - National Aerospace Laboratories (CSIR-NAL), Bangalore, India. She has a Master's Degree in Chemistry from Mysore University (1994) and she secured the first rank and won 4 gold medals. She obtained her Ph.D. from the Indian Institute of Science (IISc), Bangalore in the year 1998.

She worked as a postdoctoral fellow at Bar-Ilan University, Israel in the area of dye-sensitized solar cells from 1998-1999. She has authored ~ 140 research papers in international peer reviewed journals, 11 patents, co-authored a book and coedited a book, written 14 book chapters and 4 encyclopedia chapters. Her research papers have been well cited and her publications have an h-index of 45. Her name features in the list of top 2 per cent of the world scientists released by Stanford University. Her current research interests include development of tapecast ceramic substrates for electronics application, nanomaterials, plasma sprayed thermal and environmental barrier coatings, oxygen sensor and solid oxide fuel cells (SOFCs). She has guided 5 Ph.D students. One of her review papers has received the best cited paper award twice which was published in Current Opinion in Solid State and Materials science. She is on the editorial board of Surface Engineering Journal. She has won Sathish Dhawan Young Engineer Karnataka State Award-2021, Thermal spray excellence award-2025, Sasadhar Ray Memorial award-2023, MRSI Medal-2022, NM Sampat award -2016 and Pavan Nagpal Memorial award-2019.

Publication Ethics and Publication Malpractice Statement

The Journal of Electrochemical Society of India (JECSI) follows the Committee on Publication Ethics (COPE) *Code of Conduct and Best Practice Guidelines for Journal Editors* and the *Code of Conduct for Journal Publishers*. It is expected that authors, reviewers and editors follow the best-practice guidelines on ethical behaviour.

Responsibilities of Editorial Board

Editors evaluate submitted manuscripts only on the basis of their merit such as novelty, originality, importance, and its relevance to the journal's scope. The information or ideas imparted to the editors due to handling the manuscript will be kept confidential and will not be used for their own benefit. The editors will refrain from reviewing a manuscript in which they have conflict of interest and will be handled by other editorial board members. Editors and editorial staff will maintain confidentiality about the submitted manuscripts.

All the manuscripts submitted to the journal will undergo peer-review by at least two reviewers who are experts in that area. Based on the evaluation reports received from the reviewers, copyright permissions and plagiarism will be checked and then the Chief Editor decides on the publication of the manuscript.

The Chief Editor will take actions when ethical concerns are raised with regard to a submitted manuscript or published paper followed by a correction, retraction, expression of concern or relevant other notes will be published in JECSI.

Responsibilities of Authors

The Authors should present detailed and correct account of the work to enable others to reproduce the work. Fraudulent or inaccurate statements are not accepted. If required the authors will be asked to provide the raw data of their study if some suspicious figures are provided in the manuscript. Authors should check their manuscript for originality check using the standard software. Only manuscripts with similarity report <20% will be considered for peer review.

The authors should not simultaneously submit the same manuscript to multiple journals and is treated as unethical and such papers will be sent back to the authors and authors will be black listed.

Authors who have made significant contributions to the paper should only be included as authors in the manuscript and the role of each author has to be listed. The other peoples' name should be included in the acknowledgement section.

The authors should disclose the conflict of interest that would have influenced the results or their interpretation. Authors should also properly acknowledge the work of others and ensure proper citation of such works in the manuscript. The authors should clearly state in the manuscript if the work involved the use of hazardous chemicals, procedures or equipment. The authors should co- operate in submitting the revised manuscripts before the deadline and providing befitting replies to the reviewer comments.

The authors should inform the Chief Editor when they discover significant errors or inaccuracies in their own published work and publish a corrigendum or retract the paper.

Journal of The Electrochemical Society of India

CODEN JESIA 73 (7 & 8) Oct-Dec 2024. ISSN 0013-466X

Donor Members

M/s. Mascot Chemical Works, Bengaluru
M/s. Indian Telephone Industries Ltd., Bengaluru
M/s. Kangovi Electronics (P) Ltd., Bengaluru
M/s. Aquair Control Systems, Bengaluru
M/s. Stiver Equipment Pvt. Ltd., Bengaluru
M/s. Hindustan Aeronautics Ltd., Bengaluru
M/s. High Energy Batteries, Madurai
M/s. Electroplating Equipment Co., Bengaluru
M/s. Galvanosols Pvt. Ltd., Bengaluru
M/s. Pyro Technologies, Bengaluru
M/s. Shruthi Enterprises, Bengaluru
M/s. Grauer Weil (India) Ltd., Mumbai
M/s. Zaveri Brothers (P) Ltd., Mumbai
M/s. Standard Batteries, Mumbai
M/s. Geep Industries Syndicate Ltd.
M/s. Larsen and Toubro Ltd., Mysore
M/s. IR Technology Services Pvt. Ltd.
M/s. Brite Platers and Electrical Engineers,Bengaluru
M/s. Vijaya Metal Finishers, Bengaluru
M/s. Vinpla Plating Pvt. Ltd., Bengaluru
M/s. Surface Chem Finishers, Bengaluru

Permanent Sustaining Members

M/s. Tata Chemical
M/s Ashok Charitable Trust, Karaikudi
M/s. Mysore Paper Mills, Bhadravathi
M/s. Tata Iron and Steel Company Ltd., Jamshedpur
M/s. DCM Chemical Works
M/s. Indian Aluminum Company Ltd., Alwaye
M/s. Visveswaraya Iron and Steel Ltd., Bhadravathi

Journal of The Electrochemical Society of India

CODEN JESIA 73 (7& 8) Oct-Dec 2024. ISSN 0013-466X

Email : ecsiiisc@gmail.com

Address all communications to :
THE ELECTROCHEMICAL SOCIETY OF INDIA
Indian Institute of Science Campus
Bengaluru - 560 012
Email : ecsiiise@gmail.com

Potential of Sodium-ion Batteries for Stationary Applications

Sakshee Chandel[1*], Vinten D. Diwakar[1]

[1]*Matter Energy Private Limited, Ahmedabad-382421, Gujarat, India*

**E-mail of the corresponding author: sakshee.chandel@matter.in, saksheechandel@gmail.com*

Abstract

Sodium-ion batteries (SIBs) present a promising alternative to lithium-ion technologies, particularly for stationary energy storage applications, due to their inherent advantages in cost, resource abundance, and sustainability. However, the cost advantages of stationary SIBs alone are not enough to ensure their commercial success. Compared with lithium ions, sodium ions with large size (0.76 Å for Li and 1.02 Å for Na) and atomic weight (6.94 amu for Li and 22.99 amu for Na) suffer slower ionic transport kinetics and lower energy density. This disadvantage can be compensated by the high-rate capability of sodium containing compounds. Sodium having similar electrochemical properties compared to lithium-ion and a little less potential (-2.71 V vs. SHE) considered as a leading energy storage device for stationary and large-scale energy storage systems. Current SIBs have achieved specific capacities in the range of 100-150 mAh/g, with energy densities of approximately 100-150 Wh/kg. While these figures are lower compared to high-performance lithium-ion batteries, ongoing research is steadily closing this gap. In this review, we outline the current status of SIB technology and industry directions along with a comparison of performance metrics with lithium-ion chemistries used for storage applications.

Keywords: *Sodium-ion Batteries, Stationary Applications, Hard Carbon, Energy Storage Systems*

1. Introduction

In the quest for advancements in energy storage technologies, the spotlight has often shown on Lithium-ion batteries (LIBs) due to their high energy density (200- 250 Wh kg^{-1}), reliability, and established presence in both consumer electronics and large-scale stationary applications. Lithium Iron Phosphate (LFP) graphite and Lithium nickel Cobalt Manganese oxide (NMC)-graphite batteries, in particular, have gained recognition for their robustness, and impressive long cycle life [1, 2]. LFP batteries are renowned for their thermal stability and safety features, achieving energy densities around ~150 Wh/kg [3, 4]. As the demand for sustainable and cost-effective energy solutions continues to rise, Sodium-ion batteries (SIBs) are emerging as a formidable alternative. SIB technology leverages sodium, an abundant and inexpensive resource, to potentially reduce the cost of energy storage systems significantly [5]. Although historically considered less competitive due to lower energy densities compared to lithium-based batteries, recent advancements have demonstrated that SIBs can offer viable alternatives for stationary applications. Modern SIBs are now achieving energy densities in the range of 100-160 Wh/kg, with some advanced prototypes pushing towards 200 Wh/kg [6-7]. This progress is partly attributed to innovations in electrode materials and electrolytes, which have enhanced the performance and longevity of these batteries. For instance, researchers have developed new cathode materials, such as sodium layered oxide, polyanionic frameworks, Prussian blue analogues which have contributed to the improved energy density and cycle stability of SIBs. The practical applications of SIBs are expanding, particularly in stationary energy storage systems [7]. Their lower cost and abundant raw materials make them an attractive option for grid energy storage, peak shaving, and load leveling [8, 9].

Despite their significant potential, the development of

SIBs remains concentrated among a relatively small group of companies, including Faradion (UK), Tiamat (Europe), Altris AB (Europe), HiNa (China), and Natron Energy (USA). These companies do not adhere to a single, uniform approach to sodium battery chemistry. For instance, various types of positive electrodes are utilized, such as layered oxides, Prussian blue analogues, or vanadium-based polyanionic compounds, and these can be paired with either aqueous or non-aqueous electrolytes. This diversity in chemistry not only allows for a range of market applications but also underscores the vast potential for research and innovation in SIB materials, encompassing new developments in positive and negative electrodes as well as electrolytes.

2.Comparative Analysis of Sodium-Ion vs. Lithium-Ion for Stationary Applications.

The growth of SIBs has been extensively accelerated due to the comparable electrochemical properties of sodium and lithium. An examination of the physical properties of sodium and lithium highlights (Table 1) why both elements were once considered equally promising for energy storage.

Table 1. Physical properties of lithium and sodium.

Property	Lithium (Li)	Sodium (Na)
Atomic mass [g mol^{-1}]	6.94	22.99
Electron configuration	[He]$2s^1$	[Ne]$3s^1$
Cationic radius [Å]	0.76	1.02
Density [g cm^{-3}]	0.971	0.534
Standard electrode potential [V]	-3.04	-2.71
Melting point [°C]	180.5	97.7
First ionization energy [kJ mol^{-1}]	520.2	495.8
Theoretical gravimetric capacity [mAh g^{-1}]	3861	1165
Theoretical volumetric capacity [mAh cm^{-3}]	2062	1131

Both lithium and sodium belong to alkali metals in Group 1 of the periodic table, characterized by having a single electron in their valence shell. This commonality makes them highly reactive, with physical properties such as melting point, hardness, conductivity, and first ionization energy decreasing down the group. A crucial factor in comparing these metals is their redox potentials: the standard reduction potential of Na^+/Na is −2.71 V versus the Standard Hydrogen Electrode (SHE), which is approximately 330 mV higher than Li^+/Li at −3.04 V [8]. This difference means that, thermodynamically, the anodic electrode potentials for SIBs will generally be higher than those for LIBs. A comparative analysis of SIBs against well-established lithium-ion technologies, such as LFP is given below.

Energy Density: LFP-based LIBs offer around 150 to 200 Wh/kg [3, 4] while the energy density of SIBs typically ranges from 100 to 150 Wh/kg [6]. Thus, more energy can be delivered and stored by LIBs per unit of weight or volume. On the other hand, SIBs may require larger or heavier systems to store the same amount of energy

Cycle Life: In terms of cycle life, SIBs demonstrate a promising longevity with current technologies offering around 1,500 to 3,000 cycles, making them competitive with LFP, which can achieve between 2,000 and 5,000 cycles. This durability is beneficial for stationary applications that demand long-term reliability and minimal maintenance [1, 6].

Charge/Discharge Rates: SIBs generally support rates of 0.5C to 1C, which are lower compared to LFP batteries that handle up to 1C for charging and 5C for discharging. Although SIBs currently offer slower rates, ongoing advancements are expected to improve these metrics, making them more viable for applications requiring rapid energy storage and delivery [5, 10].

Cost: SIBs have notable cost advantages for stationary applications due to the abundance and lower cost of sodium compared to lithium. For some applications, this cost benefit can make SIBs more appealing, particularly in nations with limited lithium resources like India [11]. Overall, SIBs present a potentially more cost-effective solution for large-scale energy storage, aligning well with the economic constraints of stationary applications.

Safety and Stability: When it comes to safety and stability, SIBs generally offer a robust safety profile due to their stable chemistries, which reduce the risk of thermal runaway and fires [12]. LFP batteries are known for their safety and thermal stability, which makes

them a preferred choice for applications requiring high safety standards. SIBs can be discharged to 0 V and stored and transported in this discharged state unlike LIBs. Nonetheless, all three technologies are considered relatively safe, with SIBs benefiting from ongoing improvements in safety protocols.

Environmental Impact: SIBs have a lower environmental footprint because sodium is widely available, and the extraction process causes less environmental disturbance than lithium. LFP batteries involve the mining and processing of lithium, which have ecological consequences.

To make a true and fair comparison of SIBs and LIBs, that captures the differences in their cell performance as well as the materials costs, LFP//graphite battery would be a suitable reference where both chemistries are cobalt free cell. Figure 1 represents the trend of enhancement in cell-level specific energies of commercially available LIBs compared with Faradion's Na-ion pouch cells [9]. The LFP//graphite system is a good competitor as typically the energy density is similar to that of SIBs as mentioned in Figure 1.

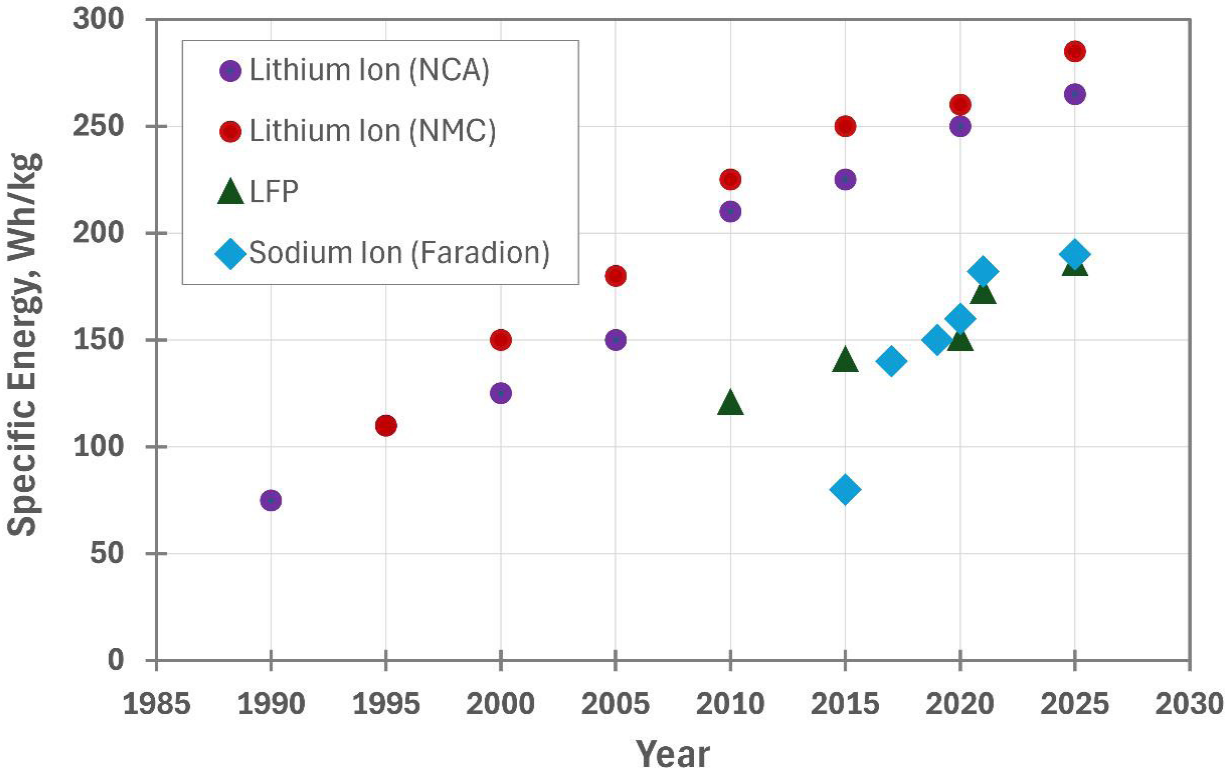

Figure 1: The trend of enhancement in cell-level specific energies of commercially available LIBs compared with Faradion's Na-ion pouch cells [Reproduced with permission from ref. 9, copyright 2025 Royal Society of Chemistry]

For stationary applications, such as grid storage or large-scale energy management systems, SIBs offer potential advantages in terms of cost, resource availability, and environmental impact. However, LIBs currently provide superior energy density and performance, making them more suitable for applications where space and weight are constraints. The choice between the two will depend on specific application needs, cost considerations, and long-term goals related to sustainability and resource management.

3.Electrochemical Mechanism in Electrode Materials

SIBs operate on the electrochemical movement of Na^+ ions between the anode and cathode during charge and discharge cycles. In the discharge process, Na^+ ions move from the anode to the cathode through the

electrolyte, releasing energy as electrons flow through an external circuit. During charging, Na^+ ions return to the anode from the cathode, with electrons flowing back through the circuit. In SIBs electrodes, charge insertion mechanisms are categorized into intercalation, alloying and conversion [5]. Intercalation involves inserting sodium ions into a host material without significant structural changes, typically seen in crystalline compounds. Although sodium ions are larger than lithium ions, causing more strain, intercalation generally results in minimal volume changes. Alloy-type anode materials, generally have high-capacity ~1000 mAh g^{-1}, can be further divided into topotactic and addition reactions. Topotactic alloying involves a solid-solution reaction with no phase changes, while addition reactions involve phase transformations. A major challenge with alloying is managing the substantial volume changes, which can lead to material degradation and poor cycling stability. Conversion-type anodes undergo large volume expansions and significant voltage hysteresis, impacting energy efficiency. However, conversion reactions can achieve very high gravimetric capacities due to their ability to exchange more than one electron per mole of host material [13, 14].

4. Electrode materials and electrolytes

4.1 Anode Materials

4.1.1 Hard Carbon

Hard carbon materials are currently the most popular choice for anodes in SIBs. These materials are derived from oxygen-rich precursors and cannot be converted into graphite, no matter the carbonization temperature. Hard carbons are characterized by a mixture of randomly oriented graphitic domains and disordered carbon regions, resulting in a complex structure with varying interlayer spacing and pore sizes. Although the exact structure of hard carbon remains elusive due to variability in precursor and carbonization conditions, it is known to provide pathways for sodium ion diffusion and storage. One of the primary challenges facing hard carbons is improving their storage capacity to match or exceed that of graphite in LIBs, which is over 372 mAh/g.

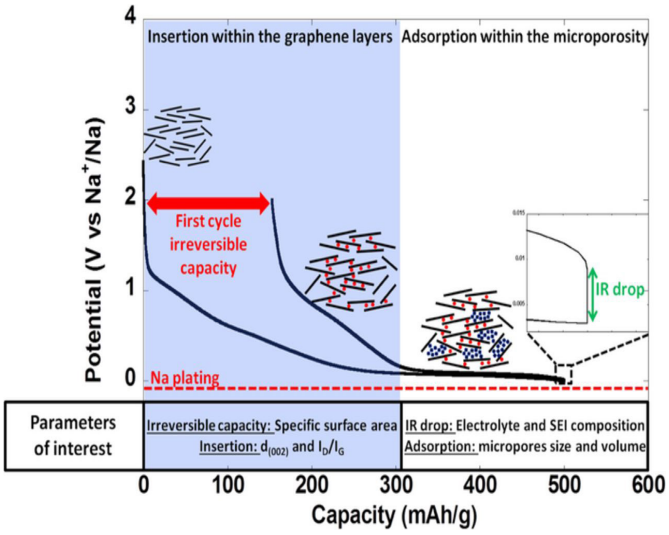

Figure 2. Na^+ storage mechanism into the hard carbon [Reproduced with permission of ref. 15, copyright 2024 IOP Publishing].

Current practical capacities for hard carbons vary from 200 to 450 mAh/g. The complexity of hard carbons, due to their heterogeneous nature and unknown storage mechanisms, complicates the accurate determination of their theoretical energy density. Hard carbon, a non-graphitizable carbon, is synthesized by pyrolyzing carbon-rich precursors such as biomass, lignin, glucose and other organic materials under an inert atmosphere (typically Ar or N_2) at high temperatures, usually around 1000°C. Theories regarding sodium storage mechanisms are evolving, with several models proposed, including intercalation-filling, adsorption-intercalation, adsorption-filling, and three-stage models. New evidence suggests simultaneous adsorption and intercalation during sodiation, with nano-pore filling occurring later. As Figure 2 illustrates, three steps are involved in the Na^+ storage process into the hard carbon: (i) Firstly, Na^+ ions adsorb at defective sites in the slope-voltage region, (ii) Then, Na^+ ions intercalate in the hard carbon lattice, and (iii) Finally, Na^+ ion adsorb at the pore surface in the plateau region.[15] Additionally, recently published articles on hard carbons and theirelectrochemical performance is summarized in Table 2.

Table 2. Summary of electrochemical performance of recently published hard carbons

Materials	Potential Range	ICE	Reversible Capacity	Capacity Retention	Ref.
Cellulose-derived hard carbon	0.0-3.0 V	87.1%	343.3 mAh g^{-1} at 20 mA g^{-1}	86.4% (1000 cycles)	[16]
Nanocrystalline cellulose-derived hard carbon	0.0-2.5 V	90.4%	314 mAh g^{-1} at 0.1 C	87% (100 cycles)	[17]
Phenolic resin-derived hard carbon	0.0-2.5 V	73.6%	304 mAh g^{-1} at 30 mA g^{-1}	87.2% (100 cycles)	[18]
Oxidized cork-derived hard carbon nanosheets	0.0-2.5 V	88%	276 mAh g^{-1} at 20 mA g^{-1}	95% (100 cycles)	[19]
Egg shell membranes-derived hard carbon	0.0-3.0 V	89%	310 mAh g^{-1} at 20 mA g^{-1}	99% (250 cycles)	[20]
Cotton-derived hard carbon	0.01-3.0 V	95%	343 mAh g^{-1} at 20 mA g^{-1}	93.5% (100 cycles)	[21]
Phenolic resin-derived hard carbon	0.0-2.0 V	90.4%	343 mA h g^{-1} at 30 mA g^{-1}	90% (150 cycles)	[22]
Hollow tremella-like carbon sphere	0.0-3.0 V	86%	278 mAh g^{-1} at 100 mA g^{-1}	80.2% (1000 cycles)	[23]
Paper towels-derived hard carbon	0.0-2.0 V	92.05%	336 mAh g^{-1} at 20 mA g^{-1}	95.8% (200 cycles)	[24]
Sucrose and phenolic resin mixture-derived hard carbon	0.0–2.0 V	87%	319 mAh g^{-1} at 100 mA g^{-1}	90% (150 cycles)	[25]
Lignin/epoxy resin-derived hard carbon	0.0-2.0 V	82%	316 mAh g^{-1} at 30 mA g^{-1}	90% (150 cycles)	[26]
Paper towels-derived hard carbon	0.0-2.0 V	94.1%	293.2 mAh g^{-1} at 20 mA g^{-1}	99% (100 cycles)	[27]
Cellulose bitumen-derived hard carbon	0.0-3.0 V	92.7%	241 mAh g^{-1} at 50 mA g^{-1}	92.3% (100 cycles)	[28]
Hard carbon@graphene carbon microspheres	0.0-3.0 V	80.1%	343 mAh g^{-1} at 25 mA g^{-1}	87.2 % (200 cycles)	[29]
Hard carbon microspheres	0.0-2.0 V	86.1%	361 mAh g^{-1} at 20 mA g^{-1}	93.4% (100 cycles)	[30]
Camphor wood residues-derived hard carbon	0.0-2.0 V	82.8%	324.6 mAh g^{-1} at 20 mA g^{-1}	90% (200 cycles)	[31]
Sucrose and phenol formaldehyde resin-derived hard carbon	0.01-2.0 V	85%	310 mAh g^{-1} at 20 mA g^{-1}	93% (100 cycles)	[32]
Hazelnut shell-derived hard carbon	0.0-2.5 V	91%	342 mAh g^{-1} at 20 mA g^{-1}	91% (100 cycles)	[33]
Bamboo-derived hard carbon	0.0-2.5 V	84.1%	348.5 mAh g^{-1} at 30 mA g^{-1}	91.6% (500 cycles)	[34]
Glucose-derived hard carbon	0.0-2.5 V	88%	478 mAh g^{-1} at 25 mA g^{-1}	90% (35 cycles)	[35]

4.1.2 Titanium-based oxides

Titanium-based oxides are promising anode materials for SIBs due to their low cost, ease of processing, and non-toxic nature. They offer safety advantages over carbon-based anodes by operating at higher voltages, thus preventing metallic sodium plating. Key titanium-based oxides include TiO_2, $Na_2Ti_6O_{13}$, and $Na_2Ti_3O_7$. TiO_2, particularly in its nanoscale form, exhibits practical capacities around 155 mAh/g, with anatase being the preferred polymorph [36, 37]. $Li_4Ti_5O_{12}$, known for its zero-strain behavior, provides a reversible capacity of 155 mAh/g. $Na_2Ti_6O_{13}$ features high Na^+ ion diffusion and minimal volume change but has a lower capacity of 49.5 mAh/g [38]. $Na_2Ti_3O_7$ offers the highest energy density in this group, with a specific capacity of 177 mAh/g, but the major challenges for titanium-based oxides, particularly $Na_2Ti_3O_7$, include poor electronic conductivity and sluggish Na^+ ion (de)insertion kinetics, leading to reduced rate performance and cycling stability. $Na_2Ti_3O_7$'s bandgap energy of approximately 3.7 eV makes it an electrical insulator, significantly hindering Na^+ diffusion. Additionally, issues like low initial coulombic efficiency (ICE) and unstable SEI layers further impact performance. Strategies to improve performance include enhancing long-term cycling stability through bulk and surface structural modifications, nanostructuring, and composite fabrication with carbon [38, 39].

4.1.3 Transition metal dichalcogenides

2D transition metal dichalcogenides (TMDs), such as MoS_2, are emerging as promising anode materials for SIBs. Their large interlayer spacings (~6.15 Å for MoS_2), high conductivity (~10^{-3} to 10^{-5} S cm^{-1} for MoS_2) and mechanical flexibility make them well-suited for accommodating the volume expansion that occurs during cycling. TMDs offer high theoretical capacities, like the 670 mAh g^{-1} of MoS_2 [40] and their ability to restack as exfoliated nanosheets enhances structural stability and facilitates efficient Na^+ diffusion. Despite their potential, TMDs face significant challenges. Understanding their charge-storage mechanisms is complex due to phase transitions that occur upon Na^+ intercalation, such as the transformation from semiconducting 2H-MoS_2 to metallic 1T-MoS_2. This phase change, along with structural distortions and lattice modulation, affects performance. Additionally, the formation and behavior of the SEI on TMD anodes remain poorly understood, impacting their overall efficiency and lifespan [41]. To address these challenges, researchers have explored strategies such as incorporating high-conductivity carbon additives (e.g., graphene, carbon nanotubes) to enhance electronic transport and designing novel nanoarchitectures (e.g., hollow structures, heterostructures) to accommodate volume changes and improve structural integrity during cycling [40-41].

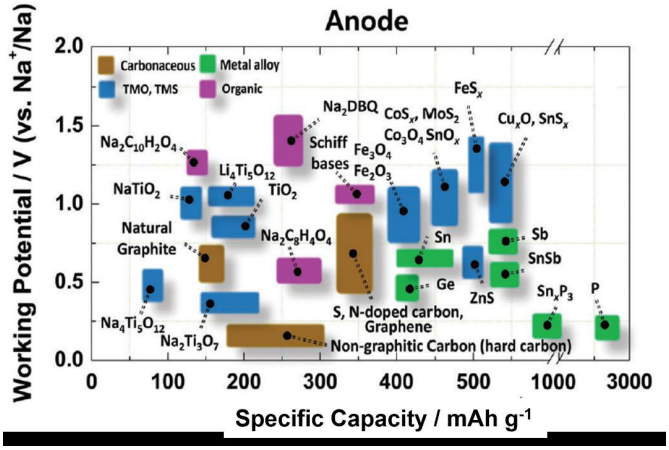

Figure 3: Recent research progress in SIBs Anode; (Reproduced with permission from ref [5]).

4.1.4 Organic electrode materials

Organic electrode materials (OEMs) are gaining attention in rechargeable battery technology due to their potential for sustainability and use of bio-derived or recycled components. Recent research has focused on small redox-active organic molecules, such as disodium terephthalate ($Na_2C_8O_4H_4$), for use in SIBs [42]. These organic systems offer structural diversity and modifiable electronic properties, making them attractive for battery applications. Redox reactions typically involve changes in π-bonds or charge stabilization mechanisms, with functional groups like carboxylates, azo, and imine being explored for their electrochemical performance. Organic anode materials face several challenges, including lower theoretical capacities due to limited redox-active sites

and issues with cycling stability. Organic electrolytes can form inactive side products or lead to solubility problems, reducing coulombic efficiency and complicating practical applications. Additionally, OEMs often have low density and poor electronic conductivity, requiring additives like conductive carbon. The capacity and working potential of various organic groups, such as carbonyl, imine, and azo bonds, also impact overall energy density. Understanding these materials' activity and addressing production costs, scalability, and stability remain critical areas for improvement [43]. These challenges are being tackled using various strategies such as polymerizing small organic molecules or embedding them into covalent organic frameworks (COFs) reduces solubility and enhances structural integrity. Modifying functional groups can stabilize redox activity and optimize voltage. Forming composites with conductive materials like carbon nanotubes improves electron transport, while using solid or gel electrolytes helps prevent material dissolution. These approaches collectively enhance the performance and durability of organic anode materials in sodium-ion batteries [42-43]. Figure 3 provides an overview of the latest advancements in research on anode for SIBs.

4.1.5 Alloy Materials

Alloy materials can store many Na^+ ions in the host structure with a relatively low operating potential (below 1.0 V). Numerous studies have been conducted on metals (Sn, Bi), metalloids (Si, Ge, As, Sb), and polyatomic nonmetal compounds (P) as possible anode materials for SIBs [5, 44]. However, the alloying and dealloying reactions involve a significant number of Na^+ ions, causing the host material to experience substantial volume changes. The repeated volume changes, constrained by the battery casing, create complex mechanical stresses within the active particles, which can eventually result in their fracture or breakdown. Extensive experimental studies on the electrochemical and mechanical behavior of these alloys during Na+ interactions have led to the exploration of optimized architectures and improved electrode designs. Here in this review, we are particularly focusing on the Phosphorous (P) and Tin (Sn) as follows.

Phosphorous (P): Phosphorus, a group 15 nonmetal, has three primary allotropes: white, red, and black. Among these, red phosphorus is relatively stable and may exist in both amorphous and crystalline states. Its potential as an anode material for SIBs with a three-electron redox reaction allowed for a high theoretical capacity of around 2600 mAh g^{-1} [44]. More recently, phosphorus-carbon composites have been investigated to improve their electrochemical performance. However, a key difficulty with phosphorus electrodes is the creation of Na_3P during sodiation, which can emit poisonous and combustible phosphine (PH_3) when exposed to moisture. Despite this constraint, phosphorus electrodes have a lower volume expansion during sodiation than other Na-based alloys. The partial covalent feature of Na_3P reduces sodium's apparent molar volume to 77% and 59% when compared to Na-metal alloys and metallic Na, respectively **[5].** However, a key concern with phosphorus anodes is the breakdown of the electrolyte at the extremely reactive surface of Na_3P. This negatively impacts cycle life. To improve the reversibility of sodium phosphide formation, non-fluorinated binders such as sodium polyacrylate (PANa) and sodium carboxymethyl cellulose (CMCNa), as well as electrolyte additives such as fluoroethylene carbonate (FEC), have been successfully used to improve electrode stability and battery lifespan [5].

Tin (Sn): Sn has been considered as one of the most capable anode materials owing to its high theoretical capacity of 847 mA h g^{-1}, corresponding to the the full sodiation state of $Na_{15}Sn_4$. Based on the theoretical calculations and experiments, there are many reports on multi-stage sodiation of Sn progressed as: $Sn \rightarrow NaSn_5 \rightarrow NaSn \rightarrow Na_9Sn_4 \rightarrow Na_{15}Sn_4$.[5, 45] Sn alloys with elements like silicon, antimony, or iron, if alloyed, can further complement the overall performance by improving the energy density of the battery. However, a few challenges still exist, including the high-volume expansion (up to 300%) during sodiation process, inducing intense mechanical stress that results in electrode cracking, pulverization and eventually capacity decline.[14] To overcome these problems, researchers have been working on several solutions including nanostructuring

Sn to counteract volume expansion effects, as smaller particles are better able to accommodate volume changes and enhancing conductivity by incorporating carbon-based materials such as graphite, graphene, or carbon nanotubes. In addition, hybrid materials that incorporate Sn with more stable elements such as antimony or iron are being created to achieve high capacity in balance with improved structural stability and longer cycling life. Optimization of the electrolyte, such as the creation of more stable SEI layers and enhanced ionic conductivity, also promises to improve the long-term performance of Sn-based anodes. Also, pre-sodiation methods might assist in reducing the initial volume expansion and enhancing the initial cycling efficiency [44]. With future developments in nanotechnology, material hybridization, and electrolyte engineering, Sn alloy anodes will be a central element in the formulation of high-performance, cost-saving, and eco-friendly sodium-ion batteries as a promising alternative to lithium-ion technology [5].

4.2 Cathode Materials

4.2.1 Layered transition Metal Oxides

In transition metal oxides ($Na_{1-x}MO_2$), mainly O3 type and P2 type materials explored as cathodes for SIBs. These crystal structures consist of edge-sharing MO_6 octahedral layers inserted between Na^+ ion layers. The number (O3 and P2) stands for the packing number of Na^+ ion octahedral or prismatic layers in each unit cell. The prime symbol (') denotes monoclinic distortion, so O'3 and P'2 symbolize monoclinic distortion of the O3 and P2 phases, respectively. The electrochemical de-/sodiation of the O3 structure proceeds with reversible structural transformation of O3 ↔ O'3 ↔ P3 ↔ P'3 [5, 46]. When Na^+ ions are partially extracted from the crystal structure, they tend to prefer a prismatic environment. This extraction causes the oxygen to be repelled from the Na layers, resulting in an increase in interlayer distance. Consequently, Na^+ diffusion occurs more rapidly in the P'3 phase due to its larger interlayer spacing compared to O3. These phase transitions are accompanied by the sliding of the MO_2 slab without the breaking of M–O bonds. In contrast, the P2 structure is stable when the Na content is between 0.3 and 0.7 in $Na_{1-x}MO2$, with the average oxidation state of M exceeding +3.3 [51-53]. Also, vacancies in the structure lead to a significant repulsion of oxygen from the Na layers, causing an increase in the interlayer distance. As a result, Na^+ ions occupy prismatic (P) sites due to the larger ionic radius of Na^+ ion [47, 54, 55]. Moreover, a major challenge lies in understanding and managing the structural complexities of both P2 and O3 materials during cycling, as these can influence the performance and longevity of the materials. Current issues involve characterizing the atomic, nano-, and meso-structural changes over many cycles and the effects of subtle substitutions on performance. Additionally, balancing power and capacity optimally remains a challenge. P2 materials offer high power performance, while O3 materials provide better capacity. Developing hybrid P2|O3 materials to meet diverse application requirements and addressing the commercial and technical issues related to these challenges are ongoing concerns [46, 56]. Table 3 summarizes the recent developments in electrochemical performance of potential cathodes for SIBs.

4.2.2 Anion redox layered transition-metal oxides

Oxygen redox reactions in SIBs have gained attention for their potential to provide higher capacity (~250–300 mAh g^{-1}) at elevated voltages (above 4.0 V) compared to traditional transition-metal redox reactions [47]. These reactions involve the overlap of M–O and (M–O)* orbitals, enabling oxygen ion electron removal [57-58]. While initial studies used expensive 4d and 5d metals, current research has shifted to more affordable 3d metals like manganese, often doped to enhance performance. Oxygen redox reactions face issues with reversibility and large hysteresis, caused by structural transformations and cation migration during cycling. High-voltage operation can lead to lattice oxygen loss and electrolyte instability. Techniques to distinguish bulk and surface phenomena in redox activity are limited, complicating the understanding of these processes [58].

4.2.3 Polyatomic anion-based materials

Polyatomic anion insertion compounds offer diverse structural chemistries, enhancing stability and enabling higher operating voltages (above 3.5 V vs. Na^+/Na). Notable examples include vanadium-containing phosphates and fluoride phosphates, such as NASICON $Na_3V_2(PO_4)_3$[59-61], $Na_3V_2(PO_4)_2F_3$[62] and $NaVPO_4F$ [63-66] which provide high ion mobility and tunable voltages. New developments like $Na_3V_2(PO_4)_2FO_2$[67] demonstrate increased energy density by accommodating additional sodium ions. Challenges include controlling polymorphic phases, which affect ionic conductivity and voltage stability. Research is needed to optimize reaction conditions and explore dopants to achieve higher redox potentials. Additionally, replacing expensive vanadium with cheaper alternatives, and addressing sluggish diffusion kinetics in new materials like $NaFeSO_4F$, are ongoing issues [68].

4.2.4 Prussian blue and analogues

Prussian blue analogues (PBAs), with the formula $Na_xM[M'(CN)_6]_{1-y}.zG$, are promising Na-ion battery cathodes due to their low cost, abundant elements, and high porosity. Despite significant progress, challenges remain in achieving high capacity and stability. PBAs show potential with capacities up to 120 mAh g^{-1} for 800 cycles using aqueous electrolytes, though non-aqueous electrolytes can offer higher capacities [69, 70].

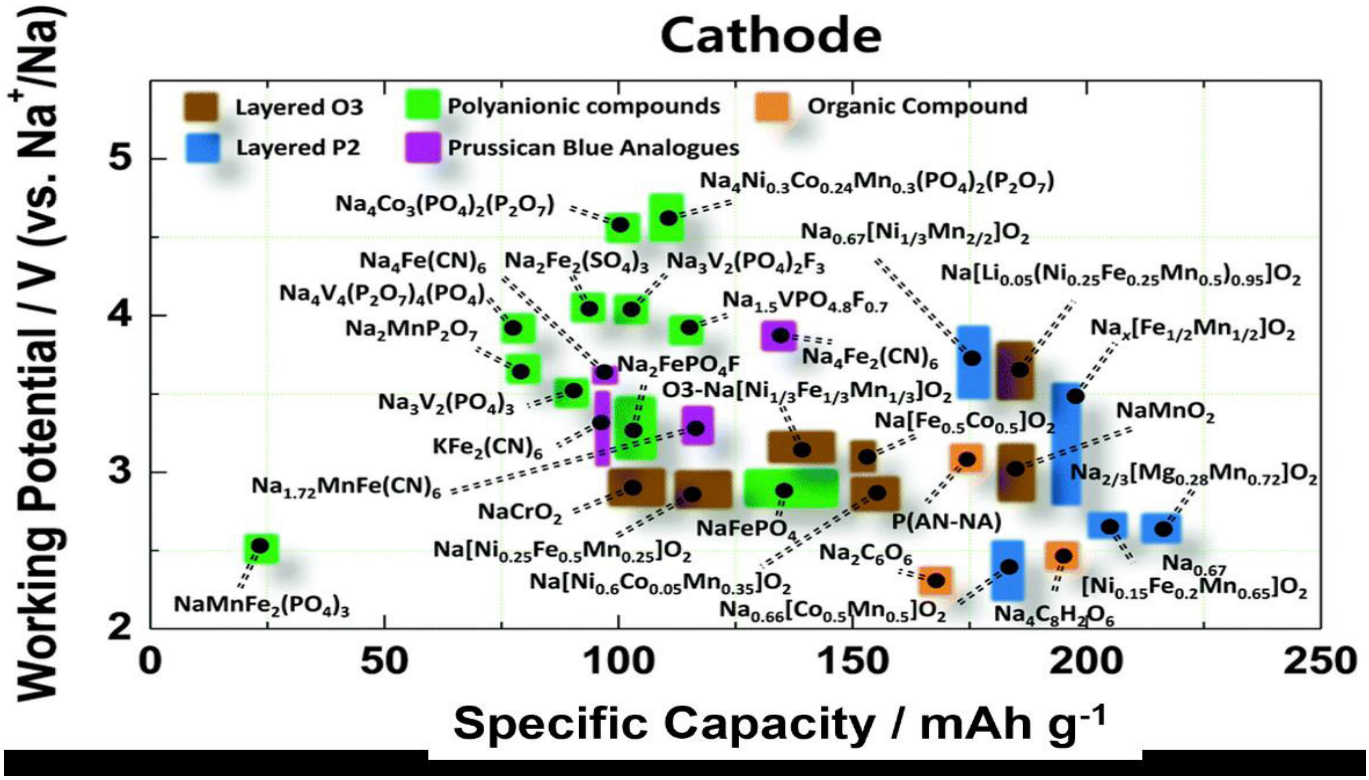

Figure 4: Recent research progress in SIBs cathode (Reproduced with permission of ref [5]).

The primary issue is maintaining structural stability and high capacity during cycling. PBAs face issues with moisture sensitivity and limited reversibility, particularly when cycling more than one sodium ion per formula unit. High vacancy concentrations from synthesis and the presence of water lead to reduced structural stability and capacity fading. Challenges include improving electronic conductivity and preventing phase transitions due to water content. The complexity of electrolyte interactions adds to the difficulty of optimizing PBAs for long-term use [71-73]. Figure 4 provides an overview of the advancements in research on cathodes for SIBs.

Table 3. Summary of electrochemical performance of developing cathodes for SIBs.

Materials	Voltage Range	Reversible Capacity	Capacity Retention	Ref.
$Na_{0.7}CoO_2$	2.0-3.8 V	125 mA h g^{-1} at 5 mA g^{-1}	86% (100 cycles)	[50]
$Na_{2/3}Ni_{1/6}Mn_{2/3}Cu_{1/9}Mg_{1/18}O_2$	2.5-4.15 V	87.9 mA h g^{-1} at 0.5C	81.4% (500 cycles)	[51]
$Na_{0.76}Cu_{0.22}Fe_{0.30}Mn_{0.48}O_2$	2.0-4.0 V	125.5 mA h g^{-1} at 0.1C	79% (300 cycles)	[52]
$Na_{2/3}Fe_{1/2}Mn_{1/2}O_2$	1.5-4.0 V	126.3 mA h g^{-1} at 13 mA g^{-1}	75.6% (30 cycles)	[47]
$Na_{2/3}Fe_{0.2}Mn_{0.8}O_2$	1.5-4.2 V	189.81 mA h g^{-1} at 0.1C	72% (50 cycles)	[48]
$Na_{0.78}Ni_{0.23}Mn_{0.69}O_2$	2.0-4.5 V	138 mA h g^{-1} at 0.1C	90% (20 cycles)	[49]
$Na_{2/3}[Mn_{0.7}Zn_{0.3}]O_2$	1.5-4.6 V	190 mA h g^{-1} at 0.1C	80% (200 cycles)	[53]
$Na_{0.55}[Ni_{0.1}Fe_{0.1}Mn_{0.8}]O_2$	1.5-4.3 V	221.5 mA h g^{-1} at 12 mA g^{-1}	75% (100 cycles)	[54]
$Na_{0.44}MnO_2$	1.5-4.0 V	118 mA h g^{-1} at 50 mA g^{-1}	67.8% (140 cycles)	[55]
$Na_{0.44}MnO_2$	2.0-4.0 V	119 mA h g^{-1} at 0.2C	63% (60 cycles)	[56]
$NaFePO_4$	1.5-4.5 V	101.4 mA h g^{-1} at 20 mA g^{-1}	90.6% (250 cycles)	[57]
$NaFePO_4$	2.0-4.5 V	158.5 mA h g^{-1} at 0.1 C	93.4% (5000 cycles)	[58]
$Na_3V_2(PO_4)_3$	2.5-4.0 V	114.5 mA h g^{-1} at 0.1 C	98.2% (2650 cycles)	[59]
$Na_3V_2(PO_4)_3$	2.4-3.8 V	104.7 mA h g^{-1} at 0.1 C	93.12% (500 cycles)	[60]
$Na_3V_2(PO_4)_3$	2.5-4.1 V	115 mA h g^{-1} at 0.1 C	95% (100 cycles)	[61]
$NaVPO_4F$	2.5-4.0 V	133.8 mA h g^{-1} at 0.2 C	94.5% (100 cycles)	[63]
$NaVPO_4F$	2.0-4.3 V	134.1 mA h g^{-1} at 0.1 C	95.1% (100 cycles)	[64]
$NaVPO_4F$	2.0-4.3 V	123.1 mA h g^{-1} at 0.1 C	87.7% (100 cycles)	[65]
$NaVPO_4F$	2.4-4.0 V	120 mA h g^{-1} at 0.1 C	97% (300 cycles)	[66]
$Na_{2-x}FeFe(CN)_6$	2.0-3.8 V	85 mA h g^{-1} at 1 C	98.9% (500 cycles)	[72]
$FeFe(CN)_6$	2.0-4.3 V	110 mA h g^{-1} at 50 mA g^{-1}	ca 64.8% (100 cycles)	[73]

4.3 Electrolytes

4.3.1 Organic electrolytes

The development of organic electrolytes for SIBs closely mirrors the advancements in LIBs, driven by similar operational needs such as high ionic conductivity, low viscosity, and stability across diverse conditions [74]. Essential characteristics include the ability to dissolve salts effectively to facilitate ion transport, as well as high thermal and chemical stability to accommodate various climates and electrode materials. Cost-effectiveness also remains a critical factor, making solvents like linear and cyclic carbonates (e.g., dimethyl carbonate (DMC), ethylene carbonate (EC), and propylene carbonate (PC) and ethers (e.g., diglyme) prominent choices [75-77]. Despite the parallels with LIB technology, SIBs face unique challenges. Linear carbonates, while useful in LIBs for adjusting viscosity and melting points, create unstable SEI layers in SIBs due to their reactions with sodium [78]. Additionally, the use of graphite, common in LIBs, is not feasible for SIBs because it cannot intercalate sodium ions. This necessitates the frequent use of solvents like PC, which are unsuitable for LIBs due to solvent co-interactions with graphite. Sodium salts

interact differently with solvents compared to lithium salts, impacting desolvation dynamics and performance [79].

4.3.2 Ionic liquids

Ionic liquids (ILs) have emerged as a promising alternative electrolyte for SIBs due to their unique properties. ILs are molten salts that are non-flammable and possess a wide electrochemical stability window. These characteristics make them safer compared to traditional organic electrolytes and capable of operating over a broad temperature range [80-83]. Additionally, ILs tend to form a more uniform and stable SEI layer, which is crucial for maintaining battery performance and longevity. This stability helps reduce the corrosion of aluminum current collectors, a common issue with organic solvents. However, the use of ILs in SIBs is not without challenges. One major drawback is their relatively high cost and the complexity of their purification processes. Furthermore, ILs, particularly those based on imidazolium and pyrrolidinium, are hygroscopic, which can introduce complications in battery performance [84-88]. Another issue is the higher viscosity and lower ionic conductivity of ILs compared to conventional organic electrolytes, which can affect the battery's efficiency, especially at room temperature.

4.3.3 Solid and Gel-Type Polymer Electrolytes

Solid and gel polymer electrolytes (SPEs and GPEs) are key components in advancing SIBs due to their potential to enhance battery safety and performance. SPEs, also known as dry solid polymer electrolytes, consist of a polymer matrix that dissolves salt ions, providing mechanical strength. However, the ionic conductivity of traditional SPEs is generally low, ranging from 10^{-2} to 10^{-4} mS cm^{-1} at ambient temperatures, making them less practical for many applications [89, 90]. To address the low conductivity issue, GPEs incorporate a significant amount of liquid electrolytes. These liquid components act as solvents and plasticizers, enhancing the ionic conductivity of the polymer matrix. While GPEs can achieve higher ionic conductivity compared to SPEs, this improvement comes at the expense of mechanical strength and electrochemical stability. In the realm of SIBs, research on gel polymer electrolytes has been more limited. However, studies on PEO-NaTFSI-based SPEs have shown high ionic conductivities, around 1 mS cm^{-1} at 70 °C. Despite these promising results, the relatively modest Na^+ transference number (0.4-0.5) and the need for high operating temperatures pose challenges for sodium-metal based rechargeable batteries, particularly given sodium's low melting point of 97.7 °C [91].

5. Industrial Status and Targets

SIBs are gaining traction as an alternative to LIBs, particularly in stationary energy storage applications. Major players in the industry (as shown in Table 4), such as Faradion, CATL and Natron Energy, are advancing SIB technology for grid storage, renewable energy integration, and backup power solutions [92-96]. These companies have moved from pilot projects to larger-scale commercial deployments, demonstrating the practical viability of SIBs. Current SIBs typically offer specific energies in the range of 100-150 Wh/kg. While this figure is lower than those of LIBs, they are competitive for many stationary applications where high energy density is less critical than cost and safety. The cost of SIBs is currently around $100-$150 per kWh [94] which could significantly reduce over period of time. This cost advantage is particularly appealing for large-scale energy storage solutions. SIBs are being deployed in various pilot projects and early-stage commercial applications. They are increasingly used in grid-scale energy storage, industrial backup power systems, and off-grid renewable energy storage. The technology is also being explored for applications in electric vehicles, although it is still in the early stages compared to LIBs.

Table 4. Current industry players and their future targets:

Company	Cathode	Anode	Cell Form Factor	Current Achievements	Future Targets
Faradion	Prussian Blue or layered oxide	Hard carbon	Pouch cells	140 Wh/kg 204 Wh/L	- Increase energy density to 200 Wh/kg - Reduce cost to $50-$80/kWh - Enhance cycle life to 5,000 cycles
CATL	Layered oxide or polyanionic	Hard carbon	Cylindrical and pouch cells	100-150 Wh/kg	- Achieve energy density of 200 Wh/kg - Lower cost - Improve cycle life and reliability
Natron Energy	Prussian Blue	Hard carbon	Prismatic cells	100-150 Wh/kg	- Increase energy density - Enhance cycle life - Expand application scope
HiNa	Layered oxide	Hard carbon	Pouch cells	120-160 Wh/kg	- Achieve higher energy density - Expand market presence - Enhance cost-efficiency
Northvolt	Prussian White	Hard carbon	Pouch and Prismatic	160 Wh/kg	- Scale up production - Expand market presence - Cost reduction

6. Conclusions and Perspectives

The progress towards the commercialization of SIBs has been substantial, marked by significant advancements in both anode and cathode materials. The discovery of hard carbon as a functional anode material has established it as a leading choice, given its current prominence among the limited options available. Capacities of HCs can be further improved by compositing them with alloy type Sn and P anodes. On the cathode side, a variety of promising materials have emerged, including NASICON structures, layered oxides, and Prussian blue analogs. Tailoring elemental compositions, nanosizing, and carbon coating have proven effective strategies for improving redox potentials, rate capability, and cycle life.

For India, this potential is particularly compelling given the country's abundant sodium resources, as sodium is the sixth most abundant element in the Earth's crust and the need for scalable, economical energy storage solutions to support its growing renewable energy sector. By leveraging sodium-ion technology, India could enhance its energy security, reduce costs, and promote local manufacturing and innovation. However, in order to achieve this, more research and development funding will be needed, together with smart government policy support to promote a strong local sector. Embracing SIBs could not only address critical energy challenges but also position India as a leader in the next generation of energy storage technologies.

References:

[1]A. Nekahi, A. K. MR, X. Li, S. Deng, K. Zaghib, Sustainable $LiFePO_4$ and $LiMn_xFe_{1-x}PO_4$ (x= 0.1–1) cathode materials for lithium-ion batteries: A systematic review from mine to chassis, Mater. Sci. Eng. R Rep. 159 (2024) 100797. https://doi.org/10.1016/j.mser.2024.100797

[2]J. M. Tarascon, M. Armand, Issues and challenges facing rechargeable lithium batteries, Nature 414 (2001) 359-367. https://doi.org/10.1038/35104644

[3]M. M. Thackeray, C. Wolverton, E. D. Isaacs, Electrical energy storage for transportation—approaching the limits of, and going beyond, lithium-ion batteries, Energy Environ. Sci. 5 (2012) 7854-7863. 10.1039/C2EE21892E

[4]L. Yang, W. Deng, W. Xu, Y. Tian, A. Wang, B. Wang, G. Zou, H. Hou, W. Deng, X. Ji, Olivine $LiMn_xFe_{1-x}PO_4$ cathode materials for lithium ion batteries: restricted factors of rate performances, J. Mater. Chem. A 9 (2021) 14214-14232. 10.1039/D1TA01526E

[5]J. Y. Hwang, S. T. Myung, Y. K. Sun, Sodium-ion batteries: present and future, Chem. Soc. Rev. 46 (2017) 3529-3614. 10.1039/C6CS00776G

[6]Y. Li, Q. Zhou, S. Weng, F. Ding, X. Qi, J. Lu, Y. Li, X. Zhang, X. Rong, Y. Lu, X. Wang, R. Xiao, H. Li, X. Huang, L. Chen, Y. S. Hu, Interfacial engineering to achieve an energy density of over 200 Wh kg^{-1} in sodium batteries, Nature Energy 7 (2022) 511-519. https://doi.org/10.1038/s41560-022-01033-6

[7]L. J. Hounjet, Comparing lithium-and sodium-ion batteries for their applicability within energy storage systems, Energy Storage 4 (2022) 309. https://doi.org/10.1002/est2.309

[8]J. Deng, W.B. Luo, S.L. Chou, H.K. Liu, S.X. Dou, Sodium-ion batteries: from academic research to practical commercialization, Adv. Energy Mater. 8 (2018) 1701428. https://doi.org/10.1002/aenm.201701428

[9]A. Rudola, A. J. Rennie, R. Heap, S. S. Meysami, A. Lowbridge, F. Mazzali, R. Sayers, C.J. Wright, J. Barker, Commercialisation of high energy density sodium-ion batteries: Faradion's journey and outlook, J. Mater. Chem. A, 9 (2021) 8279-8302. 10.1039/D1TA00376C

[10]C. Y. Huang, T. R. Kuo, S. Yougbaré, L. Y. Lin, Design of $LiFePO_4$ and porous carbon composites with excellent High-Rate charging performance for Lithium-Ion secondary battery, J. Colloid Interface Sci. 607 (2022) 1457-1465. https://doi.org/10.1016/j.jcis.2021.09.118Get rights and content

[11]C. Vaalma, D. Buchholz, M. Weil, S. Passerini, A cost and resource analysis of sodium-ion batteries, Nature Rev. Mater. 3 (2018) 1-11. https://doi.org/10.1038/natrevmats.2018.13

[12]Z. Yang, J. He, W. H. Lai, J. Peng, X. H. Liu, X. X. He, X. F. Guo, L. Li, Y. Qiao, J. M. Ma, M. Wu, S. L. Chou, Fire-retardant, stable-cycling and high-safety sodium ion battery, Angew. Chem. 133 (2021) 27292-27300. https://doi.org/10.1002/ange.202112382

[13]S. Qiao, Q. Zhou, M. Ma, H. K. Liu, S. X. Dou, S. Chong, Advanced anode materials for rechargeable sodium-ion batteries, ACS Nano 17 (2023) 11220-11252. https://doi.org/10.1021/acsnano.3c02892

[14]S. M. Zheng, Y. R. Tian, Y. X. Liu, S. Wang, C. Q. Hu, B. Wang, K. M. Wang, Alloy anodes for sodium-ion batteries, Rare Metals 40 (2021) 272-289. https://doi.org/10.1007/s12598-020-01605-z

[15]E. Irisarri, A. Ponrouch, M. R. Palacin, Review-Hard Carbon Negative Electrode Materials for Sodium-Ion Batteries, J. Electrochem. Soc. 162 (2015) A2476. 10.1149/2.0091514jes

[16]X. S. Wu, X. L. Dong, B. Y. Wang, J. L. Xia, W. C. Li, Revealing the sodium storage behavior of biomass-derived hard carbon by using pure lignin and cellulose as model precursors, Renew. Energ. 189 (2022) 630. https://doi.org/10.1016/j.renene.2022.03.023

[17]F. Xie, Z. Xu, Z. Guo, A. C. S. Jensen, J. Feng, H. Luo, F. Ding, Y. Lu, Y. S. Hu, M. M. Titirici, Achieving high initial Coulombic efficiency for competent Na storage by microstructure tailoring from chiral nematic nanocrystalline cellulose**,** Carbon Energy 4 (2022) 914. https://doi.org/10.1002/cey2.198

[18]X. Zhang, X. Dong, X. Qiu, Y. Cao, C. Wang, Y. Wang, Y. Xia, Extended low-voltage plateau capacity of hard carbon spheres anode for sodium ion batteries, J. Power Sources 476 (2020) 228550. https://doi.org/10.1016/j.jpowsour.2020.228550

[19]H. D. Asfaw, R. Gond, A. Kotronia, C. W. Tai, R. Younesi, Bio-derived hard carbon nanosheets with high rate sodium-ion storage characteristics, Sustain. Mater. Techno. 32 (2022) e00407. https://doi.org/10.1016/j.susmat.2022.e00407

[20]X. Zhao, Y. Ding, Q. Xu, X. Yu, Y. Liu, H. Shen, Low-Temperature Growth of Hard Carbon with Graphite Crystal for Sodium-Ion Storage with High Initial Coulombic Efficiency: A General Method, Adv. Energy Mater. 9 (2019) 1803648. https://doi.org/10.1002/aenm.201803648

[21]X. Li, J. Sun, W. Zhao, Y. Lai, X. Yu, Y. Liu, Intergrowth of Graphite-Like Crystals in Hard Carbon for Highly Reversible Na-Ion Storage**,** Adv. Funct. Mater. 32 (2022) 2106980. https://doi.org/10.1002/adfm.202106980

[22]H. Zhang, W. Zhang, F. Huang, Graphene inducing graphitization: Towards a hard carbon anode with ultrahigh initial coulombic efficiency for sodium storage, Chem. Eng. J. 434 (2022) 134503. https://doi.org/10.1016/j.cej.2022.134503

[23]W. Zhong, D. Cheng, M. Zhang, H. Zuo, L. Miao, Z. Li, G. Qiu, A. Cheng, H. Zhang, Boosting ultrafast and durable sodium storage of hard carbon electrode with graphite nanoribbons, Carbon 198 (2022) 278. https://doi.org/10.1016/j.carbon.2022.07.033

[24]J. Zhao, X. X. He, W. H. Lai, Z. Yang, X. H. Liu, L. Li, Y. Qiao, Y. Xiao, L. Li, X. Wu, S. L. Chou, Catalytic Defect-Repairing Using Manganese Ions for Hard Carbon Anode with High-Capacity and High-Initial-Coulombic-Efficiency in Sodium-Ion Batteries, Adv. Energy Mater. 13 (2023) 2300444. https://doi.org/10.1002/aenm.202300444

[25]H. Zhang, H. Ming, W. Zhang, G. Cao, Y. Yang, Coupled Carbonization Strategy toward Advanced Hard Carbon for High-Energy Sodium-Ion Battery, ACS Appl. Mater. Interface 9 (2017) 23766. https://doi.org/10.1021/acsami.7b05687

[26]H. Zhang, W. Zhang, H. Ming, J. Pang, H. Zhang, G. Cao, Y. Yang, Design advanced carbon materials from lignin-based interpenetrating polymer networks for high performance sodium-ion batteries, Chem. Eng. J. 341 (2018) 280. https://doi.org/10.1016/j.cej.2018.02.016

[27]X. X. He, J. H. Zhao, W. H. Lai, R. Li, Z. Yang, C. M. Xu, Y. Dai, Y. Gao, X. H. Liu, L. Li, G. Xu, Y. Qiao, S. L. Chou, M. Wu, Soft-Carbon-Coated, Free-Standing, Low-Defect, Hard-Carbon Anode To Achieve a 94% Initial Coulombic Efficiency for Sodium-Ion Batteries, ACS Appl. Mater. Interfaces 13 (2021) 44358. https://doi.org/10.1021/acsami.1c12171

[28]C. Wei, W. Dang, M. Li, X. Ma, M. Li, Y. Zhang, Hard-soft carbon nanocomposite prepared by pyrolyzing biomass and coal waste as sodium-ion batteries anode material, Mater. Lett. 330 (2023) 133368. https://doi.org/10.1016/j.matlet.2022.133368

[29]L. Yan, J. Wang, Q. Ren, L. Fan, B. Liu, L. Zhang, L. He, X. Mei, Z. Shi, In-situ graphene-coated carbon microsphere as high initial coulombic efficiency anode for superior Na/K-ion full cell, Chem. Eng. J. 432 (2022) 133257. https://doi.org/10.1016/j.cej.2021.133257

[30]L. Xiao, H. Lu, Y. Fang, M. L. Sushko, Y. Cao, X. Ai, H. Yang, J. Liu, Low-Defect and Low-Porosity Hard Carbon with High Coulombic Efficiency and High Capacity for Practical Sodium Ion Battery Anode, Adv. Energy Mater. 8 (2018) 1703238. https://doi.org/10.1002/aenm.201703238

[31]S. Guo, Y. Chen, L. Tong, Y. Cao, H. Jiao, Z. Long, X. Qiu, Biomass hard carbon of high initial coulombic efficiency for sodium-ion batteries: Preparation and application, Electrochim. Acta 410 (2022) 140017. https://doi.org/10.1016/j.electacta.2022.140017

[32]D. Sun, B. Luo, H. Wang, Y. Tang, X. Ji, L. Wang, Engineering the trap effect of residual oxygen atoms and defects in hard carbon anode towards high initial Coulombic efficiency, Nano Energy 64 (2019) 103937. https://doi.org/10.1016/j.nanoen.2019.103937

[33]J. Wang, J. Zhao, X. He, Y. Qiao, L. Li, S. L. Chou, Hard carbon derived from hazelnut shell with facile HCl treatment as high-initial-coulombic-efficiency anode for sodium ion batteries, Sustain. Materi. Techno. 33 (2022) e00446. https://doi.org/10.1016/j.susmat.2022.e00446

[34]T. Xu, X. Qiu, X. Zhang, Y. Xia, Regulation of surface oxygen functional groups and pore structure of bamboo-derived hard carbon for enhanced sodium storage performance, Chem. Eng. J. 452 (2023) 139514. https://doi.org/10.1016/j.cej.2022.139514

[35]A. Kamiyama, K. Kubita, D. Igarashi, Y. Youn, Y. Tatayama, H. Ando, K. Gotoh, S. Komaba, MgO-Template Synthesis of Extremely High Capacity Hard Carbon for Na-Ion Battery, Angew. Chem., Int. Ed. 60 (2021) 5114. https://doi.org/10.1002/anie.202013951

[36]S. Chandel, J. Kim, A. K. Rai, Effect of vanadium doping on the electrochemical performances of sodium titanate anode for sodium ion battery application, Dalton Trans. 51 (2022) 11797-11805. 10.1039/D2DT01626E

[37]S. Chandel, S. Lee, S. Lee, S. Kim, S. P. Singh, J. Kim, A. K. Rai, Hierarchically nanorod structured $Na_2Ti_6O_{13}/Na_2Ti_3O_7$ nanocomposite as a superior anode for high-performance sodium ion battery, J. Electroanal. Chem. 877 (2020) 114747. https://doi.org/10.1016/j.jelechem.2020.114747

[38]S. Chandel, C. Wang, S. P. Singh, N. Wang, A. K. Rai, Significant enhancement in the electrochemical performances of a nanostructured sodium titanate anode by molybdenum doping for applications as sodium-ion batteries, ACS Appl. Nano Mater. 5 (2022) 18591-18602. https://doi.org/10.1021/acsanm.2c04386

[39]S. Chandel, J. Singh, J. Kim, A. K. Rai, Reduced graphene oxide (rGO) integrated sodium titanate nanocomposite as a high-rate performance anode material for sodium ion batteries, J. Electroanal. Chem. 939 (2023) 117485. https://doi.org/10.1016/j.jelechem.2023.117485

[40]J. Li, H. Wang, W. Wei, L. Meng, Advanced MoS_2 and graphene heterostructures as high-performance anode for sodium-ion batteries, Nanotechnology 30 (2019) 104003. 10.1088/1361-6528/aaf76c

[41]Y. Zhang, S. Yu, H. Wang, Z. Zhu, Q. Liu, E. Xu, D. Li, G. Tong, Y. Jiang, A novel carbon-decorated hollow flower-like MoS_2 nanostructure wrapped with RGO for enhanced sodium-ion storage, Chem. Eng. J. 343 (2018) 180–188. https://doi.org/10.1016/j.cej.2018.03.003

[42]F. Wan, X. L. Wu, J. Z. Guo, J. Y. Li, J. P. Zhang, L. Niu, R. S. Wang, Nanoeffects promote the electrochemical properties of organic $Na_2C_8H_4O_4$ as anode material for sodium-ion batteries, Nano Energy 13 (2015) 450. https://doi.org/10.1016/j.nanoen.2015.03.017

[43]B. Haupler, A.Wild, U. S. Schubert, Carbonyls: Powerful Organic Materials for Secondary Batteries, Adv. Energy Mater. 5 (2015) 1402034. https://doi.org/10.1002/aenm.201402034

[44]S. M. Zheng, Y. R. Tian, Y. X. Liu, S. Wang, C. Q. Hu, B. Wang, K. M. Wang, Alloy anodes for sodium-ion batteries, Rare Met. 40 (2021) 272–289. https://doi.org/10.1007/s12598-020-01605-z

[45]S. Komaba, Y. Matsuura, T. Ishikawa, N. Yabuuchi, W. Murata, S. Kuze, Redox reaction of Sn-polyacrylate electrodes in aprotic Na cell, Electrochem. Commun. 21 (2012) 65-68. https://doi.org/10.1016/j.elecom.2012.05.017

[46]Y. Gupta, P. Siwatch, R. Karwasra, K. Sharma, S. K. Tripathi, Recent progress of layered structured P2- and O3- type transition metal oxides as cathode material for sodium-ion batteries, Renew. Sustain. Energy Rev. 192 (2024) 114167. https://doi.org/10.1016/j.rser.2023.114167

[47]L. Bai, L. Zhao, C. Wu, H. Li, Y. Li, F. Wu, Enhanced sodium ion storage behavior of P2-type $Na_{2/3}Fe_{1/2}Mn_{1/2}O_2$ synthesized via a chelating agent assisted route, ACS Appl. Mater. Interfaces 8 (2016) 2857-2865. https://doi.org/10.1021/acsami.5b11848

[48]W. M. Dose, N. Sharma, J. C. Pramudita, H. E. A. Brand, E. Gonzalo and T. Rojo, Structure-electrochemical evolution of a Mn-rich P2 $Na_{2/3}Fe_{0.2}Mn_{0.8}O_2$ Na-ion battery cathode, Chem. Mater. 29 (2017) 7416-7423. https://doi.org/10.1021/acs.chemmater.7b02397

[49]C. Ma, J. Alvarado, J. Xu, R. J. Clement, M. Kodur, W. Tong, C. P. Grey, Y. S. Meng, Exploring oxygen activity in the high energy P2-type $Na_{0.78}Ni_{0.23}Mn_{0.69}O_2$ cathode material for Na-ion batteries, J. Am. Chem. Soc. 139 (2017) 4835-4845. https://doi.org/10.1021/jacs.7b00164

[50]Y. Fang, X. Y. Yu and X. W. D. Lou, A practical high-energy cathode for sodium-ion batteries based on uniform P2-$Na_{0.7}CoO_2$ microspheres, Angew. Chem., Int. Ed. 56 (2017) 5801-5805. https://doi.org/10.1002/anie.201702024

[51]B. Fu, X. Zhou, Y. Wang, High-rate performance electrospun $Na_{0.44}MnO_2$ nanofibers as cathode material for sodium-ion batteries, J. Power Sources 310 (2016) 102-108 https://doi.org/10.1016/j.jpowsour.2016.01.101

[52]B. Fu, Y. Su, J. Yu, S. Xie, J. Li, Single crystalline nanorods of $Na_{0.44}MnO_2$ enhanced by reduced graphene oxides as a high rate and high capacity cathode material for sodium-ion batteries, Electrochim. Acta 303 (2019) 125-132. https://doi.org/10.1016/j.electacta.2019.02.074

[53]A. Konarov, J. H. Jo, J. U. Choi, Z. Bakenov, H. Yashiro, J. Kim, S. T. Myung, Exceptionally highly stable cycling performance and facile oxygen-redox of manganese-based cathode materials for rechargeable sodium batteries, Nano Energy 59 (2019) 197-206. https://doi.org/10.1016/j.nanoen.2019.02.042

[54]J. Y. Hwang, J. Kim, T. Y. Yu, Y. K. Sun, A new P2-type layered oxide cathode with extremely high energy density for sodium-ion batteries, Adv. Energy Mater. 9 (2019) 1803346. https://doi.org/10.1002/aenm.201803346

[55]Y. Xiao, Y. F. Zhu, H. R. Yao, P. F. Wang, X. D. Zhang, H. Li, X. Yang, L. Gu, Y. C. Li, T. Wang, Y. X. Yin, X. D. Guo, B. H. Zhong, Y. G. Guo, A stable layered oxide cathode material for high-performance sodium-ion battery, Adv. Energy Mater. 9 (2019) 1803978. https://doi.org/10.1002/aenm.201803978

[56]Q. Y. Shen, X. D. Zhao, Y. C. Liu, Y. P. Li, J. Zhang, N. Zhang, C. H. Yang, J. Chen, Dual-strategy of cation-doping and nanoengineering enables fast and stable sodium-ion storage in a novel Fe/Mn-based layered oxide cathode, Adv. Sci. 7 (2020) 2002199. https://doi.org/10.1002/advs.202002199

[57]L. Zhao, L.Yu, G. Wan, N. Ahmad, X. Ma, Z. Tao, G. Zhang, Co-manipulation of ultrafine nanostructure and uniform carbon layer activates maricite-structured $NaFePO_4$ as a high-performance cathode for sodium-ion batteries, Small Science 3 (2023) 2300122. https://doi.org/10.1002/smsc.202300122

[58]V. Munusami, K. Arutselvan, S. Vadivel, S. Govindasamy, Improved sodium storage properties $NaFePO_4$/C as cathode material for sodium-ion batteries, J Mater Sci: Mater Electron 35 (2024) 2104. https://doi.org/10.1007/s10854-024-13817-5

[59]M. Pan, Y. Wang, Y. Liu, M. Zhang, X. Liu, Y. Yuan, Y. Zhou, W. Liu, T. Chen, K. Liu, Optimizing interfacial modification for enhanced performance of $Na_3V_2(PO_4)_3$ cathode in sodium-ion batteries, Chemical Engineering Journal 495 (2024) 153396. https://doi.org/10.1016/j.cej.2024.153396

[60]Z. Wang, L. Chen, K. Yang, B. Liang, X. Guo, Z. Wu, D. Luo, Exploration of a Novel Vanadium Source for the Synthesis of a $Na_3V_2(PO_4)_3$ Cathode of Sodium-Ion Batteries, CS Sustainable Chem. Eng. 12 (2024) 1973-1983. https://doi.org/10.1021/acssuschemeng.3c06339

[61]J. Lee, S. Park, Y. Park, J. Song, B. Sambandam, V. Mathew, J. Y. Hwang, J. Kim, Chromium doping into NASICON-structured $Na_3V_2(PO_4)_3$ cathode for high-power Na-ion batteries, J. Chem. Eng., 422 (2021) 130052. https://doi.org/10.1016/j.cej.2021.130052

[62]A. Mukherjee, T. Sharabani, R. Sharma, S. Okashy, M. Noked, Effect of Crystal Structure and Morphology on $Na_3V_2(PO_4)_2F_3$ Performances for Na-Ion Batteries, Batter. Supercaps 3 (2020) 510-518. https://doi.org/10.1002/batt.201900202

[63]K. Tang, H. Tian, Y. Zhang, Y. Cai, H. Ren, Y. Wang, X. Yao, Z. Su, Fe-Doped $NaVPO_4F$/C Compounds for Sodium-Ion Battery Cathodes: Electrochemical Performance and Analysis of Kinetic Properties, Energy Fuels 38 (2024) 18035-18043. https://doi.org/10.1021/acs.energyfuels.4c02693

[64]X. Yao, L. Yin, C. Yang, Y. Lei, H. Zhang, Nitrogen-doped carbon encapsulated $NaVPO_4F$ as a promising ultra-long stability cathode for sodium ion batteries, J. Energy Storage 122 (2025) 11669. https://doi.org/10.1016/j.est.2025.116691

[65]X. Yao, L. Yin, C. Yang, Y. Lei, H. Zhang, K. Hui, Synergistic Effect of Carbon Encapsulation and Iron Doping Based on Metal–Organic Framework Precursor Enhances $NaVPO_4F$ Electrochemical Performance for Sodium-Ion Batteries, ACS Appl. Energy Mater. 7 (2024) 11890-11899. https://doi.org/10.1021/acsaem.4c02199

[66]V. K. Kumar, S. Ghosh, V. Naresh, G Ummethala, S. R. K. Malladi and S. K. Martha, Binder and conductive diluents free $NaVPO_4F$ based free-standing positive electrodes for sodium-ion batteries, J. Electrochem. Soc. 169 (2022) 010512. 10.1149/1945-7111/ac47eb abani, S. Taragin, R. Yemini, A. Maddegalla, I. Perelshtein, A. Mukherjee, M. Noked, Boosting the capacity and stability of $Na_3V_2(PO_4)$

$2F_{3-2x}O_{2x}$ microspheres, using atomic layer deposition of artificial CEI, J. Energy Storage 84 (2024) 111507. https://doi.org/10.1016/j.est.2024.111507

[68]Y. M. Yin, C. Pei, W. Xia, X. Luo, D. S. Li, Recent Advances and Perspectives on the Promising High-Voltage Cathode Material of $Na_3(VO)_2(PO_4)_2F$, Small 19 (2023) 2303666. https://doi.org/10.1002/smll.202303666

[69]J. Peng, W. Zhang, Q. Liu, J. Wang, S. Chou, H. Liu, S. Dou, Prussian Blue Analogues for Sodium-Ion Batteries: Past, Present, and Future, Adv. Mater. 34 (2022) 2108384. https://doi.org/10.1002/adma. 202108384

[70]G. Du, H. Pang, Recent advancements in Prussian blue analogues: Preparation and application in batteries, Energy Storage Mater. 36 (2021) 387-408. https://doi.org/10.1016/j.ensm.2021.01.006

[71] X. Liu, Y. Cao, J. Sun, Defect Engineering in Prussian Blue Analogs for High-Performance Sodium-Ion Batteries, Adv. Energy Mater. 12 (2022) 2202532. https://doi.org/10.1002/aenm.202202532

[72] W. Wang, Y. Gang, J. Peng, Z. Hu, Z. Yan, W. Lai, Y. Zhu, D. Appadoo, M. Ye, Y. Cao, Q. Gu, H. K. Liu, S. X. Dou, S. L. Chou, Effect of Eliminating Water in Prussian Blue Cathode for Sodium-Ion Batteries, Adv. Funct. Mater. 32 (2022) 2111727. https://doi.org/10.1002/adfm.202111727

[73] S. Qiao, S. Dong, L. Yuan, T. Li, M. Ma, Y. Wu, Y. Hu, T. Qu, S. Chong, Structure defects engineering in Prussian blue cathode materials for high-performance sodium-ion batteries, J. Alloys and Comp. 950 (2023) 169903. https://doi.org/10.1016/j.jallcom.2023.169903

[74] H. Qu, W. Hu, Y. Huang, T. Zhang, H. Fang, F. Li, Recent Advances and Practical Challenges in Organic Electrolytes of Sodium-Ion Batteries, Energ. Fuels 38 (2024) 12472-12486. https://doi.org/10.1021/acs.energyfuels.4c01974

[75] Z. Lin, Q. Xia, W. Wang, W. Li, S. Chou, Recent research progresses in ether-and ester-based electrolytes for sodiumion batteries, InfoMat 1 (2019) 376-389. https://doi.org/10.1002/inf2.12023

[76] Y. Yu, H. Che, X. Yang, Y. Deng, L. Li, Z. Ma, Non-flammable organic electrolyte for sodium-ion batteries, Electrochem. Commun. 110 (2020) 106635. https://doi.org/10.1016/j.elecom.2019.106635

[77] A. V. Cresce, S. M. Russell, O. Borodin, J. A. Allen, M. A. Schroeder, M. Dai, J. Peng, M. P. Gobet, S. G. Greenbaum, R. E. Rogers, K. Xu, Solvation behavior of carbonate-based electrolytes in sodium ion batteries, Phys. Chem. Chem. Phys. 19 (2017) 574-586. https://doi.org/10.1039/C6CP07215A

[78]Y. Huang, L. Zhao, L. Li, M. Xie, F. Wu, R. Chen, Electrolytes and Electrolyte/Electrode Interfaces in Sodium-Ion Batteries: From Scientific Research to Practical Application, Adv. Mater. 31 (2019) 1808393. https://doi.org/10.1002/adma.201808393

[79]K. Pan, H. Lu, F. Zhong, X. Ai, H. Yang, Y. Cao, Understanding the electrochemical compatibility and reaction mechanism on Na metal and hard carbon anodes of PC-based electrolytes for sodium-ion batteries, ACS Appl. Mater. Interfaces 10 (2018) 39651-39660. https://doi.org/10.1021/acsami.8b13236

[80]K. Sirengo, A. Babu, B. Brennan, S. C. Pillai, Ionic liquid electrolytes for sodium-ion batteries to control thermal runaway, J. Energy Chem. 81 (2023) 321-338. https://doi.org/10.1016/j.jechem.2023.02.046

[81]R. Hagiwara, K. Matsumoto, J. Hwang, T. Nohira, Sodium ion batteries using ionic liquids as electrolytes, Chem. Rec. 19 (2019) 758-770. https://doi.org/10.1002/tcr.201800119

[82]L. S. Domingues, H. G. de Melo, V. L. Martins, Ionic liquids as potential electrolytes for sodium-ion batteries: an overview, Phys. Chem. Chem. Phys. 25 (2023) 12650-12667. https://doi.org/10.1039/D3CP00238A

[83]A. Lahiri, F. Endres, Electrodeposition of nanostructured materials from aqueous, organic and ionic liquid electrolytes for Li-ion and Na-ion batteries: a comparative review, J. Electrochem. Soc. 164 (2017) D597. 10.1149/2.1011709jes

[84]D. Monti, E. Jonsson, M. R. Palacin, P. Johansson, Ionic liquid based electrolytes for sodium-ion batteries: Na^+ solvation and ionic conductivity, J. Power Sources 245 (2014) 630-636. https://doi.org/10.1016/j.jpowsour.2013.06.153

[85]N. Aslfattahi, L. Samylingam, M. S. Kiai, K. Kadirgama, V. Kulish, M. Schmirler, Z. Said, State-of-the-art review on electrolytes for sodium-ion batteries: Potential recent progress and technical challenges, J. Energy Storage 72 (2023) 108781. https://doi.org/10.1016/j.est.2023.108781

[86]P. Quan, L. T. M. Linh, H. T. K. Tuyen, N. V. Hoang, V. D. Thanh, T. V. Man, L. M. L. Phung, Safe sodium-ion battery using hybrid electrolytes of organic solvent/pyrrolidinium ionic liquid, Vietnam J. Chem. 59 (2021) 17-26. https://doi.org/10.1002/vjch.202000078

[87]A. Hofmann, D. Rauber, T. M. Wang, R. Hempelmann, C. W. Kay, T. Hanemann, Novel phosphonium-based ionic liquid electrolytes for battery applications, Molecules 27 (2022) 4729. https://doi.org/10.3390/molecules27154729

[88]C. R. Pope, M. Kar, D. R. MacFarlane, M. Armand, M. Forsyth, L. A. O'Dell, Ion dynamics in a mixed-cation alkoxy-ammonium ionic liquid electrolyte for sodium device applications, Chem. Phys. Chem. 17 (2016) 3187-3195. https://doi.org/10.1002/cphc.201600692

[89]S. M. Johari, N. A. Tajuddin, H. Hanibah, S. K. Deraman, A review: ionic conductivity of solid polymer electrolyte based polyethylene oxide, Int. J. Electrochem. Sci. 16 (2021) 211049. https://doi.org/10.20964/2021.10.53

[90]L. Ding, J. Shi, C. Yang, S. Dong, Ionic conductivity of solid polymer electrolytes based on modified alternating maleic anhydride copolymer with oligo (oxyethylene) side chains, Polym. J. 29 (1997) 410-416. https://doi.org/10.1295/polymj.29.410

[91]S. Vasudevan, S. Dwivedi, P. Balaya, Overview and perspectives of solid electrolytes for sodium batteries, Int. J. Appl. Ceram. Technol. 20 (2023) 563-584. https://doi.org/10.1111/ijac.14267

[92]Natron Collaborates with Clarios on Mass Manufacturing of Sodium-Ion Batteries (Available at: https://natron.energy/our-technology/our-chemistry)

[93]CATL Unveils Its Latest Breakthrough Technology by Releasing Its First Generation of Sodium-ion Batteries (Available at: https://www.catl.com/en/news/6015.html)

[94]Sodium-ion-batteries: A real challenger or another passerby for Indian-storage tech (Available at: https://evreporter.com/sodium-ion-batteries-a-real-challenger-or-another-passerby-for-indian-storage-tech/)

[95]CnEVPost, 23 February 2023 (Available at: Hina Battery becomes 1st battery maker to put sodium-ion batteries in EVs in China)

[96]Sodium ion cells: Sustainable. And Attainable (Available at: https://northvolt.com/products/cells/sodium-ion/)

High configurational entropy: Strategy to design P2-type layered oxide cathode for Na-ion batteries

*Amrapali Patil [1], Sagar Mitra[2]**

[1, 2] *Energy Science and Engineering Department Electrochemical Energy Laboratory (ECEL)*

IIT Bombay, Maharashtra, 400076, India

(*sagar.mitra@iitb.ac.in)

Abstract

Recent advances in renewable energy have increased the demand for efficient electrical energy storage technologies, driven by global energy needs and climate change concerns. With nearly two billion people lacking access to reliable electricity, energy storage devices are crucial, especially for integrating renewable sources into local grids. Li-ion batteries, however, are the most advanced technology, limited lithium resources make them unsustainable for large-scale deployment. Na-ion batteries provide a promising substitute because of the presence of sodium and low cost. In Na-ion batteries, cathode materials are critical, as they account for a greater mass fraction than anodes and significantly influence the battery's cost, safety, capacity, and energy density. Among potential cathode candidates, P2-type $Na_{0.67}Ni_{0.33}Mn_{0.67}O_2$ is particularly attractive due to its simple synthesis, high operating potential (~3.5 V vs. Na/Na^+), theoretical capacity (173 mAh g^{-1}), and specific capacities exceeding 140 mAh g^{-1}. Additionally, its P2 structure enables faster Na^+ ion transport than O3-type counterparts. However, its practical use is hindered by capacity fading and limited cycle life. To address these issues, the high entropy material strategy provides a new avenue for cathode development. The generic thought is to maximize the configurational entropy of the system to stabilize the single phase. By tuning the entropy of the system with multiple elements, a more flexible system can be achieved, which is found to be advantageous in increasing the specific capacity, energy density, and reversibility. This review proposes designing P2-type layered oxide cathodes using high configurational entropy to develop advanced, stable, and high-capacity materials for next-generation sodium-ion batteries.

Keywords: *Energy storage device, Na-ion batteries, P2-type layered oxide cathode, high configurational entropy.*

1. Introduction

Na-ion batteries (NaBs) have garnered significant interest in academic excellence and commercial industrial sectors since the 2000s. They offer several advantages that make them a compelling alternative or complement to lithium-ion batteries. NaBs are low-cost, environmentally friendly, have a reduced supply risk in the future, and are considered safer, making them a promising alternative for various applications [1–3]. There are plenty of merits to NaBs but are still tough to commercialize due to their limitations. **Figure 1** shows the schematic representation and mechanism of Na^+-ion (de)/insertion during charging and discharging. During charging, an oxidation event involving Na^+-ions (de)/insertion and electron (e^-) loss takes place at the cathode (e.g. Na_xMnO_2). In this process, e^- moves from the outer circuit and Na^+-ions move through the internal pathway (i.e. electrolyte) to the anode (e.g. hard carbon). During discharge opposite process happens where Na^+-ions are inserted at the cathode as a result, a reduction reaction takes place [4]. The ideal battery should be defined with a lower cost, reliable safety, high energy density, long-term cycling life, and large specific power, especially for grid energy storage and portable electronic devices [4]. As of right now, some significant anode materials show specific capacities of 300–600 mAh g^{-1} and operating potentials of 0.1–0.6 V (close to the potential of Na plating) [5–7], while cathode materials show specific capacities of 120–200 mAh g^{-1} and operating potentials of 2.6–3.2 V (much lower than the oxidation potential of electrolytes, >4.0 V) [8–10]. Moreover, due to the low gravimetric and volumetric energy densities of positive electrode material for NaBs which are not sufficient to reach up to the capacities of negative electrode material,

it is difficult to achieve broader voltage windows which some extent hinders the commercial expansion of NaBs in the next-generation energy storage devices [1,4]. In addition, it occupies a larger mass fraction and bigger space in the battery after mass balancing with the anode capacity.

The overall performance in terms of cost, safety, specific energy, cycling life, and specific power is greatly influenced by cathode material selection. Therefore, cathode materials exhibit attention for increasing the NaBs voltage window.

Structural stability in the high voltage range determines the cathode's longevity with the electrochemical stability of the electrolyte [4]. The main limiting factor for the large-scale application is the poor performance and slow reaction kinetics at low temperatures [11,12]. The slow movement of Na^+-ion at low temperatures reduces the capacity of the battery, other is the phase transition [13], and irreversible lattice anionic redox affects the structural integrity that results in the transition metal migration (i.e. cation) and lattice distortion leads to severe voltage decay and poor cycling performance [14,15].

This review article summarizes the advances of high configurational entropy (HCEs) in NaBs. Recently, HCEs raised significant attention towards particular uses for energy storage in rechargeable batteries. The combination of various elements in the system gives rise to tailorable properties and opens up opportunities for creating high-performance batteries [16–18]. Generally, we know that entropy is the degree of randomness, which creates a lot of confusion in explaining the high entropy materials (HEMs). Here, we focus on understanding the definition of HCEs which clarifies the differences between configurational entropy (CE) and randomness in the structure. Also, we aim to propose HCEs, a strategy to develop highly efficient cathodes for NaBs that offers new opportunities to address the challenges associated with P2-type layered oxide cathodes.

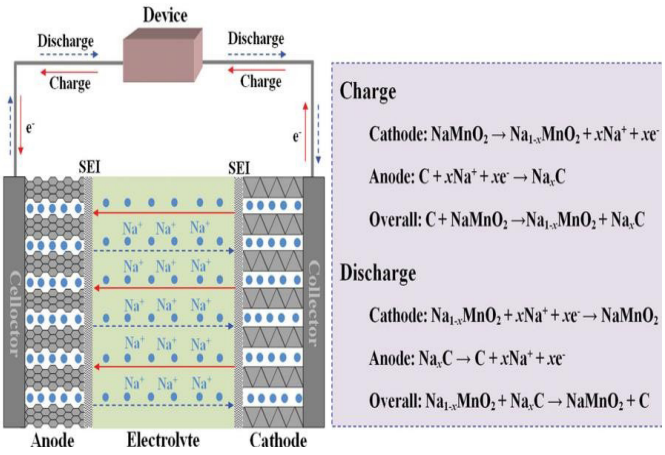

Figure 1. Schematic representation and Na+-ion (de)/insertion mechanism in NaBs [ref. 4].

2. Layered oxide material

Various cathode materials were discovered in recent years which include oxides, among the various materials studied for NaBs, polyanionic compounds, Prussian blue, and organic compounds have shown significant potential. However, layered oxide materials are considered one of the leading contenders for practical industrial applications. This is due to their high structural balance with reversible Na^+ (de)/intercalation chemistry, which is crucial for efficient energy storage and retrieval in NaBs.

The framework of layered oxide material is made up of oxygen anions which were arranged in a hexagonal closed packing, the two layers of anions form alternate octahedral and tetrahedral voids, and the transition metal ion is present in the octahedral void, tetrahedral voids remain empty. This is known as an MO_2 slab, (where M-represents the transition metal) these MO_2 slabs are arranged parallelly and form a layered structure. In between the two MO_2 slabs, there is a space known as interlayer spacing which acts as a host for Na^+-ions, shown in **Figure 2 (a-e)**. Based on the oxygen anionic packing, two types of interlayer spaces were formed: prismatic and octahedral thus layered oxide material is classified as P2, P3, O2, and O3 type, P stands for prismatic void and O stands for octahedral void which is the environment of Na^+-ion. The large cationic size of Na^+-ion always tries to remain in the octahedral and prismatic void with a 6-coordination number rather than in the tetrahedral void [19,20].

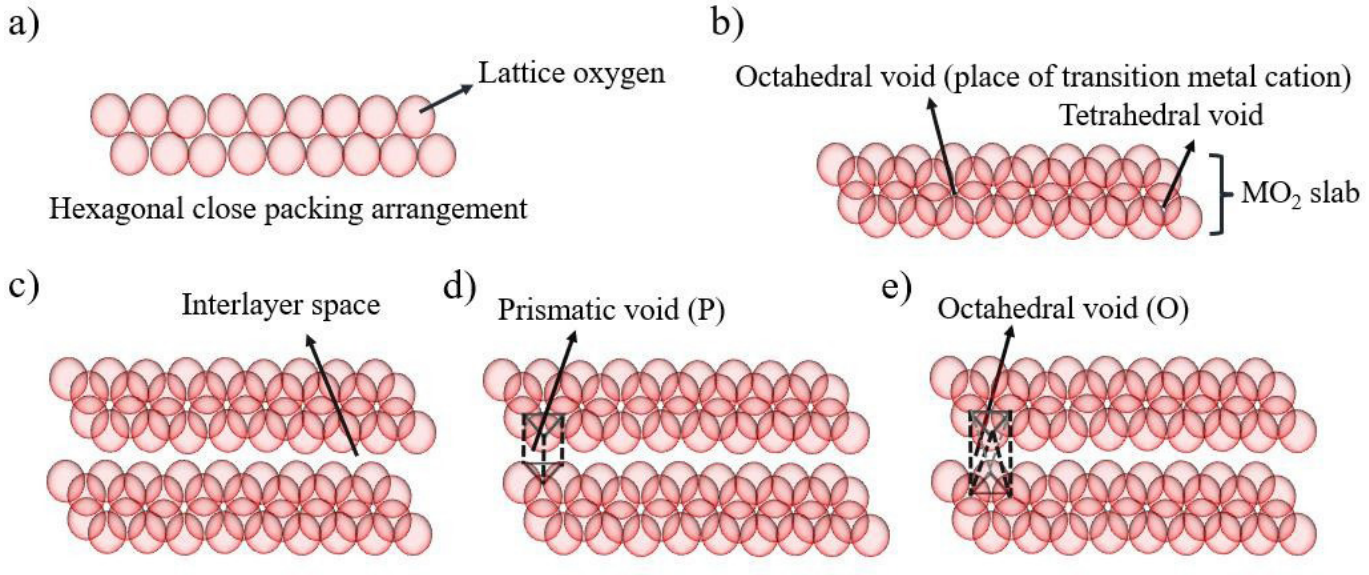

Figure 2. (a) Lattice oxygen packing, (b) void formation, (c) parallel arrangement of MO_2 slabs, (d) prismatic and (e) octahedral void formation respectively.

The structure is important in reaching electrons' high ionic and eltectronic conductivity. P2-type material offers a lower energy conduction pathway than O2-type material for Na^+-ion mobility. Na^+-ions can be moved from one octahedral site to an adjacent site in an O2-type phase occupying a tetrahedral site as shown in **Figure 3 (a)**, this entails passing through a common triangular face that stands between the octahedral-tetrahedral site, which results in a comparatively high activation barrier. The intermediate state's energy is increased by the potent coulombic repulsions between the transition metal ions (cation) in the MO_2 layers and the ions in the tetrahedral locations due to the closely packed system [21]. On the other hand, Na^+-ions in P2-type layered phases are dispersed over several trigonal prisms i.e. the Na sublattice is only partially filled, sharing their rectangular faces and offering extensive pathways and wider passage for the transport of Na^+-ions.

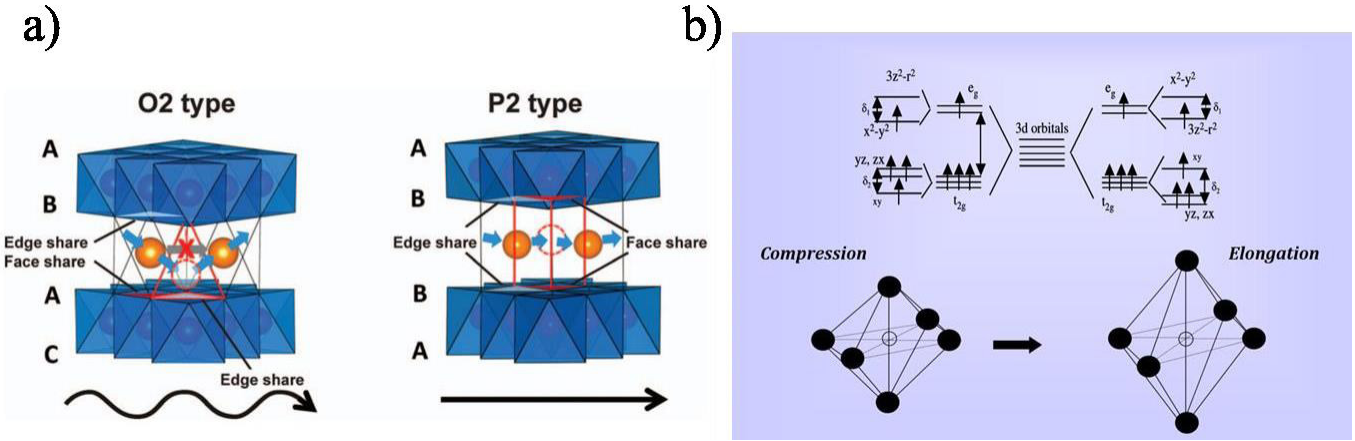

Figure 3. a) Na^+-ion conduction pathways in layered oxide O2-type and P2-type material [22], b) a schematic view of Jahn-Teller active species (Mn^{3+} ion)

Despite these advantages of P2-type layered cathode material, it undergoes poor reversibility and severe capacity loss due to the structure's instability. Various factors affect the structural integrity; phase transition is common in P2-type layered oxide material. In the high potential window while charging, Na^+-ions are extracted from the interlayer

spacing between the MO_2 slabs and a few ions maintain the initial structure. When the maximum number of Na^+ ions are extracted, the O^{2-} ions, positioned directly above one another, begin to repel each other. This repulsion is alleviated by the sliding of the oxygen layer, resulting in the formation of the more energetically stable O2-type phase. Consequently, Na^+-ion vacancies are less stable in the P2-type phase [23].

Another one is the presence of the Jahn-Teller (JT) active species in layered systems, Mn-based NaBs are low-cost, sustainable, and environmentally friendly energy storage technologies. Layered P2-type Na_XMnO_2 is more commonly investigated than the other [19]. The P2-type Na_XMnO_2 crystallizes in the two-phase tunnel-like structure with low sodium content (e.g. $Na_{0.2}MnO_2$, $Na_{0.4}MnO_2$, $Na_{0.44}MnO_2$), and layered structure with MO_2 slabs at high sodium content (e.g. $Na_{0.7}MnO_2$, $NaMnO_2$) [19].

In P2-type Na_XMnO_2, Mn^{3+} with electronic configuration t_{2g}^3 e_g^1 is JT active. In the MO_2 slab, the JT active species disturb the unit cell's symmetrical arrangement due to the elongation and compression of the bonds [24] shown in **Figure 3 (b)**. Na^+-ion conduction is affected by the activation energy barrier for Na^+-ion migration between neighboring sites when vacancy ordering or JT active cations (like Mn^{3+}) are present [25]. The strongly disfavoured unoccupied prismatic sites in a partially charged state and sudden change to an O2-like structure, as was previously described, can be challenging to create a stable P2 structure in practice [23].

The distortion highly depends on the synthesis conditions, low-temperature condition with a highly oxidizing environment stabilizes the Mn^{4+} state which reduces the distortion in the P2-type material. A study of the tunnel-like Na_XMnO_2 (x = 0.19–0.44) cathode material, reveals the anisotropic expansion during cycling is due to the presence of mixed valance Mn^{3+}/Mn^{4+} leads to the poor cycling performance of P2-type Na_XMnO_2. Initially, the structure of Na_XMnO_2 as the sodium content x increases from 0.22 to 0.66, the material's structure expands along the b-axis. Additionally, further expansion occurs along the a- and c-axes as x increases from 0.44 to 0.66. This anisotropic expansion behavior is crucial for understanding the material's performance in NaBs. The presence of JT Mn^{3+} species at different lattice positions leads to anisotropic changes in the lattice parameter along the a-, b-, and c-axis, resulting in the loss of capacity [26]. Apart from this, irreversible anionic redox causes severe capacity decay and disturbs the structural integrity. Generally, it occurs in the high potential window (> 4.3 V vs Na^+/Na), and forms unstable recombination of over-oxidized lattice oxygen (O^{2-}) further releases as O_2 gas which leads to the structural transformation from layered to spinel [27–29]. Recent studies indicate that the O_2 molecule can be trapped in the bulk [30–32]. O_2 gas evolution occurs at the surface of the particle and enters into the bulk of the material which generates vacancies and causes capacity degradation [33,34].

The oxygen release in P2-type Na_xMnO_2 is still unclear. Enhancing the performance of cathode materials is a critical focus in the expansion of high-efficiency NaBs. Several strategies are employed to achieve this, aiming to address challenges such as low energy density, poor cycling stability, and limited rate capability. One key practice is the optimization of cathode material composition. Researchers are investigating doping strategies, where small amounts of specific elements are introduced to stabilize the cathode structure, improve electronic conductivity, and facilitate sodium ion diffusion.

3. Strategies to address the issues

3.1 To design a high-capacity cathode

The P2-type phase is only stable with a limited amount of sodium i.e. Na_X where $x \leq 2/3$ [35]. It is impossible to increase the Na amount up to 0.9 with a stable P2-phase [36,37]. The as-synthesized P2-type phases can have their Na content raised by transition metal substitution, as **Figure 4** illustrates. The MnO_2 layers have been doped to increase the P2-type Na_XMnO_2's maximum capacity. Mn can be partially substituted for Ni, Li, or both to stabilize P2 structures with a Na concentration as high as 0.85. The maximum cutoff

voltage is restricted to approximately 4.2 V to avoid any structural alterations that would impact the reversible reinsertion of Na^+-ion into the structure after discharge. Therefore, materials in which part of the Mn has been replaced by Ni and Li have only moderate reversible capacities (63 to 140 mAh g^{-1}) [38–40].

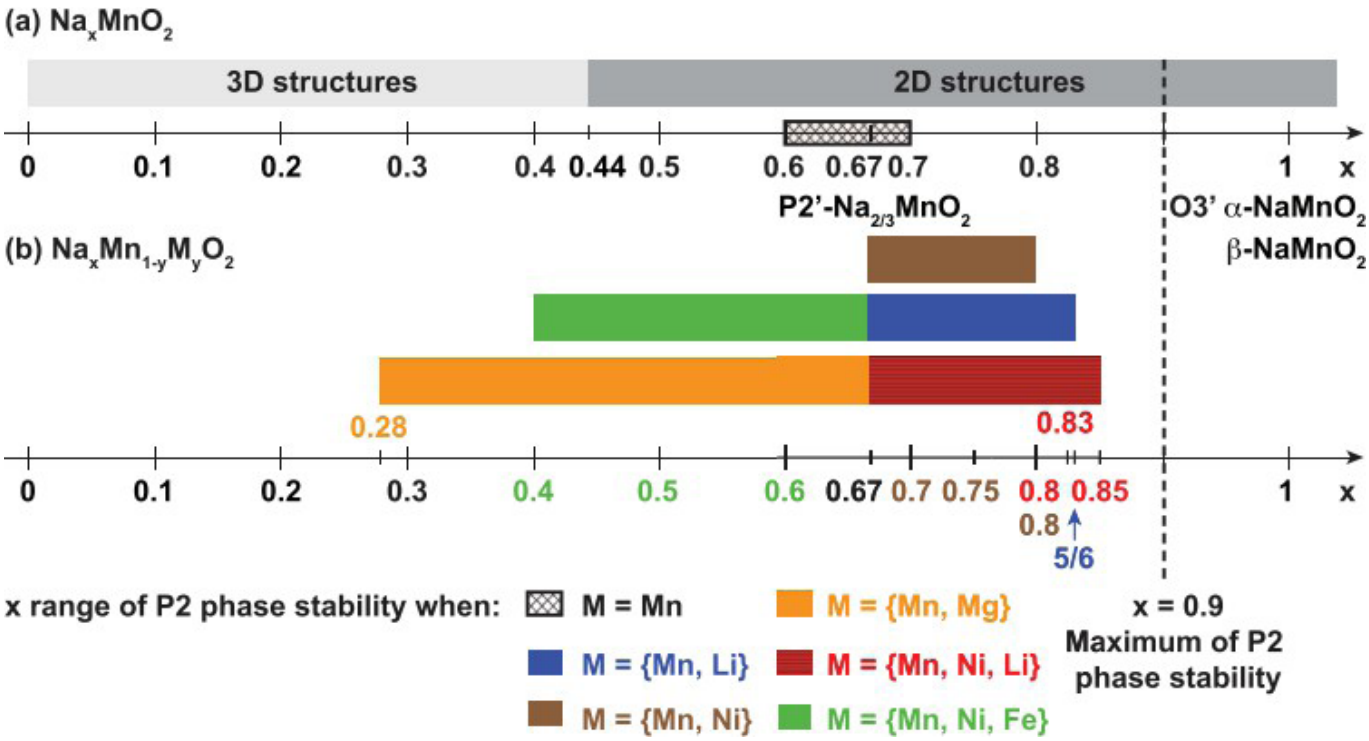

Figure 4. (a) Range of sodium content [77] in P2-Na_xMnO_2 compound observed for 3D and 2D structural stability [41,42], (b) doping of various elements on the Mn site to stabilize the P2-phase of the Na_xMnO_2 compound M = {Mn, Ni}[43]{Mn, Li} [35] {Mn, Mg}[44] {Mn, Ni, Li}[45–47] {Mn, Ni, Fe} [48].

3.2 To raise the potential window of P2-type cathode material

In the context of A_xMO_2 (A=Li, Na) materials, the electrochemical performance is highly influenced by substituting transition metals. This substitution can adjust key features, such as the value of voltage wherein the system material (de)/intercalates Li^+/Na^+ ions. For instance, P2-Na_xMnO_2 has been observed to operate within a narrow voltage range of approximately 2.8 V vs. Na^+/Na, but it offers a high capacity between 175 mAh g^{-1} and 190 mAh g^{-1} [49,50]. However, research into Fe-based systems, such as O3-$NaFeO_2$, which exhibits a higher redox potential of around 3.3 V vs. Na^+/Na, has led to new developments [51]. Yabuuchi and colleagues explored the stabilization of the P2-phase by partially substituting Mn^{3+} with Fe^{3+} in P2-$Na_xFe1/2Mn1/2O2$. Their findings demonstrated that both Mn^{3+}/Mn^{4+} and Fe^{3+}/Fe^{4+} redox couples were active, resulting in a reversible capacity of 190 mAh g^{-1} when cycled between 1.5 and 4.2 V at a 12 mA g^{-1} rate. However, contrary to expectations, this Fe/Mn bimetallic oxide did not demonstrate an increase in average working voltage, remaining around 2.75 V, similar to P2-Na_xMnO_2 [9]. Furthermore, Lu and Dahn synthesized the P2-$Na_{2/3}Ni_{1/3}Mn_{2/3}O_2$ electrode to investigate the influence of Ni replacement within the electrochemical characteristics of P2-Na_xMnO_2, adding another layer of complexity and potential for performance enhancement in these materials [52].

3.3 To suppress P2-O2 phase transition in P2-type cathode m15

single-phase behavior in P2-type layered oxides during cycling is crucial for ensuring their electrochemical stability and longevity. Investigations are concentrated on fine-tuning the composition and structure of these materials to avoid undesirable cation-ordering transitions and to enhance their performance in NaBs. The stability of P2 phases is essential for achieving high-rate performance in Na cells. However, prolonged cycling can lead to side reactions that compromise the P2 phase, resulting in increasedoverpotential and capacity loss, often due to low reversible capacity and poor capacity retention. To address these challenges, careful selection of synthetic conditions such as the choice of precursors, preparation temperature, and cooling method (slow cooling vs. quenching) is critical in achieving single-phase behavior. Additionally, composition plays a key role in preserving the stability of the P2 structure during cycling. A common approach to restrict the oxygen layer from sliding after Na deintercalation and to extend the stability range of the P2 structure over varying Na content is the addition of dopants into the MO_2 layer. For instance, as presented in **Figure 4**, substitutedNa_xMnO_2 phases benefit from such doping. Specifically, Li-doped P2-Na_xMO_2 (M = Ni, Mn) compounds have been shown to remain stable up to a potential of 4.2 V, which corresponds to a Na amount of 0.35 [40,47]. Despite these advancements, the exact content of Na required to remain in the Na_xMO_2 structure to resist the structural changes at high voltage continues to be a topic of ongoing research and debate [46]. The balance between stability and performance remains a key area of focus for optimizing these materials for practical applications.

3.4 To ensure structural stability by diluting the Jahn-Teller species

In P2-type intercalation electrode materials, structural stability is crucial for ensuring reversible electrochemical behavior and achieving a long cycle life. One of the significant challenges in maintaining structural stability is the presence of Jahn-Teller (JT) active Mn^{3+} species, which can induce distortions during cycling. These distortions create large stresses on the lattice parameters, leading to the accumulation of extended defects and even amorphization, particularly after prolonged cycling [53]. To mitigate the effects of JT distortions, the dilution of Mn^{3+} is an effective strategy. By substituting Mn^{3+} with other elements, the influence of JT active species can be reduced. Paulsen and Dahn demonstrated that the monoclinic distortion observed in β-$Na_{0.7}MnO_2$ transitions to an orthorhombic structure when weakly substituted with elements like Co, Li, or Ni in $Na_{2/3}Mn_{1-x}M_xO_2$. In heavily substituted samples, an ideal P2 structure is observed, indicating that substitution plays a key role in stabilizing the material [54]. Substituting Mn^{3+} with lower valence elements not only decreases the amount of Mn ions in the material but also increases the average Mn oxidation state from +3 to +4. This change in oxidation state reduces the extent of JT distortions, contributing to a more stable structure during cycling. Furthermore, doping can create a more flexible structure with minimal volume changes during cycling, enhancing the material's overall stability. The insertion of low valence spectator ions, such as Li^+, can also effectively stabilize the P2 phase across a wide voltage range. This approach helps maintain structural integrity, even under high-voltage conditions, making the material more suitable for long-term cycling in battery applications.

Doping elements into cathode materials is a crucial strategy for improving the performance of NaBs. This technique involves adding specific elements to the cathode structure to enhance its electrochemical properties, such as stability, capacity, and conductivity. By selecting appropriate dopants, researchers can address common challenges associated with Na-ion battery cathodes, like low energy density and poor cycling stability. For instance, doping with transition metals such as Mg, Zn, or Al can help stabilize the crystal structure of layered oxide cathodes, reducing structural degradation during charge-discharge cycles and thereby extending the battery's lifespan. Additionally, dopants can improve the electronic and ionic conductivity of the cathode material, leading to faster sodium ion diffusion and better rate

capability. Some dopants also help in mitigating the volume changes that occur during cycling, which can otherwise lead to capacity fading. Overall, element doping is a versatile and effective approach to developing high-performance cathodes, which are essential for advancing the efficiency and reliability of NaBs. Hence, doping opens the way to introduce HCE in the material, which offers a more flexible structure with low volumetric expansion and contraction, it helps to reduce the P2-O2 phase transition upon cycling in the high voltage range. By introducing various dopant elements such as active, inactive, and high valent, one can stabilize the P2-type phase of the material. Doping also helps to reduce the JT active species, lowering the energy barrier for the Na^+-ion conduction during charging and discharging. Incorporating doping elements into cathode materials can increase the CE, thereby enhancing the stability and electrochemical performance of NaBs.

2. Concept of configurational entropy

Based on thermodynamics, entropy is the microstructure combination that constitutes a specific macroscopic state. The concept itself originated from the thought experiment and approach of postulates. The thought experiment consists of a macroscopic closed composite system with total volume (V), and internal energy (U), composed of several particles (N) separated by an impermeable membrane that divides the system into two regions, in which system 1 is defined as (V_1, U_1, N_1) with entropy S_1 and system 2 described as (V_2, U_2, N_2) with entropy S_2. If the membrane is permeable the two systems try to reach the equilibrium as shown in **Figure 5 (a, b)**. After some time, at equilibrium state particles will be randomly arranged, and the entropy of the system will become $S = S_1 + S_2$. N_1 (number of particles of system 1) and N_2 (number of particles of system 2) can access a larger volume (V) to spread randomly throughout the system. There exists a function S (entropy) in the absence of the internal constraints (without impermeable membrane) which maximizes S (entropy) at the equilibrium state and this is known as the entropy of the system (entropy is additive in nature) [55].

A macroscopic system as discussed above can be thought of in another way, with a permeable membrane, N_1 and N_2 can occupy the maximum number of possible microstates available in volume (V). The probability of occupying each available state in the system gives the number of configurations and is calculated by the formula given below shown in **Figure 5 (c, d)**.

$$\Omega = N! / N_1! N_2!$$

After some time, the system reaches equilibrium, with the maximum possible configurations for N_1 and N_2 particles. This builds the connection between the macroscopic system and a number of available microstates (microscopic system) given by the Boltzmann relation stated as below [55].

$$\Delta S_{conf} = \kappa \ln \Omega \text{ (fundamental postulate)}$$

Where κ is the Boltzmann constant and Ω is the number of available microstates for the particles in the system.

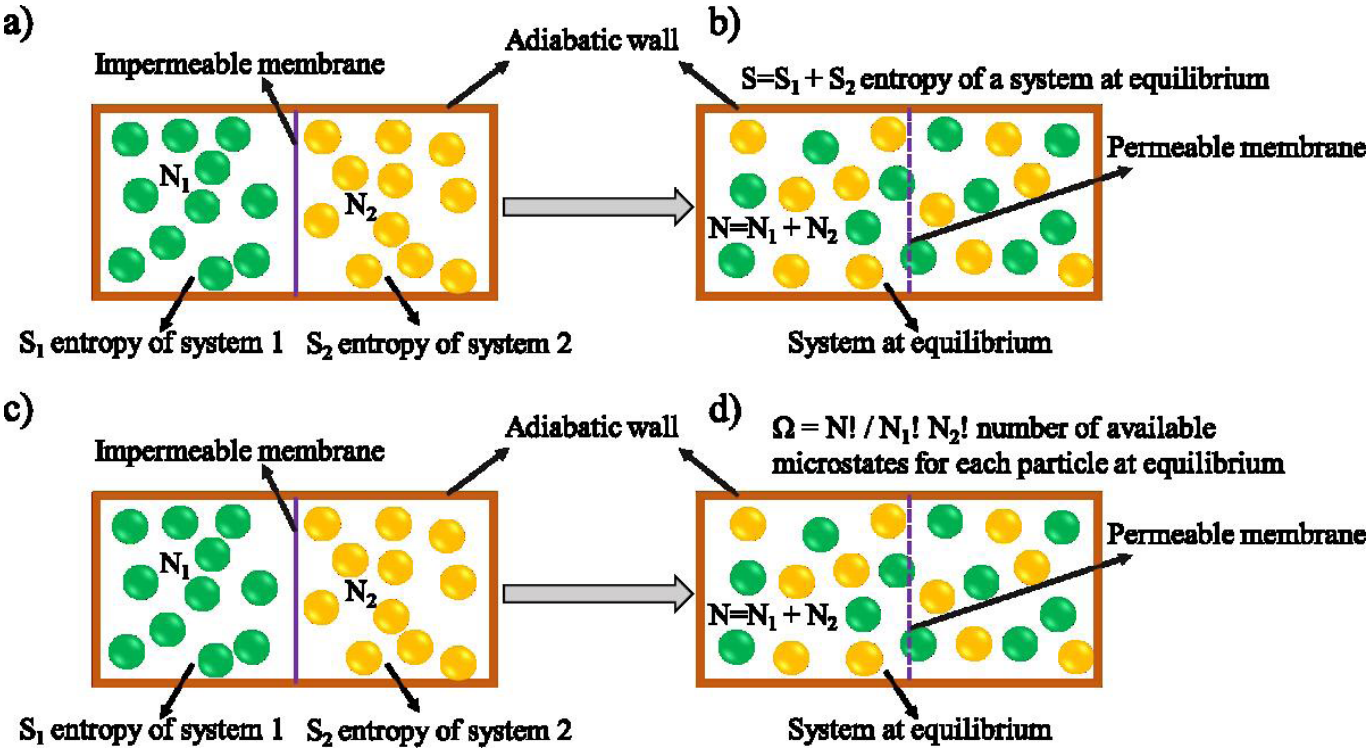

Figure 5. (a, b) Entropy of the system at equilibrium based on the entropy postulate, (c, d) number of configurations at equilibrium [55].

For a 2-component system, with n1 and n2 a lattice, where total number of molecules are **n = n1 + n2**

Therefore, the number of lattice sites can be calculated by the permutation and combination for the given system and is provided by the formula **(Ω = n! / n1! n2!).** By applying Stirling's approximation for the factorial of a large integer CE can be given as follows;

ΔSconf = κ ln Ω

ΔSconf = - R [n1/n *ln* n1/n + n2/n *ln* n2/n] x1 = n1/n; x2 = n2/n

ΔSconf = - R [x1 *ln* x1 + x2 *ln* x2]

The CE change per mole for n components with xi mole fraction when forming a solid solution is given as [56].

ΔSconf = - R [$\sum_{i=1}^{n}$ xi *ln* xi]

4.1 Definition

The investigation of unexplored areas in the field of alloying engineering gives birth to HEMs [57]. The evolution of HEMs was initiated by conventional alloys; pure single crystalline material consists of a single element placed on a fixed lattice position. The demand for more advanced materials was fulfilled by the binary and ternary compounds, in which two or three elements were mixed in small amounts with a non-equimolar ratio to substitute the pure elements lattice position and known as conventional alloys that may or may not be crystallized in a single phase. In 2004, researchers explored the equimolar region with five or more than five elements where the position of the component/element is not fixed and it arranges itself randomly throughout the lattice, surprisingly found that it crystallizes in a single phase known as high entropy alloys [58,59]. Recently, in 2018 the focus has been on the non-equimolar composition around the center [60] of the hyperdimensional compositional diagram as shown in **Figure 6 (a)**, which was explored intensively and again represents the random arrangement of elements in

the system leads to an increase in the entropy known as complex concentrated alloys (CCAs) [61].

The entropy of mixing in a solid solution refers to the increase in disorder when different types of atoms or species mix in a crystalline solid. This entropy is composed of several contributions, each related to different types of disorder and energy states within the material. This is the most significant contributor to the entropy of mixing in a solid solution. It arises from the random arrangement of different atoms (or ions) on a lattice site. For an ideal solid solution, CE $\Delta\mathbf{Sconf} = -\mathbf{R}\left[\sum_{i=1}^{n} \mathbf{xi}\ \boldsymbol{ln}\ \mathbf{xi}\right]$. The more randomly distributed the different atoms are, the greater the CE. Vibrational entropy arises from the atomic vibrations within the solid. Different atoms or ions have distinct masses and bonding strengths, which influence the vibrational modes of the solid. When atoms of different types mix, the vibrational frequencies shift, which can either increase or decrease the vibrational entropy. This effect is more pronounced in alloys or systems where there is a significant difference in atomic mass between the components. This contribution is relevant in materials where the atoms have magnetic moments. Magnetic dipole entropy arises from the disorder in the orientations of magnetic moments (spins) in the material. For materials that exhibit magnetic ordering, such as ferromagnets or antiferromagnets, the mixing of different atoms with varying magnetic properties can lead to changes in the magnetic dipole entropy. The degree of disorder in the magnetic system, particularly at temperatures near or above the Curie or Néel temperature, adds to the overall entropy. This is often referred to as residual entropy, which occurs when the system remains disordered even at very low temperatures. This type of entropy is present in systems that have more than one equivalent ground state, such as certain frustrated magnetic materials or systems with random occupancy of certain lattice sites (without long-range order). Residual entropy can arise when the system does not achieve perfect order even as temperature approaches absolute zero. Overall, the entropy of mixing in a solid solution is a combination of various forms of disorder, CE relates to the atomic arrangement, vibrational entropy comes from atomic vibrations, and magnetic dipole entropy is due to the disorder in magnetic moments. Random (residual) entropy arises from the inherent disorder at low temperatures. Together, these components contribute to the total entropy of the solid solution, influencing its stability and behavior, especially in thermodynamic processes like phase transitions [62].

CE is dominant in all, which usually represents the entropy of mixing and depends on the elemental proportion [63]. Hence, an efficient way to reach the HCE is to introduce various elements in a specific system. The HCE materials are commonly identified based on the composition of the system and the entropy calculation. The definition of HCE is still unclear and can be divided into two, 1st is based on the composition which describes a system with five or more elements in the equimolar ratio (range of elements 5 to 35%) [59], 2nd is based on entropy which defines the system with HCE i.e. the entropy must be larger than 1.5R, without any restriction on the elemental composition [64]. The maximum S_{conf} is 1.61R, which may be obtained in a system with five cations at equiatomic proportions. Materials with $S_{conf} < 1R$ are classified as "low entropy," those with $1.5R > S_{conf} \geq 1R$ are classified as "medium entropy," and materials with $S_{conf} \geq 1.5R$ are classified as "high entropy" systems. Thus, to create materials with significant CE, the systems intentionally integrate a major proportion of numerous elements in about equal proportions. This method differs from traditional doping procedures as it extends beyond the trace amount of doping and is typified by a more broad and well-balanced compositional range of elemental variety [65]. A system with five or more elements tends to form a single-phase solid solution with HCEs but this is not always the case [66]. To understand how entropy affects a compound's phase stability, consider the Gibbs free energy of mixing ΔG_{mix} as given by the below equation;

$$\Delta\mathbf{Gmix} = \Delta\mathbf{Hmix} - \mathbf{T}\Delta\mathbf{Smix}$$

Where ΔS_{mix} denotes the mixing entropy in the above equation, the mixing enthalpy by ΔH_{mix}, and the mixing CE by ΔS_{conf}, which usually dominates in ΔS_{mix}. The absolute temperature is indicated by T.

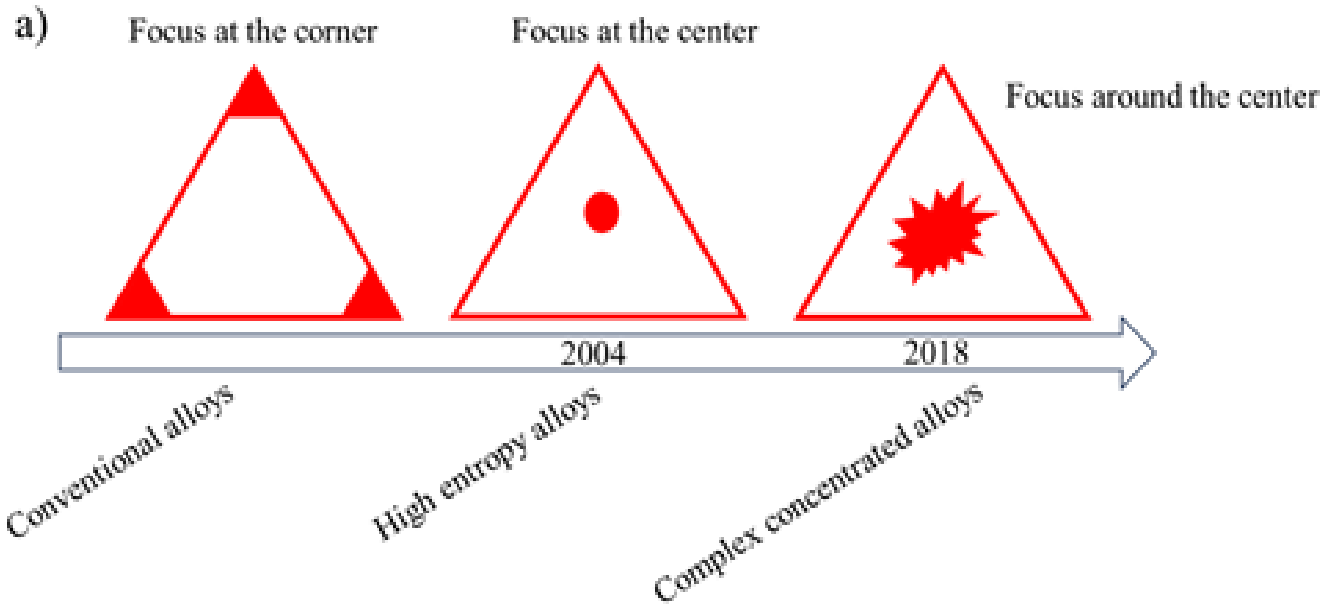

Figure 6. (a) Evolution of material innovation and the birth of high-entropy material

In the formation of HCEs and to stabilize the phase of the material there is always a competition between enthalpy and entropy. The enthalpy of a multi-component system varies significantly since the nature of the constituent elements in a solid solution plays a critical role in determining the resulting phase under near-equilibrium conditions. These elements influence various factors, including atomic size, electronegativity, crystal structure, and bonding characteristics, which in turn dictate phase stability and transitions. If the elemental composition has highly positive values of negative ΔH_{mix} (indicative of repulsive forces), this can lead to immiscibility and phase segregation. Conversely, highly negative ΔH_{mix} values (indicative of attractive forces) promote structural ordering, such as the formation of intermetallic compounds. If all ΔH_{mix} pairs in the multi-element composition are near-zero, indicating minimal attraction or repulsion between elements, the entropic term becomes dominant. This entropic dominance promotes homogeneous random elemental mixing, leading to HCE. However, natural single-phase mixing, especially in solid solutions, is indeed challenging and relatively rare due to the inherent complexities of atomic interactions and structural stability. Several factors contribute to this difficulty, making it hard to achieve and maintain a homogeneous single-phase structure in nature or even in controlled environments due to the significant physicochemical differences among different elements, which result in a wide range of ΔH_{mix} values [67,68]. For metal oxides, each cation is surrounded by anions (i.e. oxygen lattice), which have the same environment. This leads to $\Delta H_{mix} = 0$ and leaves only the entropy term in the Gibbs free energy equation, hence phase stabilization is affected by the entropy of mixing [18].

$$\Delta G_{mix} = \Delta H_{mix} - RT \sum_{i=1}^{n} x_i \ln x_i$$

It is possible to reach one phase in many cases when $S_{conf} \geq 1.5$ R. In these situations, entropy stabilization is established by the dominance of the $T\Delta S_{mix}$ term in the free energy landscape, which surpasses ΔH_{mix} and results in a negative overall ΔG_{mix} [69]. It's crucial to remember that entropy and temperature are strongly related, and synthesis at higher temperatures typically encourages the creation of single-phased systems with higher CEs.

4.2 How to achieve high configurational entropy

Generally, it was observed that the existence of numerous elements in the system will give the maximum CE. However, this is not always feasible. The CE of the system is dependent on the number and the mole fraction of the elements in the system. For a two-component system (e.g., system A and system B maximization of CE takes place at XA=XB=0.5, it was calculated mathematically by using the formula which indicates that the maximum possible achievable entropy in two components is 5.76 J/K mol as shown in **Table 1 (a)**. This suggests that the multi-component system in an equimolar ratio always maximizes the CE [56]. In addition, the CE can be maximized by increasing the number of elements. Where we observe that the HCE will be achieved with five or more than five elemental compositions in the given system as shown in **Table 1 (b)**.

Table 1. (a) Entropy calculation for a 2-component system, (b) entropy calculation with increasing number of elements

a)

x_A	x_B	$\Delta S_{conf} = -R [x_A \ln x_A + x_B \ln x_B]$
1	0	0
0.9	0.1	2.7
0.8	0.2	4.16
0.7	0.3	5.07
0.6	0.4	5.59
0.5	0.5	5.76
0.4	0.6	5.59

b)

No. of components	Equimolar ratio	$S_{conf} = -R [\sum x_A \ln x_A]$
1	1	0
2	0.50	5.76
3	0.33	9.220
4	0.25	11.64
5	0.20	13.38

4.3. Recent progress of P2-type material towards high configurational entropy

Recent advancements in P2-type materials have shown significant promise for improving the performance of NaBs. These materials, characterized by their layered structure, offer high Na-ion mobility and structural stability, making them ideal candidates for cathodes in NaBs. Research has focused on optimizing their composition, such as through element doping to enhance their electrochemical properties. These improvements have led to better capacity retention, increased energy density, and prolonged cycle life, positioning P2-type materials as a leading option in the development of next-generation NaBs. Research on phase shifts in layered materials during electrochemical cycling has been a fascinating topic for a long time. The P2 structure, while interesting, faces some challenges. Na^+ vacancy ordering and troublesome P2-O2 phase transitions can negatively affect material capacity & cycle performance. Manganese (Mn) is very important, it's a key part of layered oxides and also plays a crucial role in P2-type materials. At higher potentials (more than 2.0 V), Mn^{+4} ions help keep the structure stable during discharge (when it gets sodiated). But as the electrode discharges below 2.0 V, those Mn^{4+} ions get reduced to Mn^{3+}. This change increases the concentration of JT-active Mn^{3+}, which plays a major role in degrading electrochemical characteristics. This can lead to lattice deformation, active material loss, and even create new phases. To tackle these issues, one of the best strategies is to reduce unwanted phase transitions & control Mn loss during cycling.

In 2022, Wang et al. synthesized three different P2-type layered oxide cathode materials using a solid-state method: Na0.67(Mn0.55Ni0.21Co0.24)O2, Na0.67(Mn 0.45Ni0.18Co0.24Ti0.1Mg0.03)O2, and Na0.67(Mn0.4 5Ni0.18Co0.18Ti0.1Mg0.03Al0.04Fe0.02)O2. Named as 3, 5, and 7 NTMO2 and according to their entropy properties, low (0.99 R), medium (1.34 R), and high (1.52 R) respectively [70]. The material with the highest entropy showed amazing reversibility with less Mn depletion and structural deterioration within the voltage ranges of 1.5–4.6 V and 2.6–4.6 V, while medium & low entropy materials experienced moderate to rapid

capacity loss respectively. It turns out that improving CE is a smart way to avert phase transition while boosting structural stability. In 2023, Dreyer et al. used sonic emission to check how an increase in CE affected phase-transition properties in those high entropy oxides we talked about 3, 5 & 7 NTMO2. The distinct sound signatures linked to fracture creation were quite noticeable [71]. Shen et al. shared details about a P2-type cathode ($Na_{0.80}Li_{0.08}Ni_{0.22}Mn_{0.67}O_2$) aimed at raising the cut-off voltage to start anionic redox [72]. Similarly, Jin et al. crafted a new $Na_{0.75}Ca_{0.04}[Li_{0.1}Ni_{0.2}Mn_{0.67}]O_2$ P2-cathode helping with anionic redox-related capacity loss using Manganese (+3/+4) redox complementary mechanism. At a remarkable rate of 5C over two hundred cycles, this cathode held on strong with an impressive retention of around 95% [73]. The $P2\text{-}Na_{0.62}Mn_{0.67}Ni_{0.23}Cu_{0.05}Mg_{0.09-2y}Ti_yO_2$ showed better Na^+ diffusion thanks to its higher fraction regarding facets {010} along with improved entropy, this was highlighted by Fu et al. The kinetics of anionic redox reactions were also improved due to features from the crystal structure in the P2 phase [74]. Also noteworthy is that the Na^+ diffusion coefficient related to various cathode materials such as CuMgTi-571 and $NaMNO_2$ during Na (de)intercalation looks promising. Plus, managing energy through entropy fluctuation can contribute positively to performance. For example, $Na_{0.62}Mn_{0.67}Ni_{0.23}Cu_{0.05}Mg_{0.07}Ti_{0.01}O_2$ showed an extraordinary capacity of about 82 mAh g^{-1} at a rate of 1200 mA g^{-1}. Ma et al. developed another cathode called $P2\text{-}Na_{0.667}Mn_{0.667}Ni_{0.167}Co_{0.117}Ti_{0.01}Mg_{0.01}Cu_{0.01}Mo_{0.01}Nb_{0.01}O_2$ (HCE-NMNC). In this case, five cations share equal proportions at TM sites [75]. High entropy doping helps minimize strain change by widening voltage ranges for the highly reversible P2 phase. The HCE-NMNC managed a capacity of 111 mAh g^{-1} at 5C which was steady over one hundred cycles at 1C (130 mAh g^{-1}). The reversible oxygen redox process from its lattice site during cycling, and the charge compensation by metals like Ni, Co & Mn contributed to this high potential capacity.

Recently many reports about medium entropy oxides (MEOs) have come out. Yan et al., back in 2021 published their first report using MEOs in NaBs [76]. They developed two types of P2-compositions using solid-state methods: $Na_{2/3}Ni_{1/3}Mn_{1/3}Fe_{1/3-x}Al_xO_2$ (NaNMF) and $Na_{2/3}Ni_{1/3}Mn_{1/3}Fe_{1/3-x}Al_xO_2$ (NaNMFA) featuring three & four cation replacements respectively. The four-cation system NaNMFA showed better cycle stability between two volts & four point two volts compared to the three-cation system NaNMF with around 125.6 mAh g^{-1} reversibility. Research suggested that HCE led to smoother charge-discharge curves which also helped inhibit structural transitions raised due to damaging Mn^{3+}, preserving crystal structure integrity. Wang et al. worked on HCE-($P2\text{-}Na_{0.65}Mn_{0.65}Cu_{0.2}Li_{0.06}Mg_{0.015}Ti_{0.015}Al_{0.015}Zr_{0.015}Y_{0.015}La_{0.015}O_2$) showing potential against those irreversible phase transitions while minimizing significant volume changes when charging or discharging batteries [77]. They reported on another cathode via Liu et al. called P2-type $Na_{0.85}Li_{0.12}Ni_{0.198}Be_{0.011}Mg_{0.011}Mn_{0.66}O_2$ designed with a lower Mn^{3+}/Mn^{4+} ratio too. In this case, widening interlayer distances ensures amazing rate performance. The two published patents for positive electrode materials concerning P2-HCE oxide recently, the first patent on $P2\text{-}Na_{0.67}Ni_{0.18y}Cu_{0.1}Zn_{0.05}Fe_xMn_{0.67-x+y}O_2$ stated a capacity around 105.3 mAh g^{-1} at 1C with retention of nearly 93%.

The second patent discussed $P2\text{-}Na_{0.75}Mn_{0.5625}Ni_{0.25}Cu_{0.0625}Mg_{0.0625}Ti_{0.0625}O_2$ showcasing 98%. It shows incredible retention after 100 cycles starting from approximately 108 mAh g^{-1} around 120 mA g^{-1} (2–4.3 V) [77].

5. Discussion and future direction for the development of cathode

The dependence on energy storage devices especially in developing next-generation cathode material for NaBs, performance enhancement like energy density, reversibility, structural stability, and phase transition is crucial. Traditional aspects of cathode modification like elemental doping are still insufficient to achieve the aim of superior-performance batteries. Fortunately, the

advancement of HCEs aims to preserve the single-phase with a highly flexible structure and diverse material compositions and architectures, unlocking new pathways to enhance battery materials development. Research into HCE materials for batteries is still in the early stages, but the potential for these materials to revolutionize battery technology is significant. As our understanding of HCE behavior in electrochemical systems deepens, we can expect to see more HCE material-based components in commercial batteries, leading to higher performance and more durable energy storage solutions. Hence, HCE can indeed be a promising strategy for developing cathode materials for NaBs. By incorporating multiple cations in a single lattice (often five or more), the CE of the system is increased. This entropy can stabilize the crystal structure even at room temperature, preventing phase separation and ensuring a more stable cathode material over multiple charge/discharge cycles. In NaBs, cathodes face challenges like phase transitions and structural degradation during cycling. HCE can help mitigate these issues by stabilizing different phases that might otherwise be unstable. This leads to improved cycle life and performance. The presence of multiple different metal ions can lead to synergistic effects, improving electronic conductivity, ionic conductivity, and overall electrochemical performance. This is particularly important for NaBs, where finding suitable cathode materials has been more challenging than for their Li-ion counterparts. HCE materials offer the flexibility to fine-tune the composition by adjusting the ratio of different elements. This tunability allows researchers to optimize properties such as capacity, voltage, and stability for specific applications. In summary, HCE offers a pathway to develop a P2-type layered oxide cathode for NaBs with enhanced stability, good performance, and sustainability.

Acknowledgment

Amrapali appreciates the funding support from STARS ID-2023- and 0738, Code: RD/0123-STARS00-005, Grant:10018185. Also, acknowledges the Department of Energy Science and Engineering of the Indian Institute of Technology, Bombay, for offering the Institute Teaching Assistant (TA-category) Research Fellowship.

Conflict of interest

The author declares no conflict of interest.

References:

[1] E. Goikolea, V. Palomares, S. Wang, I.R. de Larramendi, X. Guo, G. Wang, T. Rojo, Na-Ion Batteries–Approaching Old and New Challenges, Adv Energy Mater 10 (2020). https://doi.org/10.1002/aenm.202002055.

[2] J.F. Peters, M. Baumann, J.R. Binder, M. Weil, On the environmental competitiveness of sodium-ion batteries under a full life cycle perspective-a cell-chemistry specific modelling approach, Sustain Energy Fuels 5 (2021) 6414–6429. https://doi.org/10.1039/d1se01292d.

[3] P.K. Nayak, L. Yang, W. Brehm, P. Adelhelm, Von Lithium- zu Natriumionenbatterien: Vorteile, Herausforderungen und Überraschendes, Angewandte Chemie 130 (2018) 106–126. https://doi.org/10.1002/ange.201703772.

[4] X. Xiang, K. Zhang, J. Chen, Recent advances and prospects of cathode materials for sodium-ion batteries, Advanced Materials 27 (2015) 5343–5364. https://doi.org/10.1002/adma.201501527.

[5] M. Dahbi, N. Yabuuchi, K. Kubota, K. Tokiwa, S. Komaba, Negative electrodes for Na-ion batteries, Physical Chemistry Chemical Physics 16 (2014) 15007–15028. https://doi.org/10.1039/c4cp00826j.

[6] Y. Kim, Y. Kim, A. Choi, S. Woo, D. Mok, N.S. Choi, Y.S. Jung, J.H. Ryu, S.M. Oh, K.T. Lee, Tin phosphide as a promising anode material for Na-ion batteries, Advanced Materials 26 (2014) 4139–4144. https://doi.org/10.1002/adma.201305638.

[7] J. Qian, X. Wu, Y. Cao, X. Ai, H. Yang, High capacity and rate capability of amorphous phosphorus for sodium ion batteries, Angewandte Chemie - International Edition 52 (2013) 4633–4636. https://doi.org/10.1002/

anie.201209689.

[8] S. Guo, H. Yu, Z. Jian, P. Liu, Y. Zhu, X. Guo, M. Chen, M. Ishida, H. Zhou, A high-capacity, low-cost layered sodium manganese oxide material as cathode for sodium-ion batteries, ChemSusChem 7 (2014) 2115–2119. https://doi.org/10.1002/cssc.201402138.

[9] N. Yabuuchi, M. Kajiyama, J. Iwatate, H. Nishikawa, S. Hitomi, R. Okuyama, R. Usui, Y. Yamada, S. Komaba, P2-type Nax [Fe1/2 Mn1/2[O2 made from earth-abundant elements for rechargeable NaÂ batteries, Nat Mater 11 (2012) 512–517. https://doi.org/10.1038/nmat3309.

[10] A. Ponrouch, E. Marchante, M. Courty, J.M. Tarascon, M.R. Palacín, In search of an optimized electrolyte for Na-ion batteries, Energy Environ Sci 5 (2012) 8572–8583. https://doi.org/10.1039/c2ee22258b.

[11] Z. Bai, X. Lv, D.H. Liu, D. Dai, J. Gu, L. Yang, Z. Chen, Two-Dimensional NiO@C-N Nanosheets Composite as a Superior Low-Temperature Anode Material for Advanced Lithium-/Sodium-Ion Batteries, ChemElectroChem 7 (2020) 3616–3622. https://doi.org/10.1002/celc.202000747.

[12] Q. Li, D. Yang, H. Chen, X. Lv, Y. Jiang, Y. Feng, X. Rui, Y. Yu, Advances in metal phosphides for sodium-ion batteries, SusMat 1 (2021) 359–392. https://doi.org/10.1002/sus2.19.

[13] B. Song, E. Hu, J. Liu, Y. Zhang, X.Q. Yang, J. Nanda, A. Huq, K. Page, A novel P3-type Na 2/3 Mg 1/3 Mn 2/3 O 2 as high capacity sodium-ion cathode using reversible oxygen redox, J Mater Chem A Mater 7 (2019) 1491–1498. https://doi.org/10.1039/c8ta09422e.

[14] X. Cao, H. Li, Y. Qiao, X. Li, M. Jia, J. Cabana, H. Zhou, Stabilizing Reversible Oxygen Redox Chemistry in Layered Oxides for Sodium-Ion Batteries, Adv Energy Mater 10 (2020). https://doi.org/10.1002/aenm.201903785.

[15] J. Vergnet, M. Saubanère, M.L. Doublet, J.M. Tarascon, The Structural Stability of P2-Layered Na-Based Electrodes during Anionic Redox, Joule 4 (2020) 420–434. https://doi.org/10.1016/j.joule.2019.12.003.

[16] N. Qiu, H. Chen, Z. Yang, S. Sun, Y. Wang, Y. Cui, A high entropy oxide (Mg0.2Co0.2Ni0.2Cu0.2Zn0.2O) with superior lithium storage performance, J Alloys Compd 777 (2019) 767–774. https://doi.org/10.1016/j.jallcom.2018.11.049.

[17] Q. Wang, A. Sarkar, D. Wang, L. Velasco, R. Azmi, S.S. Bhattacharya, T. Bergfeldt, A. Düvel, P. Heitjans, T. Brezesinski, H. Hahn, B. Breitung, Multi-anionic and -cationic compounds: New high entropy materials for advanced Li-ion batteries, Energy Environ Sci 12 (2019) 2433–2442. https://doi.org/10.1039/c9ee00368a.

[18] C.M. Rost, E. Sachet, T. Borman, A. Moballegh, E.C. Dickey, D. Hou, J.L. Jones, S. Curtarolo, J.P. Maria, Entropy-stabilized oxides, Nat Commun 6 (2015). https://doi.org/10.1038/ncomms9485.

[19] R.J. Clément, P.G. Bruce, C.P. Grey, Review—Manganese-Based P2-Type Transition Metal Oxides as Sodium-Ion Battery Cathode Materials, J Electrochem Soc 162 (2015) A2589–A2604. https://doi.org/10.1149/2.0201514jes.

[20] C. Delmas, D. Carlier, M. Guignard, The Layered Oxides in Lithium and Sodium-Ion Batteries: A Solid-State Chemistry Approach, Adv Energy Mater 11 (2021). https://doi.org/10.1002/aenm.202001201.

[21] K. Kang, G. Ceder, Factors that affect Li mobility in layered lithium transition metal oxides, Phys Rev B Condens Matter Mater Phys 74 (2006). https://doi.org/10.1103/PhysRevB.74.094105.

[22] N. Yabuuchi, K. Kubota, M. Dahbi, S. Komaba, Research development on sodium-ion batteries, Chem Rev 114 (2014) 11636–11682. https://doi.org/10.1021/cr500192f.

[23] C. Delmas, C. Fouassier, P. Hagenmuller, STRUCTURAL CLASSIFICATION AND PROPERTIES OF THE LAYERED OXIDES, n.d.

[24] J.B. Goodenough, JAHN-TELLER PHENOMENA IN SOLIDS, 1998.

[25] G.J. Shu, F.C. Chou, Sodium-ion diffusion and ordering in single-crystal P2 -Nax CoO2, Phys Rev B Condens Matter Mater Phys 78 (2008). https://doi.org/10.1103/PhysRevB.78.052101.

[26] F. Sauvage, L. Laffont, J.M. Tarascon, E. Baudrin, Study of the insertion/deinsertion mechanism of sodium into Na 0.44MnO2, Inorg Chem 46 (2007) 3289–3294. https://doi.org/10.1021/ic0700250.

[27] A.R. Armstrong, M. Holzapfel, P. Nová, C.S. Johnson, S.-H. Kang, M.M. Thackeray, P.G. Bruce, Demonstrating Oxygen Loss and Associated Structural Reorganization in the Lithium Battery Cathode Li[Ni 0.2 Li 0.2 Mn 0.6]O 2, (2006). https://doi.org/10.1021/ja062027.

[28] H. Koga, L. Croguennec, M. Ménétrier, K. Douhil, S. Belin, L. Bourgeois, E. Suard, F. Weill, C. Delmas, Reversible Oxygen Participation to the Redox Processes Revealed for Li 1.20 Mn 0.54 Co0.13 Ni 0.13 O 2 , J Electrochem Soc 160 (2013) A786–A792. https://doi.org/10.1149/2.038306jes.

[29] Y. Wang, E. Wang, X. Zhang, H. Yu, High-Voltage "single-Crystal" Cathode Materials for Lithium-Ion Batteries, Energy and Fuels 35 (2021) 1918–1932. https://doi.org/10.1021/acs.energyfuels.0c03608.

[30] R.A. House, J.J. Marie, J. Park, G.J. Rees, S. Agrestini, A. Nag, M. Garcia-Fernandez, K.J. Zhou, P.G. Bruce, Covalency does not suppress O2 formation in 4d and 5d Li-rich O-redox cathodes, Nat Commun 12 (2021). https://doi.org/10.1038/s41467-021-23154-4.

[31] R.A. House, J.J. Marie, M.A. Pérez-Osorio, G.J. Rees, E. Boivin, P.G. Bruce, The role of O2 in O-redox cathodes for Li-ion batteries, Nat Energy 6 (2021) 781–789. https://doi.org/10.1038/s41560-021-00780-2.

[32] R.A. House, G.J. Rees, M.A. Pérez-Osorio, J.J. Marie, E. Boivin, A.W. Robertson, A. Nag, M. Garcia-Fernandez, K.J. Zhou, P.G. Bruce, First-cycle voltage hysteresis in Li-rich 3d cathodes associated with molecular O2 trapped in the bulk, Nat Energy 5 (2020) 777–785. https://doi.org/10.1038/s41560-020-00697-2.

[33] P.M. Csernica, S.S. Kalirai, W.E. Gent, K. Lim, Y.S. Yu, Y. Liu, S.J. Ahn, E. Kaeli, X. Xu, K.H. Stone, A.F. Marshall, R. Sinclair, D.A. Shapiro, M.F. Toney, W.C. Chueh, Persistent and partially mobile oxygen vacancies in Li-rich layered oxides, Nat Energy 6 (2021) 642–652. https://doi.org/10.1038/s41560-021-00832-7.

[34] P. Yan, J. Zheng, Z.K. Tang, A. Devaraj, G. Chen, K. Amine, J.G. Zhang, L.M. Liu, C. Wang, Injection of oxygen vacancies in the bulk lattice of layered cathodes, Nat Nanotechnol 14 (2019) 602–608. https://doi.org/10.1038/s41565-019-0428-8.

[35] N. Yabuuchi, R. Hara, M. Kajiyama, K. Kubota, T. Ishigaki, A. Hoshikawa, S. Komaba, New O2/P2-type Li-excess layered manganese oxides as promising multi-functional electrode materials for rechargeable Li/Na batteries, Adv Energy Mater 4 (2014). https://doi.org/10.1002/aenm.201301453.

[36] R. Berthelot, D. Carlier, C. Delmas, Electrochemical investigation of the P2-NaxCoO2 phase diagram, Nat Mater 10 (2011) 74–80. https://doi.org/10.1038/nmat2920.

[37] M. Guignard, C. Didier, J. Darriet, P. Bordet, E. Elkaïm, C. Delmas, P2-Na x VO 2 system as electrodes for batteries and electron-correlated materials, Nat Mater 12 (2013) 74–80. https://doi.org/10.1038/nmat3478.

[38] J. Xu, H. Liu, Y.S. Meng, Exploring Li substituted O3-structured layered oxides NaLixNi1/3 - XMn1/3 + xCo1/3 - XO2 (x = 0.07, 0.13, and 0.2) as promising cathode materials for rechargeable Na batteries, Electrochem Commun 60 (2015) 13–16. https://doi.org/10.1016/j.elecom.2015.07.023.

[39] N.K. Karan, M.D. Slater, F. Dogan, D. Kim, C.S. Johnson, M. Balasubramanian, Operando Structural Characterization of the Lithium-Substituted Layered Sodium-Ion Cathode Material P2-Na 0.85 Li 0.17 Ni 0.21 Mn 0.64 O 2 by X-ray Absorption Spectroscopy, J Electrochem Soc 161 (2014) A1107–A1115. https://doi.org/10.1149/2.088406jes.

[40] D. Kim, S.H. Kang, M. Slater, S. Rood, J.T. Vaughey, N. Karan, M. Balasubramanian, C.S. Johnson, Enabling sodium batteries using lithium-substituted sodium layered transition metal oxide cathodes, Adv Energy Mater 1 (2011) 333–336. https://doi.org/10.1002/aenm.201000061.

[41] A. Mendiboure, C. Delmas, P. Hagenmuller, Electrochemical Intercalation and Deintercalation of NaxMnOz Bronzes, 1985.

[42] J.-P. Parant, R. Olazcuaga, M. Devalette, C. Fouassier, Sur Quelques Nouvelles Phases de Formule Na,MnO, (x G 1), 1971.

[43] J. Cabana, N.A. Chernova, J. Xiao, M. Roppolo, K.A. Aldi, M.S. Whittingham, C.P. Grey, Study of the transition metal ordering in layered NaxNi x/2Mn1-x/2O2 (2/3 ≤ x ≤ 1) and consequences of Na/Li exchange, Inorg Chem 52 (2013) 8540–8550. https://doi.org/10.1021/ic400579w.

[44] D. Buchholz, C. Vaalma, L.G. Chagas, S. Passerini, Mg-doping for improved long-term cyclability of layered Na-ion cathode materials - The example of P2-type NaxMg0.11Mn0.89O2, J Power Sources 282 (2015) 581–585. https://doi.org/10.1016/j.jpowsour.2015.02.069.

[45] R.J. Clément, D. Kitchaev, J. Lee, Gerbrand Ceder, Short-Range Order and Unusual Modes of Nickel Redox in a Fluorine-Substituted Disordered Rocksalt Oxide Lithium-Ion Cathode, Chemistry of Materials 30 (2018) 6945–6956. https://doi.org/10.1021/acs.chemmater.8b03794.

[46] N.K. Karan, M.D. Slater, F. Dogan, D. Kim, C.S. Johnson, M. Balasubramanian, Operando Structural Characterization of the Lithium-Substituted Layered Sodium-Ion Cathode Material P2-Na 0.85 Li 0.17 Ni 0.21Mn0.64O2 by X-ray Absorption Spectroscopy, J Electrochem Soc 161 (2014) A1107–A1115. https://doi.org/10.1149/2.088406jes.

[47] D. Kim, S.H. Kang, M. Slater, S. Rood, J.T. Vaughey, N. Karan, M. Balasubramanian, C.S. Johnson, Enabling sodium batteries using lithium-substituted sodium layered transition metal oxide cathodes, Adv Energy Mater 1 (2011) 333–336. https://doi.org/10.1002/aenm.201000061.

[48] I. Hasa, D. Buchholz, S. Passerini, J. Hassoun, A comparative study of layered transition metal oxide cathodes for application in sodium-ion battery, ACS Appl Mater Interfaces 7 (2015) 5206–5212. https://doi.org/10.1021/am5080437.

[49] J. Billaud, G. Singh, A.R. Armstrong, E. Gonzalo, V. Roddatis, M. Armand, T. Rojo, P.G. Bruce, Na0.67Mn1-xMgxO2 (0 ≤ x ≤ 0.2): A high capacity cathode for sodium-ion batteries, in: Energy Environ Sci, Royal Society of Chemistry, 2014: pp. 1387–1391. https://doi.org/10.1039/c4ee00465e.

[50] N. Yabuuchi, R. Hara, M. Kajiyama, K. Kubota, T. Ishigaki, A. Hoshikawa, S. Komaba, New O2/P2-type Li-excess layered manganese oxides as promising multi-functional electrode materials for rechargeable Li/Na batteries, Adv Energy Mater 4 (2014). https://doi.org/10.1002/aenm.201301453.

[51] N. Yabuuchi, H. Yoshida, S. Komaba, Crystal structures and electrode performance of alpha-NaFeO2 for rechargeable sodium batteries, Electrochemistry 80 (2012) 716–719. https://doi.org/10.5796/electrochemistry.80.716.

[52] Z. Lu, J.R. Dahn, In Situ X-Ray Diffraction Study of P2-Na[sub 2/3][Ni[sub 1/3]Mn[sub 2/3]]O[sub 2], J Electrochem Soc 148 (2001) A1225. https://doi.org/10.1149/1.1407247.

[53] A. Caballero, L. Hernán, J. Morales, L. Sánchez, J. Santos Peña, M.A.G. Aranda, Synthesis and characterization of high-temperature hexagonal P2-Na0.6 Mno_2 and its electrochemical behaviour as cathode in sodium cells, J Mater Chem 12 (2002) 1142–1147. https://doi.org/10.1039/b108830k.

[54] PII: S0167-2738(99)00147-2, 1999. www.elsevier.com/locate/ssi.

[55] Herbert B. Callen - Thermodynamics and an Introduction to Thermostatistics-Wiley (1985), (n.d.).

[56] B.S. Murty, J.W. Yeh, S. Ranganathan, P.P. Bhattacharjee, High-entropy alloys: basic concepts, in: High-Entropy Alloys, Elsevier, 2019: pp. 13–30. https://doi.org/10.1016/b978-0-12-816067-1.00002-3.

[57] B.S. Murty, J.W. Yeh, S. Ranganathan, A Brief History of Alloys and the Birth of High-Entropy Alloys, in: High Entropy Alloys, Elsevier, 2014: pp. 1–12. https://doi.org/10.1016/b978-0-12-800251-3.00001-8.

[58] B. Cantor, I.T.H. Chang, P. Knight, A.J.B. Vincent, Microstructural development in equiatomic multicomponent alloys, Materials Science and Engineering: A 375–377 (2004) 213–218. https://doi.org/10.1016/j.msea.2003.10.257.

[59] J.W. Yeh, S.K. Chen, S.J. Lin, J.Y. Gan, T.S. Chin, T.T. Shun, C.H. Tsau, S.Y. Chang, Nanostructured high-entropy alloys with multiple principal elements: Novel alloy design concepts and outcomes, Adv Eng Mater 6 (2004) 299–303. https://doi.org/10.1002/adem.200300567.

[60] K. Liu, S.S. Nene, M. Frank, S. Sinha, R.S. Mishra, Extremely high fatigue resistance in an ultrafine grained high entropy alloy, Appl Mater Today 15 (2019) 525–530. https://doi.org/10.1016/j.apmt.2019.04.001.

[61] S.S. Nene, Some Distinct Features of Transformative High Entropy Alloys for Metal Additive Manufacturing, Front Mater 9 (2022). https://doi.org/10.3389/fmats.2022.873911.

[62] D.B. Miracle, O.N. Senkov, A critical review of high entropy alloys and related concepts, Acta Mater 122 (2017) 448–511. https://doi.org/10.1016/j.actamat.2016.08.081.

[63] A. Manzoor, S. Pandey, D. Chakraborty, S.R. Phillpot, D.S. Aidhy, Entropy contributions to phase stability in binary random solid solutions, NPJ Comput Mater 4 (2018). https://doi.org/10.1038/s41524-018-0102-y.

[64] J.W. Yeh, Alloy design strategies and future trends in high-entropy alloys, JOM 65 (2013) 1759–1771. https://doi.org/10.1007/s11837-013-0761-6.

[65] H. Gao, J. Li, F. Zhang, C. Li, J. Xiao, X. Nie, G. Zhang, Y. Xiao, D. Zhang, X. Guo, Y. Wang, Y.M. Kang, G. Wang, H. Liu, Revealing the Potential and Challenges of High-Entropy Layered Cathodes for Sodium-Based Energy Storage, Adv Energy Mater 14 (2024). https://doi.org/10.1002/aenm.202304529.

[66] Y. Chen, H. Fu, Y. Huang, L. Huang, X. Zheng, Y. Dai, Y. Huang, W. Luo, Opportunities for High-Entropy Materials in Rechargeable Batteries, ACS Mater Lett 3 (2021) 160–170. https://doi.org/10.1021/acsmaterialslett.0c00484.

[67] R. Guo, L. Yu, Z. Liu, J. Pan, Y. Yao, L. Liu, Enthalpy induced phase partition toward hierarchical, nanostructured high-entropy alloys, Nano Res 15 (2022) 4893–4901. https://doi.org/10.1007/s12274-021-3912-z.

[68] M.C. Troparevsky, J.R. Morris, P.R.C. Kent, A.R. Lupini, G.M. Stocks, Criteria for predicting the formation of single-phase high-entropy alloys, Phys Rev X 5 (2015). https://doi.org/10.1103/PhysRevX.5.011041.

[69] Y. Yao, Q. Dong, A. Brozena, J. Luo, J. Miao, M. Chi, C. Wang, I.G. Kevrekidis, Z.J. Ren, J. Greeley, G. Wang, A. Anapolsky, L. Hu, High-entropy nanoparticles: Synthesis-structureproperty relationships and data-driven discovery, Science (1979) 376 (2022). https://doi.org/10.1126/science.abn3103.

[70] J. Wang, S.L. Dreyer, K. Wang, Z. Ding, T. Diemant, G. Karkera, Y. Ma, A. Sarkar, B. Zhou, M. V. Gorbunov, A. Omar, D. Mikhailova, V. Presser, M. Fichtner, H. Hahn, T. Brezesinski, B. Breitung, Q. Wang, P2-type layered high-entropy oxides as sodium-ion cathode materials, Materials Futures 1 (2022). https://doi.org/10.1088/2752-5724/ac8ab9.

[71] S.L. Dreyer, R. Zhang, J. Wang, A. Kondrakov,

Q. Wang, T. Brezesinski, J. Janek, The effect of configurational entropy on acoustic emission of P2-type layered oxide cathodes for sodium-ion batteries, JPhys Energy 5 (2023). https://doi.org/10.1088/2515-7655/acd41a.

[72] Q. Shen, Y. Liu, X. Zhao, J. Jin, X. Song, Y. Wang, X. Qu, L. Jiao, Unexpectedly High Cycling Stability Induced by a High Charge Cut-Off Voltage of Layered Sodium Oxide Cathodes, Adv Energy Mater 13 (2023). https://doi.org/10.1002/aenm.202203216.

[73] J. Jin, Y. Liu, Q. Shen, X. Zhao, J. Zhang, Y. Song, T. Li, X. Xing, J. Chen, Unveiling the Complementary Manganese and Oxygen Redox Chemistry for Stabilizing the Sodium-Ion Storage Behaviors of Layered Oxide Cathodes, Adv Funct Mater 32 (2022). https://doi.org/10.1002/adfm.202203424.

[74] F. Fu, X. Liu, X. Fu, H. Chen, L. Huang, J. Fan, J. Le, Q. Wang, W. Yang, Y. Ren, K. Amine, S.G. Sun, G.L. Xu, Entropy and crystal-facet modulation of P2-type layered cathodes for long-lasting sodium-based batteries, Nat Commun 13 (2022). https://doi.org/10.1038/s41467-022-30113-0.

[75] S. Ma, P. Zou, H.L. Xin, Extending phase-variation voltage zones in P2-type sodium cathodes through high-entropy doping for enhanced cycling stability and rate capability, Mater Today Energy 38 (2023). https://doi.org/10.1016/j.mtener.2023.101446.

[76] S. Yan, S. Luo, L. Yang, J. Feng, P. Li, Q. Wang, Y. Zhang, X. Liu, Novel P2-type layered medium-entropy ceramics oxide as cathode material for sodium-ion batteries, Journal of Advanced Ceramics 11 (2022) 158–171. https://doi.org/10.1007/s40145-021-0524-8.

[77] H. Liu, Y. Wang, X. Ding, Y. Wang, F. Wu, H. Gao, A high-entropy layered P2-type cathode with high stability for sodium-ion batteries, Sustain Energy Fuels 8 (2024) 1304–1313. https://doi.org/10.1039/d3se01597a.

Effect of current density on the properties of electrodeposited Ni-mullite composite coatings

*Ann Miriam, N. Balaji, S.T. Aruna**
Surface Engineering Divisi
CSIR-National Aerospace Laboratories
HAL Airport Road, Bangalore-560017, INDIA
**Email corresponding author:aruna_reddy@nal.res.in*

Abstract

In recent years there is a great demand for the development of electrodeposited Ni-composite coatings due to their improved corrosion and wear resistance. The properties of the electrodeposited coatings are dictated by the nature and amount of the distributed particles, the particle size and its distribution, the applied current density, the magnetic stirrer speed, etc. In the present study, the less explored mullite particles are chosen as the distributive phase and the effect of applied current density on the microhardness, corrosion and wear resistant properties of the coating is studied. The mullite powder is obtained by ball milling the commercial alumina and silica powders. The microhardness, corrosion resistance and wear resistance of the coatings are evaluated. The Ni-mullite composite coating electrodeposited at a current density of 3.1A/dm^2 exhibits improved corrosion resistance with a corrosion rate of 1.1cm/yr . Ni-mullite coatings showed a lower coefficient of friction (0.4) and higher wear loss when compared to plain nickel coating.

Keywords: Electrodeposition; mullite; Ni; corrosion; wear; microhardness

1. Introduction

There is a great demand for electrodeposited composite coatings for various engineering applications as electrodeposition is a relatively low-cost method compared to other coating techniques like thermal spraying or chemical vapor deposition [1]. Electrodeposited composite coatings are used in a wide range of industries, including aerospace, automotive, and electronics. They are used for improving the wear resistance of components such as gears, bearings and valves. The composite coatings are used in marine and chemical industries to impart corrosion resistance to the components [2].

Basically, electrodeposited composite coatings consists of metal matrix and non-metallic particles as distributed phases. The most common metals used as matrices in composite electrodeposition are nickel, copper, and chromium [3]. Other metals such as silver, gold, and cobalt are also employed depending on the application. The non-metallic particles, also called reinforcement materials or distributive phase, are selected based on the desired property enhancement. For example, ceramic particles like alumina, silica, zirconia, titania, ceria, etc are used to enhance hardness, wear resistance, and thermal stability of the metal matrix [4-16]. Polymer materials like polytetra fluroro ethylene (PTFE) and polyamide are used to improve the lubricity and reduce friction. Carbon based materials such as graphite and carbon nanotubes are used for enhancing the wear resistance and conductivity of the matrix and diamond particles are used to enhance the hardness and abrasion resistance of the matrix. The non-metallic particles gets co-deposited along with the metal matrix during the electroplating process. The process parameters—such as bath composition, temperature, current density, and agitation—can significantly affect the distribution and properties of the composite coating. The uniformity of particle distribution, the adherence between particles and metal, and the final mechanical and electrochemical properties depend on these factors. There is a vast literature on the electrodeposited Ni-composite coatings containing SiC, alumina, zirconia, ceria, titania, carbon

nanotubes, diamond, etc [5-15]. Ni-SiC is most widely studied coating and is being commercially exploited in automotive industry and also for coating the trochoid of the Wankel engine to improve the wear resistance [16].

Mullite is an important high temperature oxide material, chemically stable alumino-silicate ceramic with the general formula **$3Al_2O_3 \cdot 2SiO_2$. It exhibits** excellent thermal stability, low thermal expansion, and good mechanical strength at high temperatures [17]. It is most widely used in furnaces, kiln linings, and aerospace components. Its needle-like crystal morphology also enhances fracture toughness in composite materials. Due to its desirable combination of properties, mullite is widely used not only in structural and thermal insulation applications but also as a reinforcement in advanced ceramic matrix composites and coatings. In addition, the petrochemical and aluminium industries use mullite-based aggregates for applications that necessitate thermal shock resistance, chemical attack resistance, and hot-load strength. Mullite is also a desirable material for high-strength infrared transmitting windows. Protective coatings and electronic substrates are other applications of mullite [18].

There is limited literature on the electrodeposited Ni-composite coating containing mullite particles. Radomysel'skii et al. [19] have reported the development of electrodeposited Ni composite containing mullite whiskers and explored the high temperature oxidation resistance of the coating and observed improved oxidation resistance vis-à-vis plain nickel coating. The paper by Meenu et al. [20] explored the effect of the addition of mullite particles derived from sillaminite.

The present study is aimed at the synthesis of mullite powder by ball milling followed by the development of electrodeposited N-mullite composite coating. The effect of applied current density on the microhardness and corrosion resistance has been studies. Also, the wear behavior of the best coating is also studied and it is compared with plain Ni.

2. Experimental Procedure

2.1. Mullite powder synthesis and characterization

Mullite powder was synthesized by mechanical alloying, which is a very high-energy ball milling process. 27.2 g alumina (Loba Chemie) and 10.7 g cabosil (Cabot Sanmar Ltd) powders were mixed with ethanol and ball milled for three hours at 350 rpm using a planetary ball mill (Fritsch Pulveristte 6 Classic). The mullite powders were characterized using a Field Emission Scanning Electron Microscope (FESEM) system integrated with Energy Dispersive X-ray Analysis (EDAX) facility (Supra 40VP model, Carl Zeiss with a Gemini column) to understand their surface morphology and to estimate their individual size. Particle size analysis was used to find the extent of agglomeration of the particles. In the present study Master sizer 2000 (Malvern, UK) particle size analyzer, which works on the principle of the laser light scattering method was employed. The X-ray Diffraction (XRD) pattern of the powder was recorded using a Bruker-Advance-D8 X-ray diffractometer with Cu Kα as the radiation source and Ni as the filter. The average crystallite size was obtained by the line-broadening method. The average crystallite size values were estimated using Scherrer formula:

$$D = \frac{0.9\lambda}{\left(B^2 - b^2\right)^{1/2} Cos\theta}$$

where D is the crystallite size, λ is the wavelength of the radiation, θ is the Bragg's angle and B and b are the FWHMs observed for the sample and standard, respectively.

2.2. Preparation and characterization of nickel-mullite composite coatings

Composite coatings were prepared by cathodic electrodeposition in which the object to be electroplated was taken as the cathode (brass) and an electrode of the same material (Ni) to be coated was taken as the anode and both cathode and anode were of the same size. The electrolyte used was a nickel sulphamate bath into which the prepared particles were dispersed. Brass substrates were used and the electrodeposition was done using a

DC power supply.

A 200 mL Ni-sulfamate bath containing 20 g of mullite powder (100 g/L) was taken in a glass beaker and stirred for 16 hours before electrodeposition [7]. Electrodeposition was carried out at 0.75 A/dm^2 for 6 h, 1.54 A/dm^2 for 3 h, 3.1 A/dm^2 for 1.5 h and 4.65 A/dm^2 for 52 min, on a magnetic stirrer (400 rpm). The pH was maintained at 4 and the electrodeposition was carried out on brass plates and mild steel substrates, respectively, for microhardness and corrosion studies.

Cross-sectional metallography specimens were prepared by sandwiching the electrodeposited brass coupons with a copper backup in a Bakelite matrix. After mechanical grinding using emery sheets of different grades (100, 240, 320, 400, 600, 800, 1000 and 1200 μm), the samples were polished with Al_2O_3 slurry down to 0.05 μm. The optical micrographs of the cross sections of Ni-mullite composite were recorded using a vertical metallurgical microscope. Microhardness indentations were made into cross sections to avoid the effect of the substrate. The microhardness measurements were performed on ten different locations on the cross-section of each coating (Micromet 2103, Buehler) using a Knoop indenter at 50 gf load.

In this study, a pin-on–disc tribometer with a track radii varying between 5-40 mm, a load of 0.5-2 kg and a speed between 10-600 rpm was used. In this method of wear measurements, a pin with the coating to be analyzed was kept stationary and fixed to a lever arm while a disc rotates at a fixed speed. In order to study the wear performance of the composite coatings, a brass pin with a hemispherical head of about 6 mm radius was used. The hemispherical region was coated with Ni and the composite coating at 3.1 A/dm^2. All wear tests were conducted at a wear track radius of 30 mm at 200 rpm at a slide speed of 0.628 m/s .The disc used was hardened EN 31 steel with a Vickers hardness of 750 HV. An LVDT transducer was used to measure the total height loss of the pin and disc. More details of the wear test are already provided in literature [7,11]. The optical micrographs of the disc after wear test was also recorded.

The corrosion behavior of Ni and Ni-composite coatings on mild steel coupons **was** studied using CHI 604 2D electrochemical workstation [11]. The test was carried out in deaerated 3.5 wt% (0.6 M) NaCl solution (200 ±2 mL) using a conventional **three-electrode** cell equipped with the coated mild steel coupon with an active area of 1cm^2 as the working electrode. A platinum foil and saturated calomel electrode (SCE) were used as counter and reference electrodes, respectively. The reference electrode was connected to a Luggin capillary and its tip was placed very close to the surface of the working electrode to minimize the IR drop. The coupon was immersed in NaCl solution for an hour in order to establish the open circuit potential (E_{OCP}). The Electrochemical Impedance Spectroscopy (EIS) studies were carried out in the frequency range of 100 kHz - 10 mHz. The amplitude of the applied alternating potential was 10 mV on the E_{OCP}. The impedance data was displayed as Nyquist and it is a plot of real (Z′) vs. imaginary impedance (Z″). After EIS measurements, the system was allowed to attain open circuit potential and then the upper and lower potential limits of linear sweep voltammetry were set at ±200 mV with respect to the E_{OCP}. The sweep rate was 1 mV/s. The Tafel plots obtained were represented as potential vs. log i plot**.** Omitting the contribution of particles for the weight loss, the corrosion rates (CR) were calculated from corrosion current by using Faraday's law [Standard Practice for calculation of corrosion rates and related information from Electrochemical measurements, American National Standards, ANSI/ASTM G 102-89 (Reapproved 1994)]:

$$CR = K\left(\frac{i_{corr}}{\rho}\right)EW$$

Where CR is given in mm/yr, K=3.27 × 10^{-3} mm g/μA cm yr, ρ= density in g/cm^3 (density of nickel is 8.9 g/cm^3) and EW (Equivalent weight of Ni) = 29.36.

The corrosion protection efficiency of Ni-mullite coatings was calculated using the Tafel extrapolation method by comparing the corrosion current density (i_{corr})

of Ni-mullite coating with that of the Ni metal coating. The protection efficiency was evaluated from the Tafel plot using the equation:

$$P = \frac{I'corr - Icorr}{I'corr} x\ 100$$

where I'corr and Icorr are the corrosion current densities in the absence and presence of particles. The protection efficiency of Ni-composite coatings was also calculated according to the following equation:

$$P = 1 - \left(\frac{R^{o}p}{Rp}\right) x \quad 100$$

Where $R^{o}p$ is polarization resistance in absence of oxide particles (i.e plain nickel) and Rp is polarization resistance in the presence of oxide particles i.e composite coating.

3. Results and discussions

The surface morphology and the particle size of the incorporated particles play an important role in the properties of composite coatings. The FESEM images (Fig.1) of mullite particles showed agglomerates of differently sized particles. The smaller particles were found to be silica particles and the bigger ones were alumina. Bigger particles were in the size range of 0.5-1µm and the smaller particles were in the size range of 10-20 nm. Figure 2 shows the powder XRD pattern of mullite powder. It shows a mixture of α-alumina and silica particles.

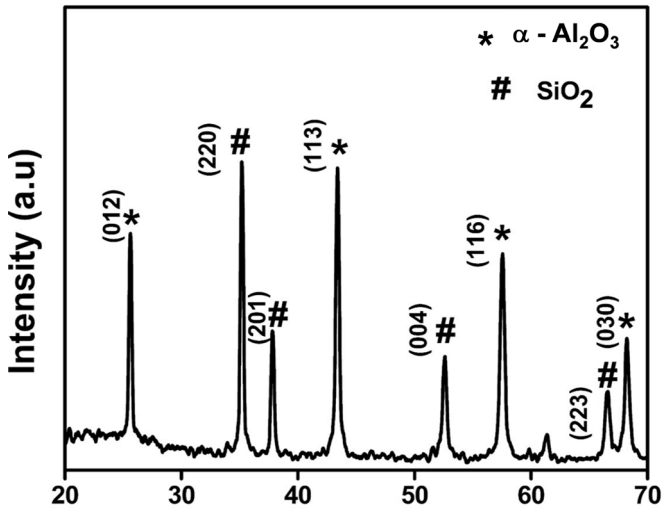

Fig.2. XRD pattern of mullite powder.

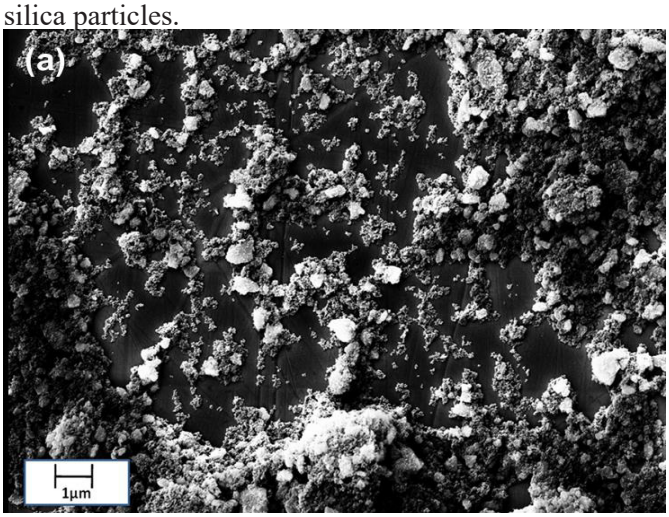

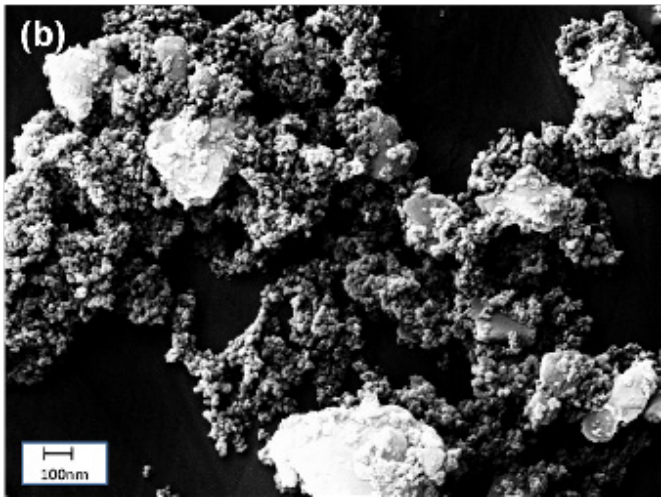

Fig. 1. FESEM of of mullite powders at different magnificatiotns

The characteristic peaks of α-Al_2O_3 and SiO_2 were observed and the average crystallite size of the mullite particles was calculated to be 42.095 nm as calculated by the Scherrer formula with the crystallite size of α-Al_2O_3 being 46 nm and that of SiO_2 as 32.8 nm. The average agglomerated particle size was found to be 3.9 µm from particle size analysis. The bimodal distribution shows the presence of two different sizes of particles (Fig.3). The broad peak covering 1-100 µm size corresponds to alumina particles and a sharp peak below 1 micron corresponds to cabosil silica which is having very high surface area and smaller size.

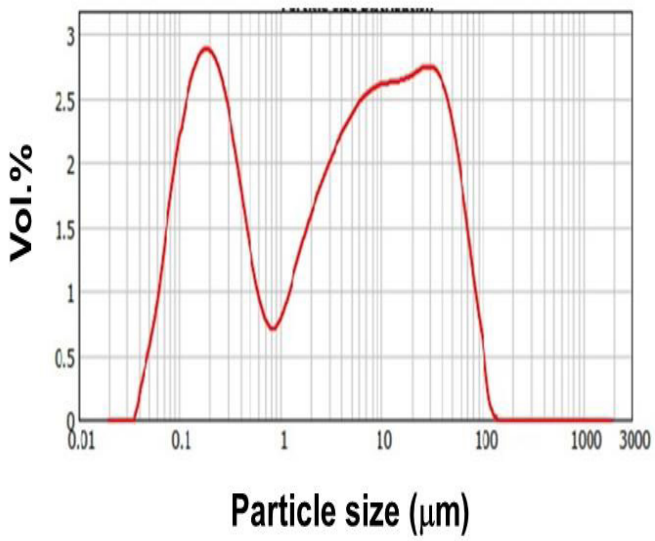

Fig.3. Particle size distribution of mullite particles.

Figure 4 shows the cross-sectional micrographs of Ni-mullite composite coatings electrodeposited at various current densities. From Fig.4, it is evident that at lower current densities, more of particle incorporation occurs. The incorporated particles seen in the optical microscope images may correspond to alumina particles. However, due to the fine nature of the silica particles, they may not be visible in the optical microscope images. The incorporated particles are responsible for increasing the microhardness of the coatings. Further, at higher current denisties, bigger agglomerates are observed in the coatings.

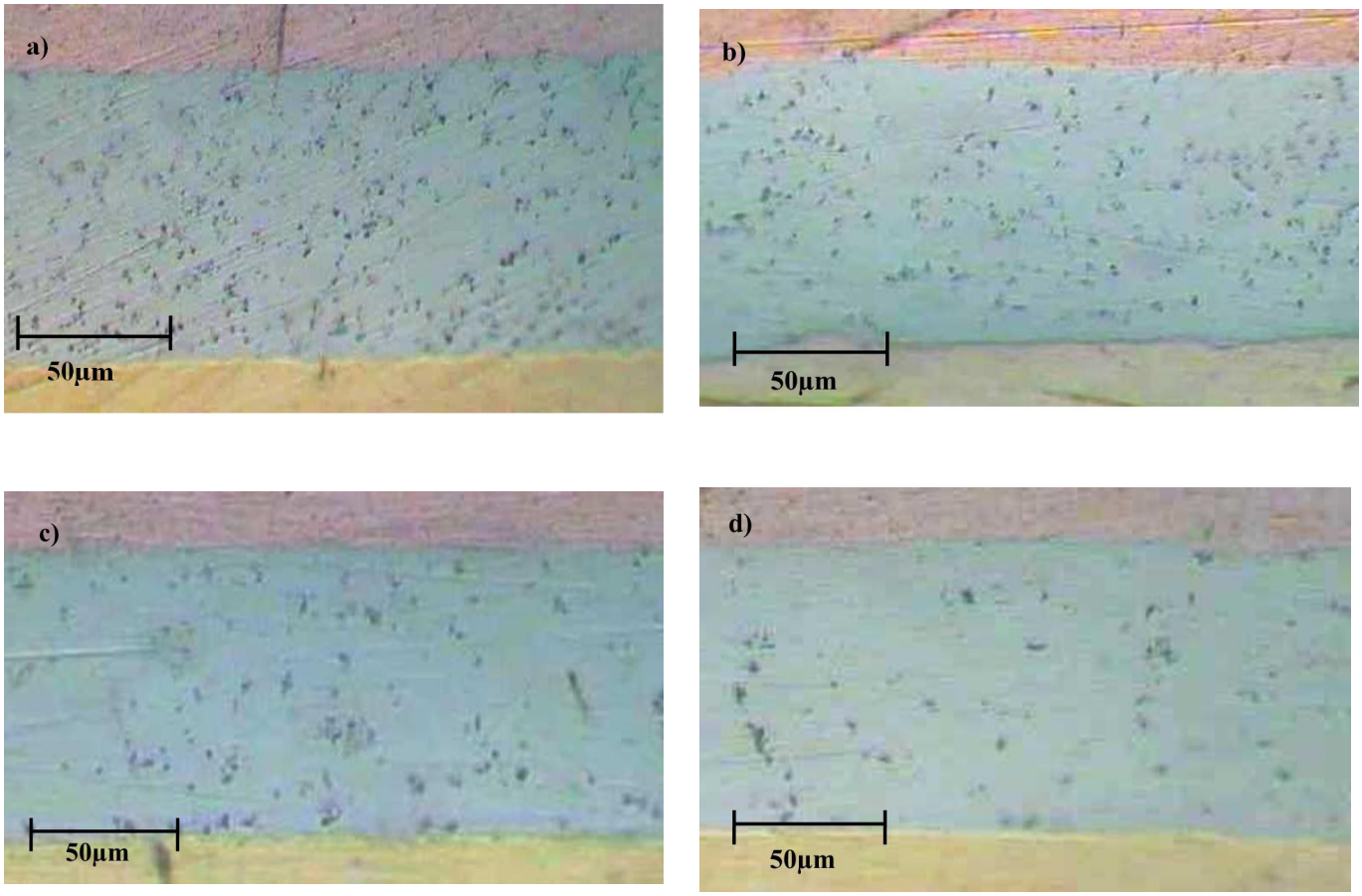

Fig.4. Optical micrographs of the Ni-mullite coating crosssection electrodeposited at various current densities (a) 0.75A/dm^2,(b) 1.54A/dm^2(c) 3.1 A/dm^2 and (d) 4.65A/dm^2

Figure 5 shows the plot of microhardness vs. current density for the Ni-mullite coating electrodeposited at various current densities. The observed microhardness is greater than that reported in the literature (400 HK at 50_{gf}). This is attributed to the lower current density used for the electrocomposite coating development in this study. The lower current density during the electrodeposition of Ni-based composite coatings generally improves the incorporation of particles due to the following reasons: (i) Lower hydrogen evolution during lower current density reduces the turbulence and there by ensures the proper adhesion of the particles and prevents the dislodgement of the particles; (ii) With lower current density, the rate of metal ion reduction slows down, allowing more time for the suspended particles in the electrolyte to reach and adhere to the cathode surface before being encapsulated by the growing nickel layer. This enhances particle entrapment; (iii) At lower current densities, the reduced electric field strength and deposition rate minimize disruption, helping maintain particle stability at the interface, (iv) Better uniformity and less agglomeration: Lower current densities promote more uniform metal deposition, which reduces the likelihood of localized roughness or defects that can either block particle incorporation or cause clustering. This results in a more homogeneous distribution of particles within the nickel matrix, and (v) Operating at lower current densities keeps the system closer to electrochemical equilibrium, which helps maintain consistent ion concentrations near the cathode. This avoids concentration gradients that could interfere with both metal deposition and particle capture. Lower current density is preferred as it provides a more controlled and less turbulent deposition environment, enhancing the likelihood that reinforcement particles are successfully embedded in the nickel matrix and distributed uniformly throughout the coating.

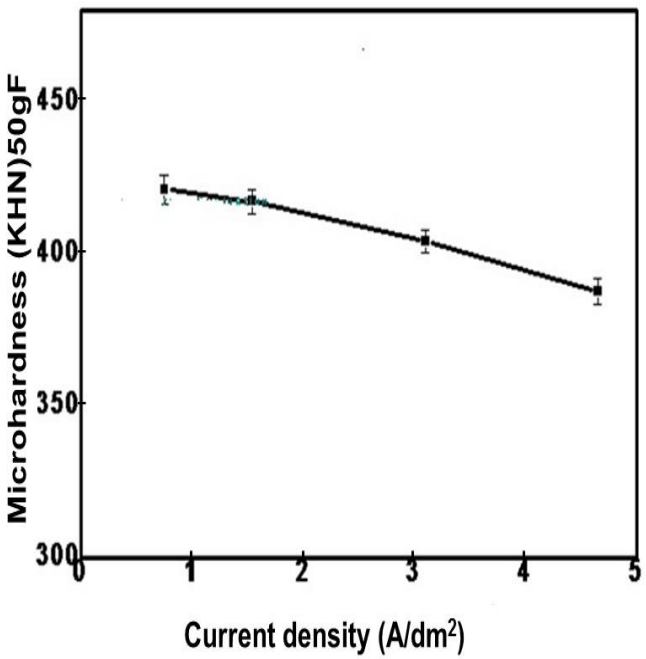

Fig.5. Microhardness vs. current density plots of Ni-mullite coatings.

Table 1 summarizes the corrosion potential, corrosion rates and Tafel plots for Ni-mullite composite coatings electrodeposited at different current densities. All the coatings show same order of corrosion resistance. However, the coating electrodeposited at 3.1 A/dm^2 shows lower icorr. The corrosion current density (μA/cm^2) is derived from Tafel plot (Fig.6). It reflects the rate of the electrochemical reactions occurring on the metal surface, specifically it indicates how fast metal atoms are oxidized and dissolve into the corroding medium. A lower corrosion current indicates improved corrosion resistance because it directly corresponds to a slower rate of metal dissolution, meaning the material is corroding more slowly.

Table 1: Corrosion potential, corrosion rates and Tafel slopes calculated from potentiodynamic polarization curves for Ni-mullite composite coatings.

Current density *A/dm²*	100gpl				
	Ecorr (V)	Icorr (μA/ cm²)	βa (V/dec)	βc (V/dec)	Rp Ω/cm²
1.54	-0.245	0.20	0.11	0.138	130686
3.1	-0.242	0.11	0.19	0.105	269248
4.65	-0.315	0.51	0.202	0.124	65361

Further, interestingly, the polarization resistance of the Ni-mullite coating electrodeposited at 3.1 A/dm^2 is double that of Ni-mullite coating electrodeposited at 1.54 A/dm^2. Polarization resistance is a measure of how much a material resists the flow of electric current during the electrochemical reaction associated with corrosion. It's typically measured using electrochemical techniques like linear polarization resistance (LPR). The value is derived from the slope of the potential vs. current plot near the open circuit potential. A higher polarization resistance in an electrodeposited coating typically means that the coating offers better protection against corrosion, making it more effective as a barrier to environmental degradation. Table-2 summarizes the corrosion protection efficiency of the coatings derived from the Tafel plot and from polarization resistance. There was a good correlation in the efficiency values derived from both the methods.

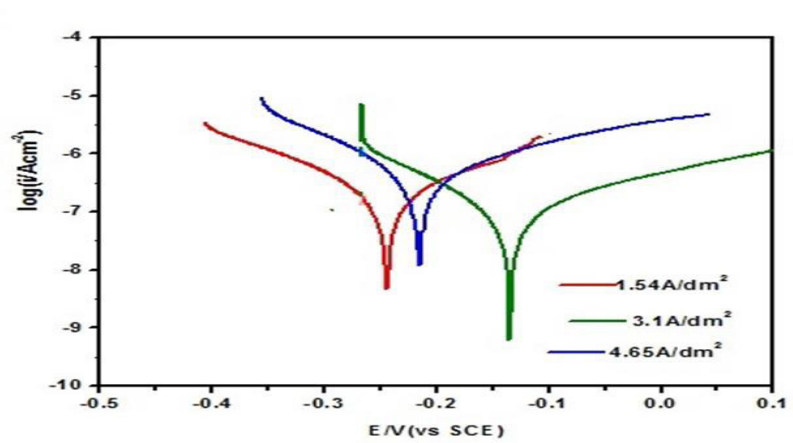

Fig. 6. Tafel plots of Ni-mullite composite coatings electrodeposited at different current densities.

Table 2. Comparison of protection efficiency obtained from Tafel plot to that obtained from the polarization resistance for 100gpl Ni-Mullite composite coating.

Current Density (A/dm²)	P% obtained from Tafel	P% obtained from Rp
1.54	96	94
3.1	98	97
4.65	91	87

The observed Tafel plots substantiate the results of Nyquist plots. The Ni-mullite composite coating electrodeposited at 3.1 A/dm^2 showed a larger semicircle compared to the coatings obtained at 1.54 and 4.65 A/dm^2 (Fig.7). In the case of Nickel-mullite coating, the corrosion resistance was found to be better in the case of 3.1A/dm^2 with a corrosion rate of 1.1 cm/yr.

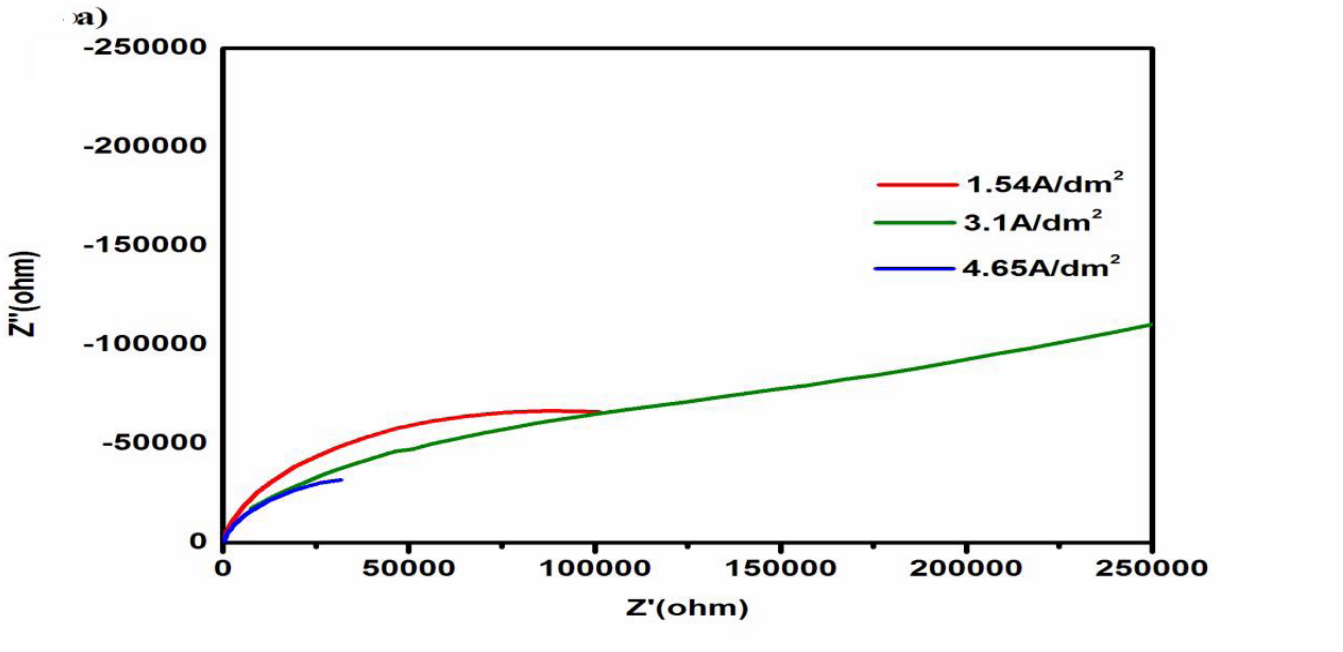

Fig. 7. Nyquist plots of Ni-mullite coatings.

Interestingly, the Ni-mullite coating exhibited higher wear loss compared to plain Ni coating (Fig.8) despite exhibiting a lower coefficient of friction (0.4) compared to plain Ni (0.75). Initially, the wear loss is constant for Ni-mullite coating and the coefficient of friction was constant at 0.45. As the wear loss increases, the coefficient of friction decreases. It is interesting to note that mullite, as a material, doesn't inherently possess lubricating properties. However, when used as an additive in lubricating materials or in composite materials, it can improve the overall tribological performance (friction and wear behavior). Mullite can enhance lubrication by reducing the friction coefficient [21].

The increased wear loss despite possessing a lower friction coefficient may be attributed to the formation of a transfer film that reduces friction in the beginning. The film will become unstable and it flakes off and further increasing the wear loss. Figure 9 shows the optical micrographs of the wear track on the discs after wear. Clearly, mullite particles are seen on the wear track of the Ni-mullite coating tested wear disk (Fig. 9(b)).

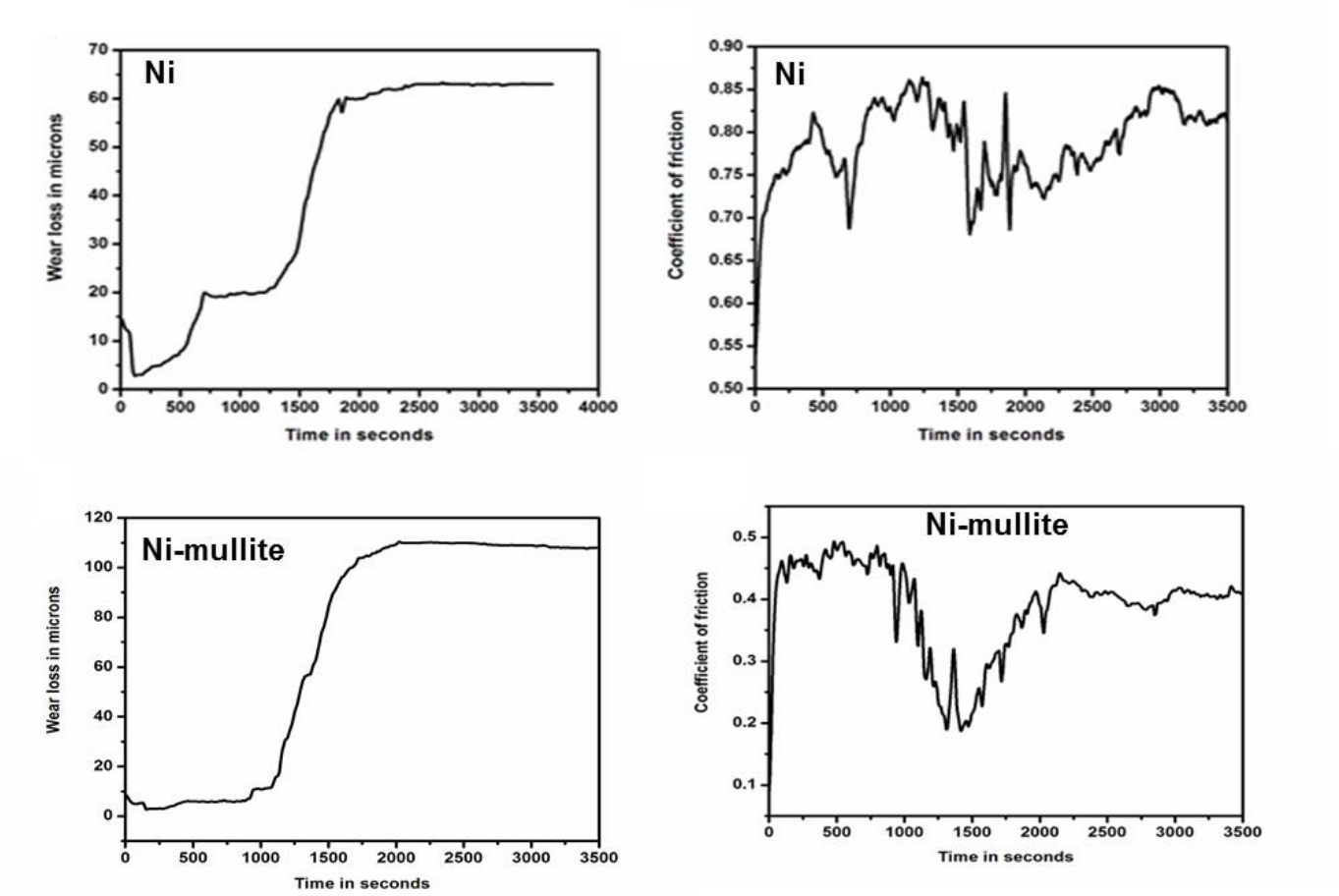

Fig.8. Wear test results of Ni and Ni-mullite coatings.

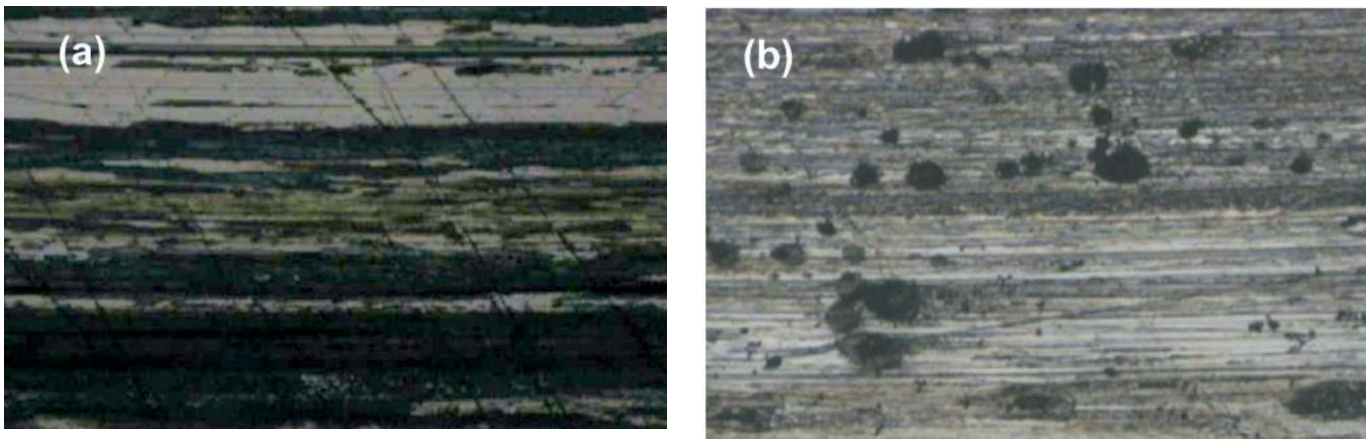

Fig. 9. Optical micrographs of the wear track on the disc after wear test with (a) Ni and (b) Ni-mullite composite coated brass pin.

Conclusions

Electrodeposited Ni-mullite composite coatings were developed using ball milled mullite powder and nickel sulphamate bath. The effect of current density on microhardness and in turn on corrosion resistance of the coatings were studied. The coating electrodeposited at lowest current density (1.54A/dm^2) exhibited higher microhardness (430 HK) and higher number of mullite particles were incorporated. Interestingly, the coating electrodeposited at 3.1 A/dm^2 exhibited better corrosion resistance as evident from the Tafel and Nyquist plots. The coating also demonstrated lower coefficient of friction (0.4) and higher wear loss. Thus Ni-mullite coatings are promising for applications that require higher microhardness and corrosion resistance.

Acknowledgement

The authors acknowledge the Director, CSIR-NAL and Head, SED for their constant support and encouragement. The authors thank Mr. Siju, Mr. Srinivas and Mr. Muni Prakash for the FESEM, XRD, microhardness and wear studies.

References

[1] L. S. Murr, Electrodeposition of composite coatings, Journal of Materials Science, 39(3) (2004) 625.

[2] G. L. Song, M. J. Scully, Electrodeposition of composite coatings for corrosion protection: a review, Corrosion Science, 40 (8) (1998) 1495-1507.

[3] Zellele DM, Yar-Mukhamedova GS, Rutkowska-Gorczyca M. A review on properties of electrodeposited nickel composite coatings: Ni-Al_2O_3, Ni-SiC, Ni-ZrO_2, Ni-TiO_2 and Ni-WC. *Materials.* 17(23) (2024) 5715.

[4] F. C. Walsh, C. Ponce de León, A review of the electrodeposition of metal matrix composite coatings by inclusion of particles in a metal layer: an established and diversifying coatings technology. Trans.IMF, 2014, 92, 83–98.

[5] Li Ruiqian, Chu Qingwei, Liang Jun, Electrodeposition and characterization of Ni–SiC composite coatings from deep eutectic solvent, RSC Adv. 5(2015) 44933-44942

[6] A. Hovestad, L. J. J. Janssen, Electrochemical codeposition of inert particles in a metallic matrix, Journal of Applied Electrochemistry 25 (1995) 519-527.

[7] S.T. Aruna, C.N. Bindu, V. Ezhil Selvi, V.K. William Grips, K.S. Rajam, Synthesis and properties of electrodeposited Ni/ceria nanocomposite coatings" Surface Coatings and technology, 200 (2006) 6871.

[8] S.T. Aruna, K.S. Rajam, Synthesis, characterisation and properties of Ni/PSZ and Ni/YSZ nanocomposites, Scripta Materialia, 48 (2003) 507.

[9] S. T. Aruna, S. Diwakar, A. Jain, K. S. Rajam, Comparative study on the effect of current density on Ni and Ni–Al_2O_3 nanocomposite coatings produced by electrolytic deposition, Surface Engineering, 21 (5) (2005) 209.

[10] S.T. Aruna, K.S. Rajam, Studies on nanocrystalline Ni/Al_2O_3 and Ni/$Al_{2-x}Co_xO_3$ films formed by electrolytic DC plating, ASTRA, 2004, pp. 473-477.

[11] S. T. Aruna, V. K. William Grips, K. S. Rajam, Synthesis and characterization of Ni–Al_2O_3 composite coatings containing different forms of alumina, Journal of Applied Electrochemistry, 40 (2010) 2161.

[12] S.T. Aruna, V. Ezhil Selvi, V.K. William Grips, K.S. Rajam, Corrosion and wear resistant properties of Ni-Al_2O_3 composite coatings containing various forms of alumina, J. Applied Electrochemistry 41 (2011) 461.

[13] S.T. Aruna, V.K. William Grips, V. Ezhil Selvi, K.S. Rajam, Synthesis and properties of electrodeposited nickel / yttria doped ceria nanocomposite coatings, Journal of Applied Electrochemistry, 37 (2007) 991.

[14] S.T. Aruna, M. MuniPrakash, V.K. William Grips, Effect of titania particles preparation on the properties of Ni-TiO_2 electrodeposited composite coatings, J. Applied Electrochemistry 43(2013) 805..

[15] S.T. Aruna, V.K. William Grips and K.S. Rajam, Ni-based electrodeposited composite coating exhibiting

improved microhardness, corrosion and wear resistance properties, Journal of Alloys and Compounds 468 (2009) 546.

[16] S.T. Aruna, C. Anandan, V.K.W. Grips, Effect of probe sonication and sodium hexametaphosphate on the microhardness and wear behavior of electrodeposited Ni–SiC composite coating, Applied Surface Science 301 (2014) 383–390.

[17] Anggono, Juliana, Mullite Ceramics: Its Properties, Structure, and Synthesis Journal Teknik Mesin, 7, 2005.

[18] https://www.azom.com/article.aspx?ArticleID=925

[19] Radomysel'skii, I.D., Apininskaya, L.M. & Vergeles, N.M. Production of composite nickel deposits with mullite additions, Powder Metall Met Ceram 9 (1970) 638–641.

[20] Meenu Srivastava, M. Muniprakash, S.K. Singh, Synthesis of fused mullite and its use in multifunctional nickel based composite coating, Surface and Coatings Technology, 245 (2014) 148-155.

[21] Qiang, H., Li, G., Du, Z., Ren, S., Xu, Z., Xu, Y. Tribological behavior and mechanism of surface-modified mullite as polyurea grease additive, ASME. *J. Tribol.* 146(4): (2024) 041701.

Waste Treatment for Discarded Electroplating Baths

Dr. Vaishali Umrania
Space Application Centre, ISRO, Ahmedabad
vaishali@sac.isro.gov.in

Abstract

In the process of Silver-plating on various metallic hardware, the electrolyte is essentially comprised of high content of cyanide ions 120 g/L along with salts of Silver metal and other required ingredients. Spent Silver plating bath needs specific treatment to destroy cyanide ions beyond detectable limit of 0.1 ppm before putting into common stream of wastewater drain. Oxidation of cyanide under alkaline condition is attempted using Sodium hypochlorite solution (10-12% W/V) to reduce cyanide content below detectable limit through the formation of bicarbonate and gaseous nitrogen. Complete destruction of cyanide ion is confirmed and allowed to release in the main stream of wastewater.

Keywords: cyanide, treatment, effluent, electroplating bath.

Introduction

Silver electroplating is carried out on various substrates majorly aluminium, kovar, invar and other such metals, which are being used for different components of electronics packages. In electroplating, silver corresponding cyanide salt along with other chemistry is used. This bath contains silver potassium cyanide, sodium or potassium cyanide and sodium carbonate. This bath contains a very high concentration of cyanides up to 90-120 g/L, silver 30-34 g/L and sodium carbonate 30 g/L. Plating is carried out batch wise from this bath. Silver metal concentration goes down than the required concentration, bath is replenished with silver plating salt. Silver is consumed from bath and carbonates concentration are increased more than 100 g/L. After long term usage, the plating efficiency decreases and results in defective plating. Dusty silver deposits are observed. At this time the bath is said to be exhausted. So it is advisable to stop the use of this exhausted bath and shift to new one. This whole bath containing high concentration of cyanides is of around 50-200 litres capacity. The main problem occurs over here is that, the existing effluent treatment plant is not designed for high concentrations of cyanides. So to prevent shock loading conditions and avoid other operational problems, we stored all these exhausted baths separately, instead of disposing this waste to treatment plant. Its dilution would require huge amount of water to bring it to safe dispose limit. This created a requirement to develop a separate treatment technique for the cyanides. It is necessary to treat cyanides before treatment of heavy metals because cyanides may interfere in heavy metal removal by forming metal complexes. Also according to central pollution control board (CPCB) standards for electroplating sector, cyanide concentration shall not be more than 0.2 mg/L. So it becomes very important to treat the cyanides in order to meet the standards.

This paper provides basic information about the treatment of extremely toxic cyanide wastes. Basic system guidelines are described along with typical operating parameters. The main objective of effluent treatment is to protect the environment from pollution and fulfil the Government's standards for emission or discharge of environmental contaminants.

Several methods are described in literature about treatment of cyanide effluent which includes use of ozonation alone and conjugation with UV radiation, biologically active species, biosorption-biodetoxification, hydrogen peroxide, photochemical process, sodium hypochlorite, calcium hypochlorite [1] , sulfur dioxide, precipitation by adding heavy metals, ion exchange, activated carbon, aldehydes, per oxygen compounds and bio oxidation [2-11].

Amongst oxidants chlorine is preferred because it is readily available and the least expensive but excess chlorine can produce cancer-causing substances by reacting with other effluent compounds. Ozonation is a

J. Electrochem Soc. India Vol.(73) 7&8 - 2024, page No. 267-280

second choice and is preferred by industries because its excess converts to oxygen, but it requires ozonator and oxygen cylinder to produce ozone. Considering safety measures to store highly flammable oxygen cylinder and hazardous smell of ozone, it was avoided to choose ozonation. Alkaline chlorination is the most popular and preferable treatment for cyanide waste in plating effluent treatment plants. It generates minimum waste. 10-12% Sodium hypochlorite was chosen based on easy availability and less hazardous properties compared to others.

Literature is available for treatment of cyanide up to concentration of 1 g/l. But there are no references found for treatment of cyanides in the concentrations ranging from 2 to 120 g/l. In this study it is exercised to treat cyanides in this higher concentration range.

2. Materials and method

Technical grade 10-12% sodium hypochlorite, 10% sodium hydroxide, pH meter, ORP meter, thermometer, pumps and reaction tanks were sourced from local supplier. During all experiment personal protective equipments such as protective apron, hand gloves, respirator mask with filter cartridge and eye goggles were used to ensure operator safety. The experiments were performed under exhaust hood with high suction capacity.

Samples were taken for discarded plating baths of silver. Initial and final silver concentration, pH, carbonate (if any) and cyanide content were analyzed by using potentiometric titretor according to guidelines [7].

For electroplating silver baths total volume was 400 litres. Silver present in the baths was plated out on SS304 plates at higher current densities. Initial and final silver content was analysed by using x-ray fluorescence spectrometer. Initial cyanide concentration of baths was 120 grams/ litre. The whole treatment was done as per directions given in reference [3]. In one batch 100 litres of solution was taken in 500 litres bath. Reaction was completed in 4 batches. Sensors were arranged for continuous monitoring of reaction. Dosing pumps were arranged for dosing of base (10% sodium hydroxide), oxidant (10-12% sodium hypochlorite) and acid (10% nitric acid). Each part of cyanide requires 9.56 parts of chlorine to oxidize it to carbon dioxide theoretically. The actual requirements exceeded the stated stoichiometric values. So, during experiment 10 gm of sodium hypochlorite was used for each 1 gram of cyanide present in the effluent. Monitoring cyanide waste water treatment by ORP measurement electrode is quite useful indicative method for demonstrating whether proper quantities of treatment chemicals have been added. Following steps were followed for waste treatment of cyanide. The reaction was carried out at room temperature of 30-35°C. Effluent treatment plant schematic diagram for cyanide containing effluent is given in figure 1.

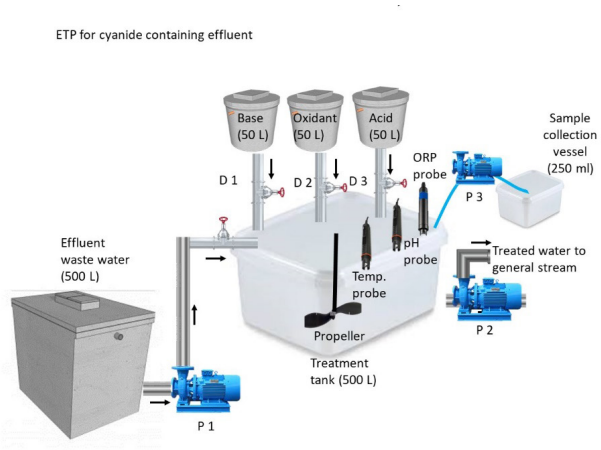

Figure 1 Effluent treatment plant schematic diagram for cyanide containing effluent

The destruction of cyanide by sodium hypochlorite was accomplished in the following stages:

1st stage:

(a) $NaCN + NaOCl + H_20 \rightarrow CNCl + 2NaOH$

(b) $CNCl + 2NaOH \rightarrow NaCNO + NaCl + H_20$

Initial value of sample pH and ORP values lies between 11-12 and 0 to -400mV respectively. ORP set point was +300 mV. The rise in ORP is easily observable with consequent addition of hypochlorite which further supports the reaction progression.

2nd stage:

$2NaCNO + 2NaOH + 3NaOCl \rightarrow 2Na_2CO_3 + 3NaCl + N_2 + H_20$

Reaction was done at pH in the range of 8.5 to 9.5. ORP set point was +750 mV. Ideal reaction time was 2 hours. If pH drop was observed, 10% sodium hydroxide was added to maintain pH 9-9.5.

Overall:

$2NaCN + 5NaOCI + 2NaOH \rightarrow 2Na_2CO_3 + 5NaCl + N_2 + H_2O$

At the end of reaction, pH nearly comes to 8-9.5 and ORP comes up to +650 to +750 mV. Carbonate increased in the solution gradually with time which also supports the completion of reaction. Ensured removal of cyanide by titration. The treated solution was alkaline. So it was neutralized to meet discharge limits. Nitric acid was used to lower pH. But before adding acid it was confirmed that all the cyanide was converted to bicarbonate and nitrogen, otherwise it would produce hazardous hydrogen cyanide gas while coming in contact with acid. Discarded treated solution.

3. Results

For electroplating silver discarded baths, silver was recovered by plating on SS304 plates at current density of 40-50 amperes per square feet at room temperature. Initial silver content was 28 g/L and after recovery silver content was 1.5 g/L. Theoretically, it should require 47 kg of sodium hypochlorite but practically it required 50 kg of sodium hypochlorite for complete removal of cyanide. This can be due to loss of chloride content from sodium hypochlorite during storing and reaction. The solution was treated with sodium hypochlorite for cyanide removal. Treatment was continued until cyanide was below detectable level. Initially the solution was having pH 12. The treatment was carried out batch wise. After cyanide removal solution was having pH above 10, which was neutralized by nitric acid to get pH between 6-8. ORP changes during the reaction is given in figure 2.

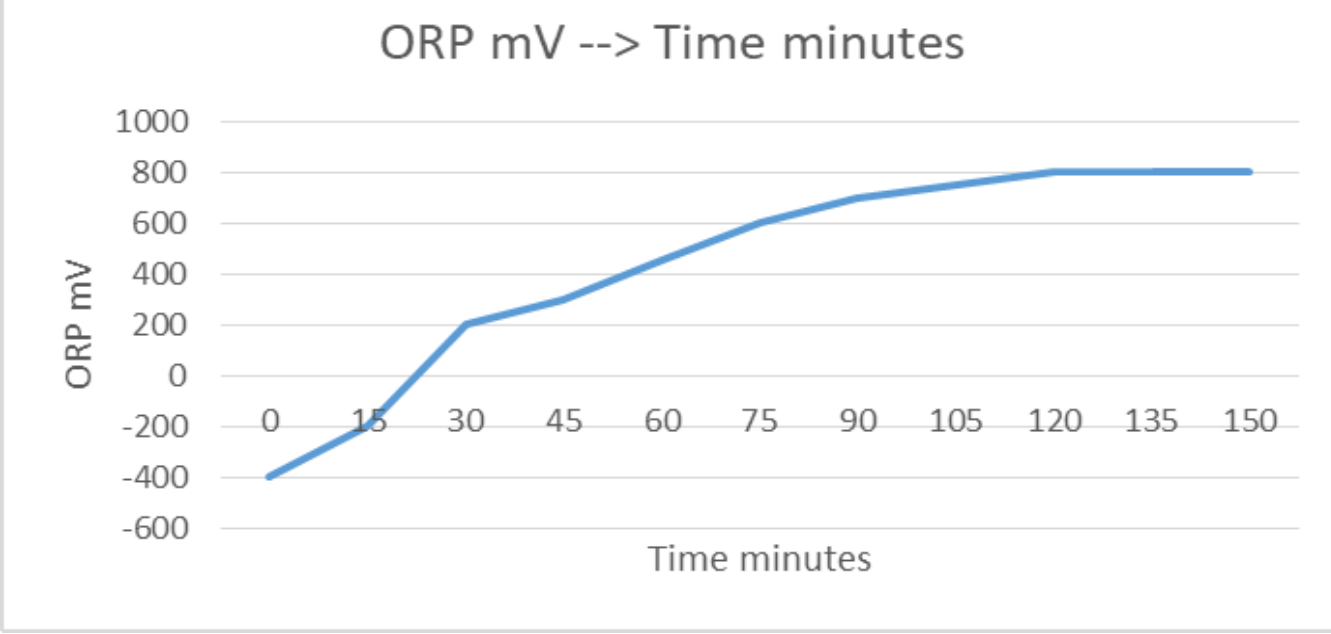

Figure 2 ORP changes during reaction

Details of pH changes during the reaction is given in Figure 3. Initially pH of solution was 12. Sodium hypochlorite was added, cyanide was converted to cyanate, and pH decreased to 9. Here the first step of reaction was completed. Again sodium hypochlorite was added for further conversion of cyanate to nitrogen and sodium carbonate. Gradually pH was decreased. At the end of reaction at about 120 minutes pH came to 8-8.5. All cyanide was destroyed. Remaining solution was treated with nitric acid to get pH between 6.5-6.

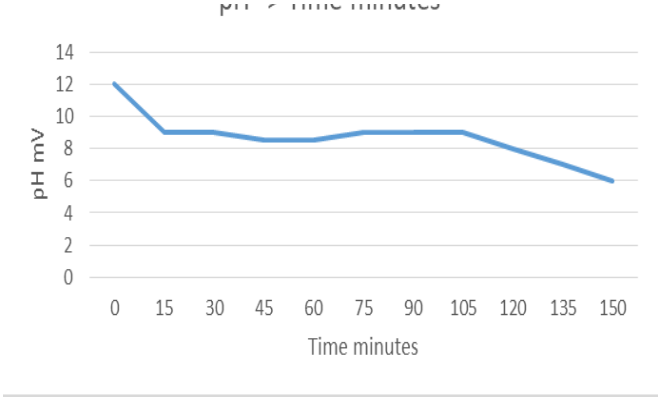

Figure 3 pH changes during reaction

During second stage of reaction bubbling of nitrogen gas was observed in the bath. Generation of carbonate was confirmed by titration.

4.Conclusion

From experiments it can be calculated that for every 100 litters electroplating silver baths having 120 ± 2 g/L cyanide required 7 litters of sodium hypochlorite to neutralize cyanide. The left over solution had pH above 8-9.5 after treatment, which was neutralized by nitric acid. This treated neutral solution was discarded into main stream effluent. During this experiments we found difficulty in storing 10-12% sodium hypochlorite solution at room temperature of 35°C and above. As soon as container is opened, sodium hypochlorite concentration started to come down. It was recommended to use it within 24-30 hours. It is quite important to maintain concentration to at least 8-10% to get efficient oxidation reaction. This process is found very useful and successfully implemented in our facility with semi-automated controls. Advantages of using sodium hypochlorite is that reaction doesn't require complex machinery and setup, process is rapid, technical grade material is easily available as by product from chemical industries, reaction is easily controllable. Disadvantage is that using hypochlorite required careful pH control to prevent formation of toxic cyanogen chloride.

Acknowledgement

The authors appreciate technical help received from STPD colleagues during the course of experiments reported in this paper. The authors gratefully acknowledge guidance received from Head STPD, Shri Ranajit Pal, the inspiration received from Shri Arun Bindal, Group Director, EFMG and best regards to reviewers for spending their valuable time in the evaluation. Sincere thanks to Shri Sumitesh Sarkar, AD SAC, and Director-SAC for their necessary guidance and facilitating us to do this experiment.

References:

[1] N. Sinbuathong and B. Kongseri, "Cyanide Removal from Laboratory Wastewater Using Sodium Hypochlorite and Calcium Hypochlorite," *Kasetsart J. (Nat. Sci.)*, no. 34, pp. 74–78, 2000.

[2] Z. Walter and H. Robert, "Cyanide waste treatment technology, The old, the new and practical," *P & SF*, pp. 56–59, Aug. 1980.

[3] D. H, L. F, and B. G Liptak, "Cyanide Waste Treatment," in *Environmental Engineers Handbook*, CRC Press LLC, 1999.

[4] J. T. Byrne, W. S. Turnley, and A. K. Williams, "Destruction of cyanide wastes by electrolytic chlorination," *J. Electrochem. Soc.*, vol. 105, no. 10, p. 607, 1958.4

[5] M. R. Hillis, "Treatment of cyanide wastes by electrolysis," *Trans. Inst. Met. Finish.*, vol. 53, no. 1, pp. 65–73, 1975.

[6] M. C. Dart, J. D. Gentles, and D. G. Renton, "Electrolytic oxidation of strong cyanide wastes," *J. Appl. Chem.*, vol. 13, no. 2, pp. 55–64, 1963.

[7] T. C. Tan, W. K. Teo, and D.-T. Chin, "Electrochemical destruction of complex cyanide," *Chem. Eng. Commun.*, vol. 38, no. 3–6, pp. 125–133, 1985.

[8] L. M. Cardoso, F. Mainier, and J. A. P. Itabirano, "Analysis voltammetry of cyanide and process electrolytic removal of cyanide in effluents," *American Journal of Environmental Engineering*, vol. 4, no. 6, pp. 182–188, 2014.

[9] N. S. Bhadrinarayana, C. A. Basha, and N. Anantharaman, "Electrochemical oxidation of cyanide and simultaneous cathodic removal of cadmium present in the plating rinse water," Ind. Eng. Chem. Res., vol. 46, no. 20, pp. 6417–6424, 2007.

[10] C.A. Young and T.S. Jordan, "Cyanide remediation: current and past technologies," in *Proceedings of the 10th Annual Conference on Hazardous Waste Research*, May 23-24 1995, p. 26

[11] Y. Gao *et al.*, "Simultaneous silver recovery and cyanide removal from electroplating wastewater by pulse current electrolysis using static cylinder electrodes," *Ind. Eng. Chem. Res.*, vol. 52, no. 17, pp. 5871–5879, 2013.

PROFORMA OF SUBSCRIPTION FORM

I /We wish to subscribe **The Journal of Electrochemical Society of India (JECSI)** for ..... year(s) for which (i) a Demand Draft vide ……..……. dated ……..…… issued from (Name of the bank…….....)favouring **ELECTROCHEMICAL SOCIETY OF INDIA JOURNAL, payable at Bengaluru or (ii) NEFT/IMPS vide UTR no……..dated for Rs/US $…….is enclosed.**

NAME…….

DESIGNATION…….

POSTAL ADDRESS…….

……PIN…….....

E-MAIL…….Phone no.……

Subscriber ID (for renewal only)……

Signature…….

Bank account details
Name: Electrochemical Society of India Journal
Account No. 110045333254
Bank Name: Canara Bank
Customer ID: 309740255
IFSC Code: CNRB0000683
MICR Code: 560015023
Indian Institute of Science
Canara Bank IISc, Bangalore - 560012

Subscription details:

Print only: For institutions & Individuals: Annual 6 issues: Rs 2000/- (India), Annual 6 issues: USD 250.00 incl. postages (abroad),

For students: Annual 6 issues: Rs 1000/-

Print & Online (customer type: institution):

USD 100.00 & INR 5000.00

Please note that institutional prices are available only for libraries of higher education institutions and research organizations.

Journal of the Electrochemical Society of India

Vol. No.73 (7 & 8), Oct- Dec 2024

CODEN-JESIA73 [7&8]2024 ISSN:0013-466X

Email : ecsiiisc@gmail.com

FROM IV

See Rule VIII

1.	Place of publication	:	Bengaluru
2.	Periodicity of its publication	:	Quarterly
3.	Printer name	:	Print Hut
	Whether the Citizen of india	:	YES
	Address of the printer		Govindarajnagar Bengaluru - 560040
4.	Publishers Name	:	**The Electrochemical Society of India**
5.	Editor's Name	:	Dr. U. Kamachi Mudali
	Whether Citizen of India	:	Yes
	Address	:	**The Electrochemical Society of India** Indian Institute of Science Campus, Bangalore - 560 012
6.	Name and Address of Individuals who own the newspaper/holders and partners and shareholders	:	**The Electrochemical Society of India** Indian Institute of Science Campus, Bangalore - 560 012. holding more than 1% of the total capital.

I, Dr. U. Kamachi Mudali hereby declare that the particulars given above are true to the best of my knowledge and belief.

Sd/-

Dr. U. Kamachi Mudali

Chief Editor, JECSI

(Publisher)

THE ELECTROCHEMICAL SOCIETY OF INDIA

Indian Institute of Science Campus, Bengaluru - 560 012, India
Phone : +91-80-22932613
E-mail : ecsiiisc@gmail.com | www.ecsi.in

CALL FOR NOMINATIONS FOR ECSI AWARDS- 2024

Shri S.K. Seshadri Memorial Mascot National Award
(Instituted in the year 1980)

With a view to stimulate interest among Scientists and Technologists in the field of corrosion, the Electrochemical Society of India has instituted the prestigious "**Shri S. K. Seshadri Memorial Mascot National Award"** for notable and outstanding contributions in the field of Industrial Corrosion. The award is sponsored by Director, M/s. Biosafe Solutions.

1. The research work considered for this award should be in the field of Corrosion Science and Technology, Corrosion Prevention and Allied aspects. Industrial Significance to be highlighted and Industrial applicability is desired.
2. The work should have been carried out to bring it to the point of application. The process of development and test schedules may have been carried out during the preceding couple of years, but should have culminated in a fruitful result. The work need not necessarily have been published.

THE N. M. SAMPAT AWARD - 2024
(Instituted in the year 1986)

With a view to recognize outstanding services rendered to the Electroplating industry andTechnology, the Governing Council of the ECSI has with great pleasure has instituted "**The N. M. Sampat Award".** This award is sponsored by M/S Canning Mitra Phoenix Limited, Mumbai. Research work considered for this award should be in the field of Metal Finishing, Electroplating, Surface Coating and Modification, and allied fields. Work carried out in these areas with possible industrial applicability or academic excellence would be considered. The work need not have been published but industrial applications should have been established.

ECSI- METROHM National Award - 2023
(Instituted in the year 2021)

With a view to recognize the contributions made by individuals in the field of basic electrochemistry, electrochemical instrumentation and devices, theoretical and; experimental electrochemistry, the Electrochemical Society of India has instituted this prestigious award **"ECSI- METROHM National Award for Electrochemical Science".** The award is sponsored by M/s Metrohm India Ltd. Chennai. Meritorious work in any field of Electrochemical Science would qualify for this award

ECSI- AMARA RAJA National Award- 2023
(Instituted in the year 2021)

With a view to stimulate interest among Scientists and Technologists in the field of Batteries, Fuel Cells and Sensors, the Electrochemical Society of India has instituted the prestigious award **"ECSI- AMARA RAJA National Award for Advanced Electrochemical Technology".** The award is sponsored by M/s. Amara Raja Batteries Ltd. Tirupathi. Meritorious work in the field of Batteries, Fuel Cells and Sensors would qualify for this award.

ECSI-Dr. K. Elayaperumal National Award- 2023
(Instituted in the year 2022)

With a view to recognize the outstanding contributions of individuals made in the area of Corrosion Mitigation in Industries, The Electrochemical Society of India has instituted the prestigious award "ECSI- Dr. K. Elayaperumal National Award for Excellence in Industrial **Electrochemical Science and Technology"** from this year. The award is sponsored by Dr. K. Elayaperumal and his family. Meritorious work in the area of corrosion mitigation in industries would qualify for this award.

GUIDELINES FOR NOMINATION

1. Nominations may be made by Research Organizations/Institution/ Industries/Individuals.
2. The nomination should be accompanied by the complete bio-data and important contributions for which the nomination is being made.
3. The work should have been carried out to bring it to the point of application. The process of development and test schedules may have been carried out during the preceding couple of years, but should have culminated into a fruitful result at least during the year of application.

Each of the above awards carries a Scroll of Honor and cash prize.

Awardees are required to present their work in the form of an **Award Lecture** and also submit a written manuscript for publication in the Journal of Electrochemical Society of India. Complete Nominations in all respects for the above awards should reach The Secretary, The Electrochemical Society of India, Indian Institute of Science Campus, Bengaluru - 560 012.

Nominations complete in all respects for the above awards should reach
Hon President or General Secretary,
The Electrochemical Society of India, Indian Institute of Science Campus,
Bengaluru - 560 012,
E-Mail: ecsiiisc@gmail.com

Dr. S. T. Aruna
Hon. President, ECSI

Dr. Ajay Krishnan
Hon. Gen. Secretary, ECSI

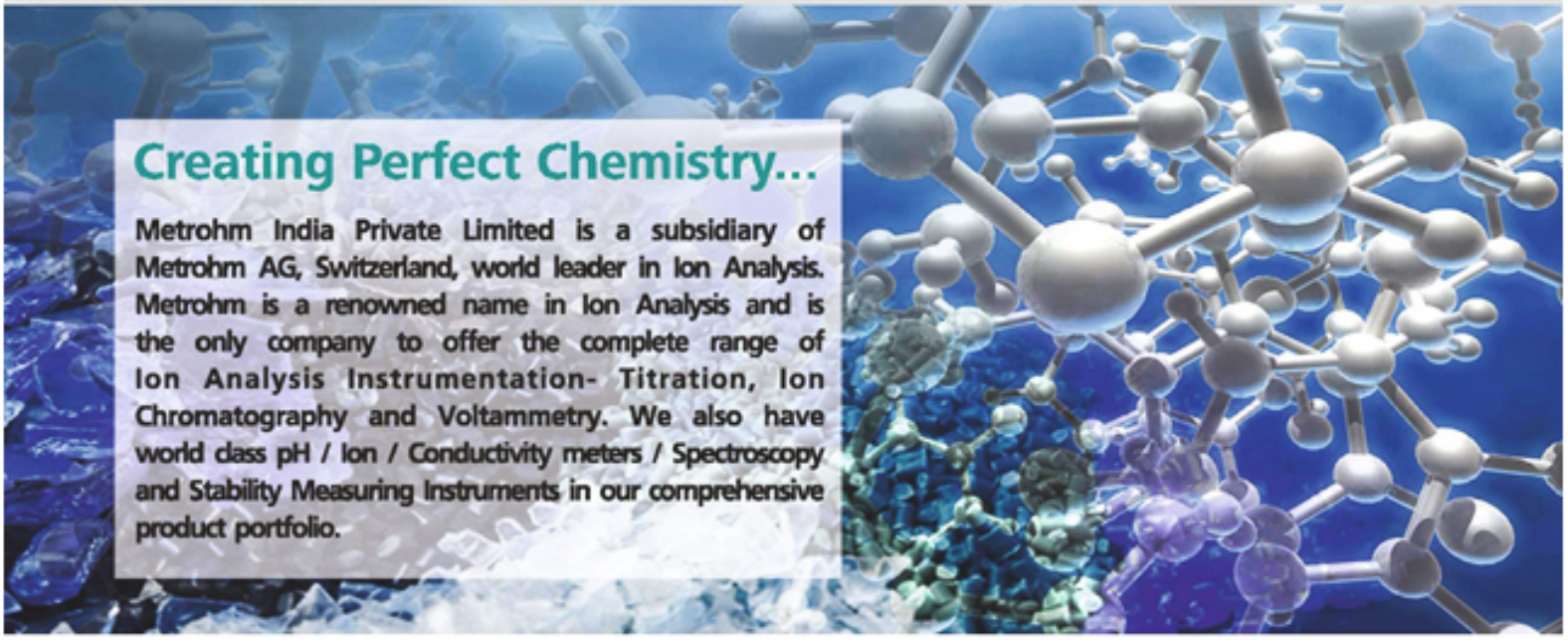

Creating Perfect Chemistry...

Metrohm India Private Limited is a subsidiary of Metrohm AG, Switzerland, world leader in Ion Analysis. Metrohm is a renowned name in Ion Analysis and is the only company to offer the complete range of Ion Analysis Instrumentation- Titration, Ion Chromatography and Voltammetry. We also have world class pH / Ion / Conductivity meters / Spectroscopy and Stability Measuring Instruments in our comprehensive product portfolio.

Titrator

Ion Chromatography

Voltammetry

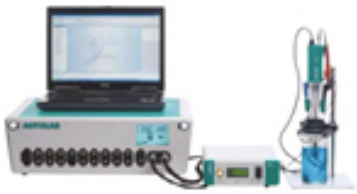

Electrochemical station

NIRS Analyzer

Raman Spectroscopy

Labwater Purification

Surface Area Analyzer

We also have:

- Electrochemical research instrumentation from Metrohm Autolab
- On-line and at-line process analyzers for process monitoring from Metrohm Process Analytics
- NIR and Raman Spectroscopy solutions from Metrohm and B&W Tek
- Innovative technology for electrochemistry research from Dropsens
- BET surface area, pore size distribution from MicrotracBEL Corp., Japan
- Testing instrumentation for the energy storage device and energy conversion device markets from Arbin instruments
- Lab water solutions from Elga
- Pipetting and dispensing solutions from Socorex

PARTICIPATE IN WATER SURVEY

SCAN ME

GET YOUR **FREE** GIFT!

Metrohm India Private Limited
Metrohm-SIRI Towers, 3&4, Fourrts Avenue, Annai Indira Nagar
Okkiyam, Thoraipakkam, Chennai - 600097, India.
Ph: +91 44 40440440 | Customer support: +91 44 40440444

For details, e-mail us at **info@metrohm.in** or visit us at **www.metrohm.in**

Metrohm
India Private Ltd.